

Interaction of Nanoscale Particles with the Skin Barrier

Dissertation
zur Erlangung des Grades
Doktor der Naturwissenschaften
der Naturwissenschaftlich-Technischen Fakultät III
Chemie, Pharmazie, Bio- und Werkstoffwissenschaften
der Universität des Saarlandes

von

Hagar Ibrahim Mohamed Ibrahim Labouta

Saarbrücken

2011

Tag des Kolloquiums: **19.12.2011**

Dekan: **Univ.-Prof. Dr. Wilhelm F. Maier**

Berichterstatter: **Jun. Prof. Dr. Marc Schneider** (*Saarland University*)

Prof. Dr. Claus-Michael Lehr (*Saarland University, HIPS institute*)

Prof. Dr. Labiba Khalil El-Khordagui (*Alexandria University*)

Prof. Dr. Eduard Arzt (*Saarland University, INM institute*)

Vorsitz: **Prof. Dr. Guido Kickelbick** (*Saarland University*)

Akademischer Mitarbeiter: **Dr. Kerstin Hirschfelder**

Die vorliegende Dissertation entstand unter der Betreuung von

Jun. Prof. Dr. Marc Schneider

In der Fachrichtung Pharmazeutische Nanotechnologie
der Universität des Saarlandes

*Ich möchte mich für die Überlassung des Themas und die wertvollen Anregungen
und Diskussionen bei Herrn Jun. Prof. Schneider herzlich bedanken.*

Scientific contributions

This thesis encompasses the following publications:

- **Hagar I. Labouta**, Tobias Kraus, Labiba K. El-Khordagui and Marc Schneider (2011).
"Combined multiphoton imaging-pixel analysis for semiquantitation of skin penetration of gold nanoparticles".
International Journal of Pharmaceutics, **413**, 279-282.
- **Hagar I. Labouta**, Martina Hampel, Sibylle Thude, Katharina Reutlinger, Karl-Heinz Kostka and Marc Schneider (2011).
"Depth profiling of gold nanoparticles and characterization of point spread functions in reconstructed and human skin using multiphoton microscopy".
Journal of Biophotonics, **5**, 85-96.
- **Hagar I. Labouta**, David C. Liu, Lynlee L. Lin, Margaret K. Butler, Jeffrey E. Grice, Anthony P. Raphael, Tobias Kraus, Labiba K. El-Khordagui, H. Peter Soyer, Michael S. Roberts, Marc Schneider and Tarl W. Prow (2011).
"Gold nanoparticle penetration and reduced metabolism in human skin by toluene".
Pharmaceutical Research, **28** (11), 2931-2944
- **Hagar I. Labouta**, Labiba K. El-Khordagui, Tobias Kraus and Marc Schneider (2011).
"Mechanism and determinants of nanoparticle penetration through human skin".
Nanoscale, **3**, 4989-4999.
- **Hagar I. Labouta**, Labiba K. El-Khordagui and Marc Schneider.
"Could chemical enhancement of gold nanoparticle penetration be extrapolated from established approaches for drug permeation?".
In due publication.

Table of contents

Short Summary.....	7
Kurzzusammenfassung.....	8
<u>Chapter 1:</u>	
Background and Literature Survey.....	9
1.1. Introduction.....	10
1.1.1. Inorganic nanoparticles and their pharmaceutical and biomedical applications.....	10
1.1.2. Significance and scope of the chapter.....	13
1.2. Current dilemma in the status of skin penetration of inorganic nanoparticles.....	15
1.3. Factors affecting skin penetration.....	22
1.3.1. Physicochemical attributes of the nanoparticles and formulation factors.....	22
1.3.2. Experimental factors.....	23
1.4. Approaches adopted to enhance skin penetration of inorganic nanoparticles.....	23
1.4.1. Physical/mechanical enhancement.....	24
1.4.2. Chemical enhancement.....	27
1.5. Mechanism of skin penetration.....	27
1.6. Penetration of inorganic nanoparticles through human skin: Dissecting the “nano” effect.....	30
1.7. Qualitative and quantitative analysis of inorganic nanoparticles in the skin.....	31
1.8. Standpoint and recommendations for future directions.....	34
<u>Chapter 2:</u>	
Aim of the Thesis and Experimental Design.....	36
<u>Chapter 3:</u>	
Publications.....	40
3.1. Combined multiphoton imaging-pixel analysis for semiquantitation of skin penetration of gold nanoparticles.....	41
3.2. Depth profiling of gold nanoparticles and characterization of point spread functions in reconstructed and human skin using multiphoton microscopy.....	48

3.3. Gold nanoparticle penetration and reduced metabolism in human skin by toluene.....	71
3.4. Mechanism and determinants of nanoparticle penetration through human skin.....	95
3.5. Could chemical enhancement of gold nanoparticle penetration be extrapolated from established approaches for drug permeation?.....	121
3.6. Statements of effort.....	136
<u>Chapter 4:</u>	
Summary.....	138
4.1. Results and discussion.....	139
4.2. Conclusion.....	143
<u>Chapter 5:</u>	
References.....	145
Curriculum Vitae.....	157
Acknowledgments.....	162

Short Summary

Skin penetration of nanoparticles was the focus of several recent studies. This is of major importance in basic research for potential future applications, e.g. designing topical and transdermal delivery systems, as well as for health risk analysis. Yet, there is a controversy among researchers on the status of their skin penetration due to different experimental setups. Meanwhile, there is little known about the mechanism and determinants of nanoparticle penetration.

The main thesis objective was hence to study the penetration of model gold nanoparticles of different physicochemical and formulation parameters through human skin of different degrees of barrier integrity. Multiphoton microscopy was used for nanoparticle detection. Imaging parameters were determined in terms of resolution and depth profiling of gold nanoparticles in skin. A semiquantitative approach based on pixel analysis of gold nanoparticles was developed to compare nanoparticle localization in different skin locations under different conditions. Based on penetration experiments, determinants that favor or limit particle penetration were determined as well as the barrier to penetration (intercellular lipids). Finally nanoparticle penetration was successfully enhanced using a chemical enhancement approach.

Results obtained are important to enhance our understanding of nanoparticle interaction with the skin barrier. Future studies are required to reduce the gap between research and applications.

Kurzzusammenfassung

Die Penetration von Nanopartikeln ist Gegenstand der aktuellen Forschung. Diese Frage ist von großer Bedeutung für die Anwendung im Bereich der Nanomedizin als auch für die Abschätzung des Risikopotenzials bei Kontakt mit solchen Systemen. Bis dato sind allerdings keine eindeutigen Aussagen möglich.

Das Ziel dieser Arbeit war daher die Untersuchung des Penetrationsverhaltens anhand von kolloidalem Gold (AuNP). Dieses Modellsystem erlaubt die Untersuchung der Penetration in Abhängigkeit von verschiedenen physikochemischen Eigenschaften der Partikel (oberflächenmodifiziert), als auch von Formulierungseigenschaften (Vehikel). Die AuNP erlauben eine Visualisierung mittels Multiphotonen Mikroskopie. Daher wurden die Auflösung und die optischen Parameter für AuNP in Haut bestimmt. Des Weiteren wurde ein Pixel-basiertes Verfahren ermittelt, das eine semiquantitative Analyse der penetrierten Objekte ermöglicht. Dies erlaubt eine Abschätzung der Partikelpenetration.

Penetrationsexperimente erlaubten die Parameter, die die Penetration beeinflussen, hinsichtlich Größe und Oberflächenpolarität einzuschränken. Außerdem konnte gezeigt werden, dass auch die Penetration von Nanopartikeln mit Hilfe von Penetrationsverbesserern gesteigert werden kann.

Die Ergebnisse dieser Arbeit sind wichtige Bausteine für das Verständnis der Interaktion von Nanopartikeln mit der Hautbarriere. Zukünftige Studien sind dennoch nötig, um die Lücke zwischen Forschung und möglicher Anwendung zu schließen.

1. Background and Literature Survey

The chapter is part of a review article in due publication:

Hagar I. Labouta and Marc Schneider, "Interaction of inorganic nanoparticles with the skin barrier: current status and critical review".

1.1. Introduction

Nanomaterials of approximately 1 – 100 nm size range show new functions and applications rather than bulk materials primarily because of their high surface to volume ratio. Additionally, unusual physical, chemical, and biological properties can emerge in materials at this nanoscale dimension. These properties may significantly differ from that of bulk materials and single atoms or molecules [1]. However, there is no guarantee that unique properties appear below such boundary, 100 nm [2]. In most cases, these unusual new properties are attributed to inorganic nanomaterials. Gold in the bulk state, for instance, is an excellent conductor of heat and electricity, but no heat transfer reaction occurs on directing light onto it. Gold nanoparticles (AuNP) can however absorb light and transfer it into heat acting like miniature thermal scalpels that can kill unwanted cells in the body, such as cancer cells [3]. Titanium dioxide and zinc oxide, used as sunscreen agents, have the disadvantage of being visible masking the skin with a white color. Titanium dioxide and zinc oxide nanoparticles are transparent and are thus preferred to microparticle counterparts in sunscreen products [4]. On the other hand, polymeric nanosystems usually acquire properties that are essentially an interpolation of that of the same material at the larger scale. It is also relatively easy to prepare inorganic nanoparticles in such size range rather than polymeric nanoparticles. Last but not least, inorganic nanoparticles have been recently the subject of several applications in nanomedicine and drug delivery. Fine-tuning the surface properties of inorganic nanoparticles by surface functionalization has further extended their applications [5]. Selected applications of some inorganic nanoparticles are highlighted in the next section and relevant review articles are cited for further more detailed readings.

1.1.1. Inorganic nanoparticles and their pharmaceutical and biomedical applications

Quantum dots (QD). QD are nanocrystals comprised of a semiconductor material, e.g. CdS. QD have attracted widespread interest in biology and medicine due to their unique electronic and optical properties over organic dyes and fluorescent proteins, e.g. size- and composition-tunable emission wavelength, improved signal to noise ratio, higher photostability, etc. Therefore, QD have rapidly emerged as a new class

of fluorescent probes for biomolecular and cellular imaging [6-7]. Surface functionalization of QD and bioconjugation to biomolecules via a covalent linkage was then adopted to enhance the dispersibility of QD, reduce toxicity and for better *in vivo* and cellular targeting. This has further allowed for the use of QD in medical diagnostics especially in cancer diagnosis [6-9]. Further development of QD might enable their application in tracking drug delivery, and monitoring the efficacy of therapeutics non-invasively in real time [7].

Silica nanoparticles. Another fascinating bioprobes are nanosized silica particles, which were also reported to be an ideal protein host because of their high chemical, physical and mechanical stability, large surface area, good dispersibility in aqueous solution and relative inertness. Silica nanoparticles have a high surface silanol concentration which facilitates a wide variety of surface reactions and the binding of biomolecules [10]. Therefore they attracted wide spread interest in applications in bioanalysis, and diagnosis especially in the diagnosis of cancer cells. Silica nanoparticles were also considered good candidates for drug and gene delivery [10-11].

Silver nanoparticles. Silver compounds are well-known for centuries as antimicrobial agents and are widely exploited in the treatment of bacterial infections encountered in burns, open wounds, and chronic ulcers [12]. Recently, however, silver nanoparticles showed higher antimicrobial efficiency compared to silver salts due to their extremely large surface area with diameters generally smaller than 100 nm containing 20-15000 silver atoms, providing better contact with microorganisms. Thus, on cellular or tissue exposure to silver nanoparticles, the active surface of silver nanoparticles would be large compared to silver compounds, and thereby exhibiting remarkably unusual physicochemical properties and biological activities [13-16]. They interact with bacteria and produce electronic effects, which enhance the reactivity of nanoparticles [16]. Thus, the bactericidal effect of silver nanoparticles was proved to be size [14] and shape [17] dependent due to different interactions with the microorganism. Several dressings for wound healing incorporating silver nanoparticles as a topical antibacterial agent have already found

their way to the market, e.g. Acticoat™ (Westaim Biomedical Inc., Fort Saskatchewan, Alberta, Canada) and Silverlon® (Argentum Medical, L.L.C., Lakemont, Georgia). They have the advantage of providing a more controlled and prolonged release of nanocrystalline silver to the wound area. This mode of silver delivery allows the dressings to be changed less frequent, thereby reducing the risk of nosocomial infection, cost of care, further tissue damage and definitely improves patient compliance [12].

Gold nanoparticles (AuNP). Applications of AuNP in biology and life sciences is a fast growing field. These bio-applications can be classified into four areas: labeling, delivery, hyperthermia, and sensing [18]. Similar to silver nanoparticles, AuNP have unique optical properties. They have the ability to resonantly scatter visible and near-infrared light upon the excitation of their surface plasmon oscillation. The scattering light intensity is sensitive to the size and shape of particles [19]. Therefore they were useful as biosensors and diagnostic agents, especially in cancer diagnosis [20-21]. AuNP hold promise as the future “magic bullet” for cancer treatment. Based on their physical properties, AuNP cause local heating when they are irradiated with light in the range of 800–1200 nm. El-Sayed group [22] has showed the potential use of AuNP in photothermal destruction of tumors. Recently, AuNP have emerged as a delivery system for various payloads [23-24] either drug molecules [25-27] or large biomolecules such as proteins [28], DNA [29-30] and RNA [31].

Magnetic nanoparticles. Nanoparticles with a magnetic core allow for the magnetic manipulation of the particles in presence of an external magnetic field. In this size range, below 100 nm, there is a fundamental change in the magnetic structure of ferro- and ferrimagnetic materials. Their superparamagnetic moment with high magnetic saturation value has resulted in exploring the use of magnetic nanoparticles as targeting agents in a number of applications including drug and gene delivery, in addition to tumor diagnostics and therapeutics. Another important therapeutic application is hyperthermia, which involves heating organs or tissues resulting in tumor cell necrosis [32-36]. Functionalization of magnetic nanoparticles has further extended their *in vivo* applications based on higher biocompatibility and

reduced toxicity, in addition to adopting additional targeting approach on coating the surface with biofunctional molecules and thus enhancing the targeting efficiency of the final developed system [35-36].

Titanium dioxide (TiO₂) and zinc oxide (ZnO) nanoparticles. TiO₂ and ZnO nanoparticles are currently used in many sunscreen formulations as UV filters to protect against UV-induced skin damage. TiO₂ and ZnO have the advantage over other chemical agents not to undergo any chemical decomposition on exposure to UV radiation. Moreover, they offer a wider range of protection against UVA and UVB types of radiation, compared to other organic compounds. Nowadays in the cosmetics industry, TiO₂ and ZnO are included as nanosized particles because in this form they are transparent and more esthetically acceptable to consumers [4, 37]. This is in addition to the size-dependent antibacterial activity of ZnO nanoparticles [38].

1.1.2. Significance and scope of the chapter

One could so far reach a conclusion that inorganic nanoparticles have found several applications, especially in cancer diagnosis and therapy and more recently in drug and gene delivery. This potential for applications has triggered the investigation of the nanoparticle interaction with the various biological barriers. An excellent biological barrier, the skin, has been addressed in several recent studies regarding nanoparticle penetration.

Skin is a unique barrier composed of several highly organized and heterogeneous layers that also includes a number of appendages such as hair follicles, sweat and sebaceous glands. Skin is composed of three layers from outwards moving deeper inside the skin: epidermis, dermis, and hypodermis. However, from a penetration perspective only epidermis and dermis are important. The outermost layer of the epidermis is the stratum corneum (SC), to which the main barrier function of the skin is attributed [39-40]. Nevertheless, topical and transdermal drug delivery systems has always been a main target of many researchers avoiding the numerous problems encountered with the oral route. Though the mechanism is still unclear,

nanoparticles were shown to enhance the skin penetration of several active agents [41-42].

Hence, studying the skin penetration of nanoparticles is crucial for the following reasons:

- Design of potential topical and transdermal nanocarriers and biomedical diagnostic agents.

Understanding the behavior of nanoparticles when coming in contact with the skin surface and their interaction with the different skin layers would ultimately lead to the design of the “ideal” carrier or diagnostic agent in terms of the physicochemical parameters of the nanoparticles, e.g. size, shape, surface chemistry, in addition to other factors, e.g. formulation and environmental factors, influencing skin penetration of nanoparticles.

- Health risk analysis.

The public could come in contact with nanomaterials intentionally on applying topical cosmetic preparations containing nanoparticles, or non-intentionally through the handling of several products used in our daily life and contain nanoparticles such as sport clothes, surface cleaning agents, computer devices, paints, etc. [16, 37]. Environmental exposure comprises water or even air contaminated with nanoparticles. This is in addition to the people handling nanoparticles in research and industry. In hospitals, physicians and patients may also come in contact with nanoparticles e.g. silver impregnated medical devices such as surgical masks and implantable devices [16]. The exposure occasions to nanoparticles are thus increasing constantly.

In this chapter, recent research on the interaction of inorganic nanoparticles with the skin barrier are discussed and analyzed in an attempt to answer still open questions; (1) How do inorganic nanoparticles, in the size range less than 100 nm, as well as sub-micron particles interact with the skin barrier? (2) Do they have the ability to penetrate the SC into the viable deeper skin layers (DSL)? And if so, (3) what is the possible mechanism of skin penetration? Finally, (4) what are the factors contributing to their penetration?

But first, it is important to define two important terms used in this chapter, “skin penetration” and “skin permeation”. The first indicates transport of an agent, here nanoparticles, across the SC into DSL. The latter however stands for transport across the whole skin into the receptor solution, (*in vitro*) or to the systemic circulation (*in vivo*) [43].

1.2. Current dilemma in the status of skin penetration of inorganic nanoparticles

Investigating the ability and the possible mechanism of particle penetration through skin is a recent area of research receiving great interest of researchers due to the aforementioned reasons. Starting from the year 2004 till now the number of studies focusing on skin penetration of inorganic particles is generally increasing. To the best of our knowledge, the total number of research papers in this field is 40 (excluding replicate studies common in skin penetration/permeation experiments and including the papers presented in this thesis), in which 125 different penetration/permeation experiments (different in particle type and size, skin type, skin treatment, etc.) were conducted. Yet, the ability of inorganic nanoparticles to overcome the barrier function of the SC into DSL is a point of debate among researchers. Different outcomes were reported for particle penetration as shown in Table 1.1. About 49% of all these experiments were reported to result in particle penetration with or without adopting a mechanical or a chemical enhancement approach or a combination thereof. Some of these studies, four studies, showed even particle permeation of the whole skin thickness either *in vitro* [44-45] or *in vivo* [44, 46-47]. The other 51% of these experiments however resulted in neither passive particle penetration nor particle penetration on physical or chemical skin treatment (discussed in section 1.4). Further analysis of the reported outcomes over the years 2008-2010, witnessing most of the conducted particle skin experiments, one could observe an increase in the frequency of research articles reporting particle penetration, increasing from ~ 38% in 2008 to ~ 67% in 2010, relative to the total number of research papers reported at that year. This could be due to implementing more and more approaches for enhancing skin penetration in addition to the improvements of the analytical techniques for detection of nanoparticles inside the

skin (discussed in section 1.7). Unfortunately, the feasibility to publish studies showing particle penetration, being more attractive to the research community could be also a contributing factor. Nevertheless, to further add to this dilemma, the size range of inorganic particles, regarded as the primary determinant of skin penetration, is overlapping for particles reported to penetrate the SC (4 nm to 1.5 μm) and particles that could not (4 nm to few microns).

Overall, the reported experimental set-ups regarding skin type, environmental and mechanical conditions, revealed a high diversity. This might be the basis of the current controversy among researchers on whether nanoparticles do or do not penetrate the SC into DSL, as highlighted in the following points:

- **Animal versus human skin.** Though excised human skin is regarded as the “gold standard” for *in vitro* skin penetration studies especially in human dermal risk assessment [48], it was only used in 51 % of the used experimental set-ups in particle penetration studies (35 % *in vitro* and 16 % *in vivo*). However, 47 % of these experiments were conducted on animal skin (pig, mouse and rat skin) *in vitro* (31 %) or *in vivo* (16 %) (Figure 1.1). This is apparently due to the limited availability of human skin driving most of the research laboratories to depend on animal skin. However, structural and morphological differences between human and animal skin especially in terms of the density of the hair follicles, SC and total skin thickness, the amount of skin lipids, in addition to variations among animal species could certainly result in different penetration behaviors [48-49]. Furthermore, only one study was conducted on an *in vitro* reconstructed human skin model using 7 nm QD [50]. However, no penetration was reported though these models are generally known to overestimate drug flux across human skin due to the lower barrier properties relative to human skin [48, 51].

All this makes it quite difficult to compare the data generated by different laboratories and reach a conclusion regarding the current status of skin penetration of inorganic nanoparticles.

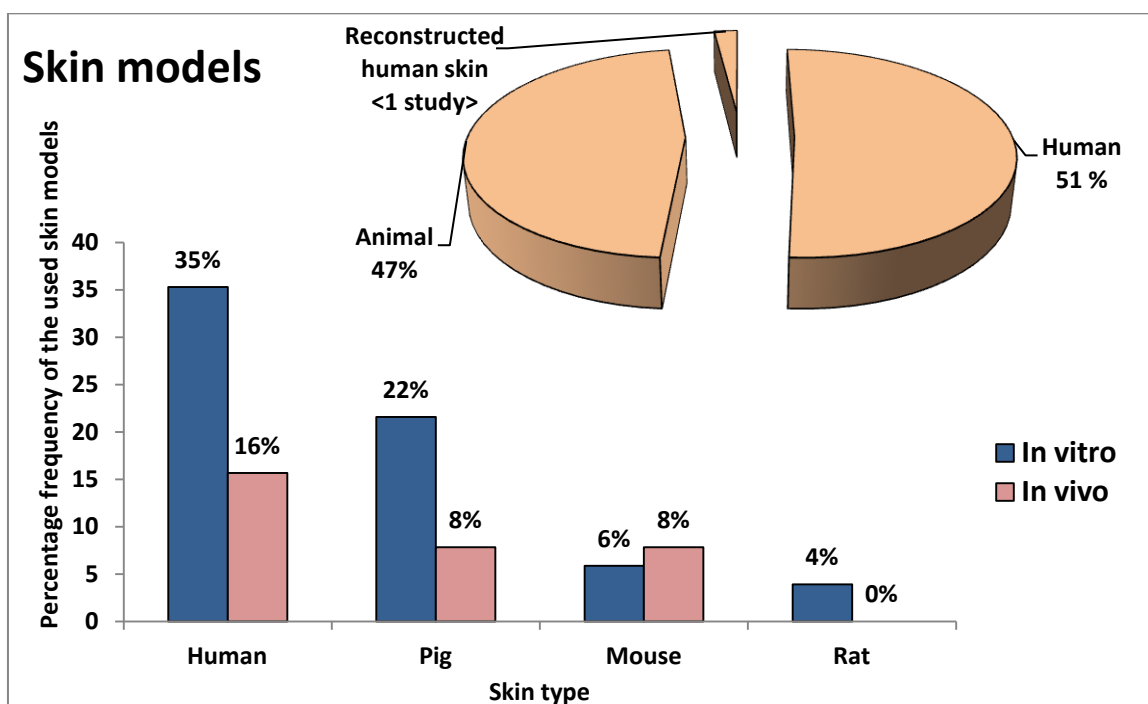


Figure 1.1: *In vitro* and *in vivo* skin penetration/permeation experiments in the literature classified according to the skin type: human, reconstructed human and animal (pig, mouse and rat) skin. Percentage frequency of using each of these skin models in examining nanoparticles penetration, either *in vitro* or *in vivo*, is indicated in the figure.

Table 1.1: Overview on the skin penetration studies of various inorganic particles applied to different skin types under different experimental conditions (including our research papers presented in this thesis).

Particle	Diameter, nm	Skin type (<i>in vitro/in vivo</i>)	Additional enhancement approach	Reported outcome	Ref
QD-COOH	4	Human (<i>in vitro</i>)	- Massage Tape-stripping Tape-stripping+Massage	No penetration No penetration No penetration Penetration	[52]
Fe ₂ O ₃ -TMAOH	4.9±1.3	"	-	Penetration	[53]
AuNP	10	"	- Dermaportation by pulsed electromagnetic field	No Penetration Penetration	[54]
AuNP-thiol ⁺ AuNP-lecithin ⁺ AuNP-cetrimide ⁺ AuNP-citrate	~6 ~6 ~15 ~15	"	- - - - CHCl ₃ /methanol Tape-stripping	Penetration Penetration Penetration No Penetration Penetration Penetration	[55- 56]
TiO ₂	10–50	Human (<i>in vivo</i>)	-	Penetration [†]	[57]
AuNP	~12.9	Human (<i>in vitro</i>)	- Dermabrasion	Penetration Penetration	[58]
AuNP	~15	"	- Urea Tween 80 SLS DMSO	No penetration No penetration Negligible penetration No penetration Penetration	[59]
ZnO	15–40	"	-	No penetration	[60]
TiO ₂	20	Human (<i>in vivo, in vitro</i>)	- -	No penetration No penetration	[61]
TiO ₂ TiO ₂ in sunscreens with and without ZnO	20	Human (<i>in vitro</i>)	-	No penetration	[62]
ZnO	20–30	Human (<i>in vitro, in vivo</i>)	-	No penetration	[63]
TiO ₂ ZnO	20–70 < 200	Human (<i>in vitro</i>)	- -	No penetration No penetration	[64]
AgNP	25±7.1	"	- Abrasion	Low penetration (both), but higher for damaged skin	[65- 66]
ZnO	30	"	-	No penetration	[67]
TiO ₂ (Hydrophobic) TiO ₂ (Amphiphilic) TiO ₂ (Hydrophilic)	20–100 nm aggregates	Human (<i>in vivo</i>)	- - -	No penetration No penetration No penetration	[68- 69]
TiO ₂ platelets ZnO platelets	not stated (nm range) 116.8 length, 57.5 width	Human (<i>in vitro</i>)	- -	No penetration No penetration	[70]
AuNP	not stated (nm range)	"	Electrophoresis	No penetration	[71]

Background and Literature Survey

Particle	Diameter, nm	Skin type (<i>in vitro/in vivo</i>)	Additional enhancement approach	Reported outcome	Ref
TiO ₂	not stated (nm range)	Human(<i>in vivo</i> , healthy) Human(<i>in vivo</i> , psoriatic)	- -	No penetration No penetration	[72]
QD-PEG, QD-PEG-amine & QD-COOH	12.65–29.35 nm (at different pH values)	Human (<i>in vitro</i>)	- Tape-stripping	Penetration of only QD-PEG at pH8.3 Penetration	[73]
QD-PEG-amine	7±2	Reconstructed human skin	-	No penetration	[50]
AuNP	4.6±1.5	Porcine-full thickness(<i>in vitro</i>) Porcine-dermatomed(<i>in vitro</i>)	Ultrasound & SLS Ultrasound & SLS	Penetration Penetration	[74]
QD-PEG, QD-PEG-amine & QD-COOH	15–45 (spherical & ellipsoid)	Porcine (<i>in vitro</i>)	-	Penetration	[75]
Polymer coated QD	20	"	Ultrasound with or without SLS	Penetration (further increased with SLS)	[76]
AgNP-uncoated AgNP -carbon coated	20, 50 & 80 25 & 35	Porcine (<i>In vivo</i>)	-	No penetration	[77]
TiO ₂ with different coatings	35uncoat.,35coat., 10x100,250 [†]	Porcine (<i>in vitro</i>)	- Tape-stripping Hair removal	No penetration No Penetration Penetration for 35coat.	[78]
PEG-coated QD	Nail shaped: 5.78 width & 8.4 length 39±1 hydrodynamic diameter	Porcine-dermatomed (<i>in vitro</i>)	-	No penetration	[79]
TiO ₂ (four formulations)	45-150 length, 17-35 width (lanceolate shape)	Porcine (<i>in vitro</i>)	-	Penetration	[80]
ZnO TiO ₂ Agglomerates	80 up to 200	"	-	No penetration	[81]
Au particles	900±600	"	Ballistic delivery	Penetration	[82]
TiO ₂ (uncoated sub- micron sized, uncoated nano- or Al(OH) ₃ , dimethicone/methico ne copolymer- coated nano-sized	207±53 [§] , 30±8 [§] & Fibrils of 57±18 length & 15±5 width [§]	Porcine (<i>in vivo</i>)	-	No penetration	[83]
QD-COOH	4.1	Mouse (<i>in vitro</i> & <i>in vivo</i>)	-	Permeation	[44]
Fe ₂ O ₃	4.6–10	Mouse (<i>in vitro</i>)	Blade incision, 1 µm width	Penetration	[84]
ZnO	10	"	- OA, EtOH & OA-EtOH	No penetration Penetration	[85]
AuNP	11.6	Mouse (<i>in vivo</i>)	-	Penetration	[86]
QD-COOH	~20 & ~33 [87]/ ~12-20 [88]	"	- UV exposure	Low penetration for both but higher on UV exposure	[87- 88]

Background and Literature Survey

Particle	Diameter, nm	Skin type (<i>in vitro/in vivo</i>)	Additional enhancement approach	Reported outcome	Ref
QD-PEG	37	"	- Acetone pretreated Tape-stripped Dermabraded	No penetration No penetration No penetration Permeation	[47]
Diphtheria toxoid-QD-COOH conjugate	Size not stated (nm range) (nail-shaped)	"	Hyperthermea	Penetration [†]	[89]
QD-COOH	6±2	Rat (<i>in vitro</i>)	- Flexion Tape-stripping Abrasion	No penetration No penetration No penetration Penetration	[90]
AuNP	15, 102, 198	"	-	Permeation	[45]
TiO ₂	4,10,21,25,60,90 4,60 10,21,25,60	Porcine (<i>in vitro</i> -1 day) Porcine (<i>in vivo</i> -30days) Mouse (<i>in vivo</i> -60 days) [#]	- - -	No penetration Penetration Permeation	[46]
TiO ₂	Width: 20, length 100	Human (<i>in vitro</i>) Porcine (<i>in vitro</i>)	-	No penetration	[91]
TiO ₂	20–100	Porcine (<i>in vitro</i>) human skin grafted on SCID mouse (<i>in vivo</i>)	- -	No penetration No penetration	[92]
TiO ₂	Size not stated (commercial formulation)	Human foreskin grafted on SCID mouse (<i>in vivo</i>)	-	No penetration	[93]

* Dispersed in toluene. † Non-statistically significant higher Ti levels in the deeper layers versus background levels of Ti normally present in the skin (non-exposed control). ‡ These reported sizes (35 nm (uncoated and coated particles), 10x100 and 250 nm) are the primary sizes, however aggregation was reported for these nanodispersions. § These sizes are not the primary size diameters but are those determined by TEM of the particles in skin after application. ¶ No proof for penetration was provided by the authors (only fluorescent images without depth information). # Different pathological lesions were observed in several organs especially the skin and liver. AgNP: silver nanoparticles, AuNP: gold nanoparticles, DMSO: dimethyl sulphoxide, DOTAP: 1,2-dioleoyl-3-trimethylammonium propane chloride (cationic surfactant), EtOH: ethanol, Fe₂O₃: iron oxide nanoparticles, OA: oleic acid, QD: quantum dots, SCID: severe combined immune deficient, SLS: sodium lauryl sulphate, TGA: thioglycolic acid, TiO₂: titanium dioxide nanoparticles, TMAOH: tetramethylammonium hydroxide, VE: viable epidermis and ZnO: zinc oxide nanoparticles.

“Skin penetration” indicates transport of nanoparticles, across the SC (stratum corneum) into the DSL (deeper skin layers). “skin permeation” stands for transport across the whole skin thickness into the receptor solution, *in vitro* or to the systemic circulation, for *in vivo* experiments.

- Among the different animal species, there are hairy animals used for conducting particle penetration experiments. Therefore, **hair removal** is often indicated to be able to apply a formulation. Removal of hair by means of a clipper, cosmetic grade hair removal cream or even by shaving before the penetration experiment possibly has an effect on the barrier function of the used skin. Consequently, particle penetration might also be affected. For instance, 11.6 nm AuNP could penetrate into mouse skin *in vivo* after hair was clipped [86]. On the other hand, no penetration was reported for QD having nearly the same size, ~ 12 nm, through hairless mouse skin *in vivo* [88]. Recently, Senzui *et al.* [78] have shown the effect of hair removal on penetration of TiO₂ nanoparticles through pig skin. Particles were shown not to penetrate through intact or stripped skin, however penetration was observed on hair removal possibly by entering empty hair follicles. Therefore, hair removal should be taken into consideration especially when assessing the safety of nanoparticles. This also implies that the dermatomed skin of thickness 200-400 µm recommended by the OECD (Organization for Economic Co-operation and Development) according to the guideline 428 for *in vitro* testing of skin absorption [94] could possibly overestimate the skin penetration/permeation of nanoparticles. Overestimation is especially the case for particles likely to accumulate in the hair follicles, because the hair follicle is cut on splitting the dermis and the nanoparticles can then diffuse into the dermis/receptor solution [78].
- **Skin exposure time** to particles also differed greatly among previous studies. Penetration of particles were tracked over a period of as short as a few hours, e.g. 1 hour [71], 3 hours [86] up to several days (60 days) [46]. However, unlike monitoring penetration of drug molecules especially lipophilic molecules, it is usually not practically feasible to generate appropriate pharmacokinetic parameters for particles, including the flux for normalizing the effect of exposure time, due to absence or a scarce concentration of particles penetrating into the skin. This further limits the ability to analyze data based on different studies raising an analytical problem in determination of the amount of nanoparticles present in the skin in typical penetration-permeation experiments. This will be discussed in detail later in section 1.7.

- The **application dose** and **volume** and the **diffusion area** are important factors that would significantly affect the results of any penetration experiment.
- Different **skin treatment approaches**, physical or chemical, were adopted for inducing or enhancing skin penetration of nanoparticles. This would rather limit the ability of a study-with-study comparison which will be discussed in detail in Section 1.4. This is in addition to other factors such as formulation factors, e.g. surface coatings, vehicle, etc. which differ greatly from one study to another. These factors were shown as important determinants of particle penetration as detailed in the next section.

1.3. Factors affecting skin penetration

In addition to the aforementioned experimental variations among different studies, there are several factors which were systematically studied and found to contribute significantly in the skin penetration of nanoparticles. Critical determinants of skin penetration of nanoparticles could be categorized into physicochemical attributes of the nanoparticles (size, surface charge and surface chemistry), formulation factors (vehicle) and experimental factors (concentration and skin exposure time to nanoparticles).

1.3.1. Physicochemical attributes of the nanoparticles and formulation factors

The physicochemical attributes of nanoparticles and the nature of the dispersing vehicle are key factors governing their skin penetration. Sonavane *et al.* [45] showed size-dependent skin permeation of AuNP through rat skin. Higher permeation for 15 nm AuNP compared to 102 nm and 198 nm AuNP was described through rat skin and the permeability coefficient was reported to decrease on increasing the particle size.

The effect of particle surface charge and shape on penetration through skin was the focus of a study by Ryman-Rasmussen *et al.* [75]. They studied the effect of different surface charge imparting coatings (cationic, anionic and neutral) on the skin penetration of two types of QD of different size and shape, spherical QD of 4.6 nm

core/shell diameter and ellipsoid QD 12 nm (major axis) by 6 nm (minor axis) core/shell diameter. Following skin exposure, confocal examination of longitudinal skin sections showed penetration of the spherical nanoparticles into the viable epidermis and dermis after only 8 h regardless of the surface charge. Similar behavior was reported for cationic and neutral ellipsoid nanoparticles. However, 24 h of contact of the anionic ellipsoid QD with the skin surface was required for their penetration into DSL. Based on these findings, the authors concluded a shape dependency for particle penetration, especially due to the fact that the two anionic spherical and ellipsoid QD had a more or less similar hydrodynamic diameter, 14 and 18 nm, respectively. Faster skin penetration for cationic and non-ionic ellipsoid QD relative to anionic ellipsoid QD could be attributed to the negative surface charge of the pig skin used in the latter study; isoelectric point of pig skin is ~ 4.4 [95].

1.3.2. Experimental factors

Concentration of the applied nanodispersion and skin exposure time could greatly influence the skin penetration of nanoparticles. For instance, Baroli *et al.* [53] studied the penetration of magnetic nanoparticles through human skin after 3, 6, 12 and 24 h, where particle penetration was reported starting from 6 h skin exposure time.

Though more studies are still required at the basic level to advance our understanding and to gain a deeper insight into the mechanism and determinants of skin penetration of nanoparticles, several approaches have been adopted by researchers in an attempt to enhance skin penetration of inorganic nanoparticles via breaching the barrier function of the skin. These approaches, however, did not always assure an increase or even occurrence of skin penetration of particles.

1.4. Approaches adopted to enhance skin penetration of inorganic nanoparticles

There is no study systemically investigating the possibilities of enhancement of particle penetration. Some approaches were however adopted to enhance skin penetration of inorganic nanoparticles. Most of these approaches were physical methods. Yet, the use of chemical enhancers was also explored.

1.4.1. Physical/mechanical enhancement

UV-exposure. UV radiation is known to have a deleterious effect on the skin barrier function by causing biophysical and morphological changes of the SC lipids [96]. As mentioned earlier, inorganic nanoparticles, titanium dioxide and zinc oxide nanoparticles, are currently used in sunscreen formulations [4]. Therefore studying particle penetration into the skin was of utmost importance for these applied particles [87-88].

Increased penetration of QD, by the effect of UV radiation, as a model particle, by the effect of UV radiation, was observed through damaged skin, by the effect of UV radiation compared to intact mouse skin [87-88]. Though in both cases, low levels of penetration were qualitatively detected. However, according to the authors, penetration was mostly detected in areas with defects in the SC or around hair follicles, referring to this as another possible mechanism for the transport of particles in addition to the SC intercellular weakening effect of UV radiation. These results should raise the public concern regarding the use of nanoparticle-based formulations intended for topical use. However, one should also consider the effect of the surface properties on skin penetration of the applied particles when extrapolating these results to commercial sunscreens containing titanium dioxide and zinc oxide nanoparticles.

Hyperthermia. Upadhyay [89] explored the application of mild local hyperthermia for transdermal delivery of diphtheria toxoid (DT) vaccine. DT-conjugated to QD were applied to mice *in vivo* with concomitant application of pads for local hyperthermia. According to the author, this has led to skin transport of the QD-labeled vaccine. However, it should be noted here that the evidence the author provided for skin penetration was based on top-view fluorescence images of QD in skin specimens with no depth information. However, the unlabeled vaccine was found to induce an immune response when applied topically to mice as effective as intramuscular injection of the vaccine. Nevertheless, care should be taken construing the results of this study with respect to particle penetration.

Iontophoresis. Iontophoresis provides a mechanism to enhance the penetration of hydrophilic and charged molecules across the skin by application of constant current [97]. Similarly, a transdermal delivery chip system was used to deliver

negatively charged citrate-stabilized AuNP across human skin [71]. At zero voltage, AuNP were localized on the surface of the SC. On application of 6 V, AuNP were shown to pass through the intercellular routes of the SC. Further transport to the DSL was not shown. The results obtained from this particular study however are quite questionable as the experimental set-up was not fully explained in terms of the particle size, surface charge, concentration and volume of the applied dispersion.

Dermaportation. Dermaportation is a novel transdermal drug delivery technology that uses pulsed electromagnetic fields to enhance the transport across the skin. A preliminary experiment by Krishnan *et al.* [54] showed enhanced penetration of 10 nm AuNP into epidermal human skin sheets. A potential mechanism proposed by the authors for enhanced transport is the formation of transient pores through which particles can diffuse more easily.

Sonophoresis. Sonophoresis, defined as the application of ultrasound, particularly at low frequency (20-100 kHz) has been shown to greatly enhance the skin permeability of a variety of drugs [98]. Based on this, low frequency sonophoresis was also applied for enhancing the skin penetration of 20 nm QD [76]. Application of ultrasound on porcine skin increased the frequency of the formation of scattered and separated lacunar spaces in the SC which are assumed to eventually lead to higher connectivity of these voids and formation of porous networks within the SC. This has induced significant transport of QD through the lipid regions of the SC into the viable tissue. However, QD were also found in few occasions in the corneodesmosomes and even occasionally inside the corneocytes [76]. Simultaneous application of this technique and sodium lauryl sulphate induced similar but more pronounced effect on the SC ultrastructure and consequently higher QD penetration. The same combined approach was recently exploited by Seto *et al.* [74] to enhance the skin penetration of smaller particles, ~ 4.6 nm AuNP, through porcine skin.

Tape-stripping and dermabrasion. In view of the fact that the skin barrier function resides primarily in the SC, its total or partial removal by tape-stripping or dermabrasion can disrupt the skin barrier enhancing transport across the skin. Tape-stripping has been commonly used to enhance drug delivery across the skin, and to obtain information about the SC function. Moreover, tape-stripping has been proposed by the FDA as a part of the standard method to evaluate the

bioequivalence of topical dermatological dosage forms [99-100]. However, tape-stripping of the SC prior to application of inorganic nanoparticles did not always lead to satisfactory results. For instance, ~ 4 nm [52], 6 nm [90] and ~ 37 nm [47] QD could not penetrate tape-stripped human (20 tape-strips), rat (10 tape-strips) and mouse (5-20 tape-strips) skin, respectively. Abrasion is another technique which involves the removal or disruption of the upper skin layers to facilitate the skin permeation of several drugs [101-103]. Dermabrasion is often used in clinical practice by dermatologists as a facial resurfacing technique in the treatment of acne, scars, hyperpigmentation, and other skin blemishes [101]. Based on this, the effect of abrasion on skin penetration of rigid inorganic nanoparticles was examined. Dermabrasion of excised rat skin [90] and mouse (*in vivo*) [47] resulted in skin penetration and permeation of 6 nm and 37 nm QD, respectively, whereas no penetration was reported through intact skin in these studies.

Skin flexion and massage. The impact of mechanical stress on the barrier function of the skin with regard to skin penetration of inorganic nanoparticles was further examined via flexion and massage. Skin flexion is a method that simulates flexing movements such as repetitive wrist bending. Zhang and Monteiro-Riviere [90] studied the effect of mechanical flexion on skin penetration of ~ 6 nm QD. However, no penetration was reported after flexing the skin on an automated apparatus for 60 min. More clinically acceptable manual approach, massaging, for short time (5-10 min) was later explored by Gratieri *et al.* [52] to drive QD to penetrate into the DSL of human skin. However, QD could be found in the DSL only after massaging of tape-stripped skin for 10 min.

Ballistic bombardment. Ballistic bombardment of particles, a needle free technique of targeting cells within defined layers of the viable epidermis, was used by Kendall *et al.* [82]. A hand-held supersonic device was used to impact porcine skin at high rate with sub-micron gold particles, 900 ± 600 nm, resulting expectedly in skin penetration. Environmental relative humidity and temperature were shown to affect particle penetration using this method.

1.4.2. Chemical enhancement

Chemical permeation enhancers are defined as agents that promote drug diffusion through the SC and the epidermis. These agents have been extensively studied and used as enhancers in favoring transdermal drug permeation. They work mainly by temporarily reducing the barrier function of the SC allowing for more drug transport [104]. Few studies however focused on the use of these enhancers for skin delivery of inorganic nanoparticles. Kuo *et al.* [85] studied the effect of chemical enhancers, oleic acid and ethanol, on the penetration of ~ 10 nm zinc oxide nanoparticles through mouse skin. They showed enhanced transport values for nanoparticles in presence of oleic acid, ethanol and oleic acid-ethanol mixture. Gopee *et al.* [47] have also pretreated mouse skin with acetone, however no penetration of QD was observed.

As a conclusion so far, many studies have focused on treating the skin physically or chemically for enhancing the skin penetration of inorganic nanoparticles based on the previous knowledge and understanding of transdermal drug delivery. However, some of these have shown contradictory results on using the same enhancing approach. In other cases, non-satisfactory results were obtained. This could be again attributed to the different experimental set-ups used in different studies. Nevertheless, the basic knowledge on the potential mechanism is still somehow missing or at least not yet clear.

1.5. Mechanism of skin penetration

The exact contribution of the relevant parameters for potential skin penetration of inorganic nanoparticles is still unknown. Studying the skin architecture could provide a possible explanation for the skin penetration of nanoparticles (Figure 1.2). The intercellular lipids in the SC arrange themselves in a head-to-head and a tail-to-tail manner. The lipophilic pores formed by tail-to-tail configuration of the lipids are estimated to be approximately ≤ 6.94 nm. The aqueous pores, hydrophilic regions delimited by lipid heads, have been estimated to have a diameter of 2.8 ± 1.3 nm [105]. However, it has been suggested that the skin may contain different types of aqueous pores, whose dimensions of superficial openings (0.4–36 nm) may not be

maintained in the internal channel [105]. Though the aqueous pores provide a possible route for penetration of hydrophilic penetrants, the penetration of water and polar molecules is reported to be poor [106]. Based on this, one could question whether the penetration of inorganic nanoparticles is dependent on these pores. Nevertheless, from an exclusively dimension point of view, agents of size $< 5\text{-}7$ nm or 36 nm can penetrate SC through lipidic intercellular route or aqueous pores, respectively. Even larger agents may enter the skin appendages, hair follicles and pilosebaceous pores ($10 - 70 \mu\text{m}$) or sweat gland pores ($60 - 80 \mu\text{m}$) but still have to penetrate the respective tissue [105].

In a study by Zhang *et al.* [79], TEM examination showed the localization of most PEG-coated QD in the intercellular lipids of the outermost SC layers, thereby concluding that nanoparticles penetrate the skin via the intercellular pathway. They suggested theoretically that since the outer PEG coating is a soft coating, it thereby allows the particles to squeeze through the intercellular spaces. In contrast, Lee *et al.* [84], showed that on application of iron oxide nanoparticles ($4.6\text{-}10$ nm) on skin after superficial skin incision, $1 \mu\text{m}$ width, particles were found to distribute in both the intercellular and intracellular spaces of the SC and viable epidermis near the area of incision, but only in the intracellular spaces of the viable epidermis at longer distances.

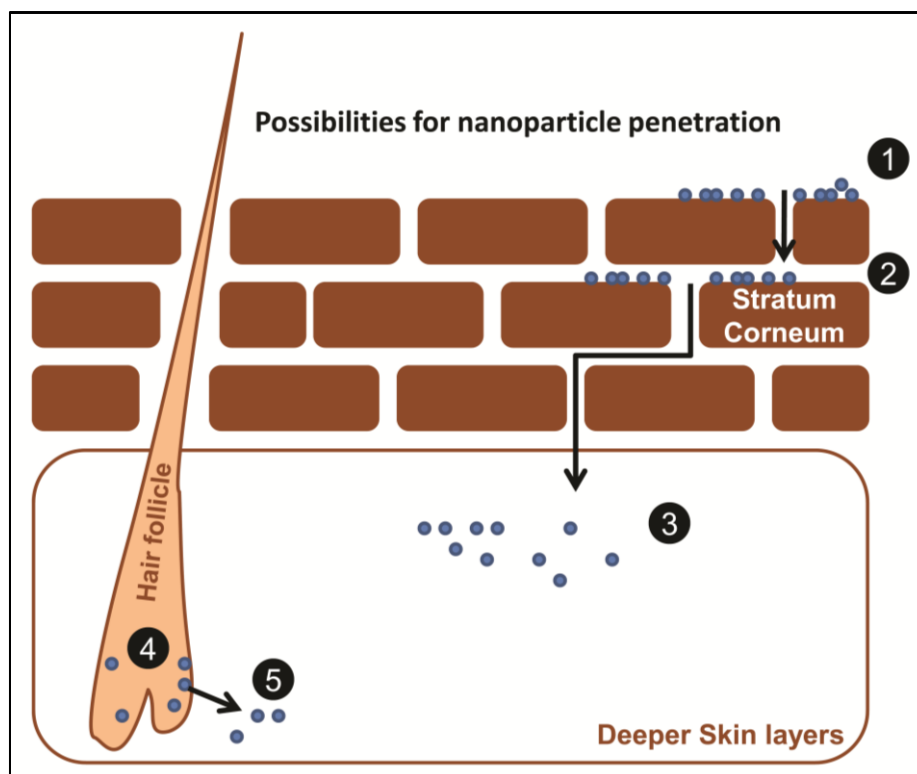


Figure 1.2: A sketch showing possibilities for nanoparticle penetration and localization in the skin barrier. Nanoparticles could penetrate the skin through intercellular pathways and localize in the stratum corneum or even permeate the whole stratum corneum into deeper skin layers. On the other hand, hair follicles could be a depot for particles that could further penetrate into the deeper skin layers.

Finally, the follicular pathway is also a possible mechanism for skin penetration of inorganic nanoparticles, however the skin appendages occupy only a small fraction (about 1/1000) of the entire skin surface [107]. It has been hypothesized by Lademann *et al.* [108] that the hair and the hair follicle might act as a pumping system pushing the nanoparticles into the hair follicles when the hair is moving (*in vivo*). Hair movement could be simulated *in vitro* by massaging excised skin. Based on this, medium-sized nanoparticles (approximately 400-700 nm) could diffuse deeper into the porcine hair follicles rather than smaller or larger particles allowing for selective follicular targeting by size modification [108-109]. Lekki *et al.* [91] have studied the possible role of the follicular pathway on the percutaneous uptake of TiO₂ nanoparticles of 20 nm width and 100 nm length. Though particles were observed as deep as ~400 nm inside the hair follicle, no particles were observed in the surrounding viable tissue. Overall, nanoparticle penetration into the appendages is apparently not sufficient for increased skin penetration.

Away from the exact mechanism of skin penetration of inorganic nanoparticles, it is important to know whether nanoparticles potentially penetrate the skin only due to the “nano” effect, i.e. passive penetration or under the influence of other factors.

1.6. Penetration of inorganic nanoparticles through human skin: Dissecting the “nano” effect

Whether particle penetration is studied for risk assessment or drug delivery purposes, the basic knowledge about the underlying mechanisms is an essential aspect. For nanoparticles, the size is the most prominent parameter. Hence the contribution and importance of the particle size was always in focus facing several difficulties.

Following *in vivo* studies on human volunteers (difficult to perform), excised human skin is regarded as the “gold standard” for *in vitro* skin penetration studies especially in human dermal risk assessment [48]. Therefore, careful analysis of the reported data using either human skin *in vivo* was done in an attempt to reach to a conclusion on the feasibility of skin penetration of nanoparticles in real-case scenarios. To our knowledge, there are 22 different studies investigating skin penetration of inorganic nanoparticles through human skin (including the studies presented in the thesis). Of these studies, 14 studies reported no particle penetration into the DSL using either *in vitro* [60-64, 67, 70, 72, 91-92] or *in vivo* [61, 63, 68, 71-72] human skin, as well as human skin grafted in severe combined immune deficient mice [92-93]. In three other studies, skin penetration was only induced by skin treatment, such as massage of tape-stripped skin [52], dermaportation using pulsed electromagnetic field [54] or by the use of chemical penetration enhancers [59]. For the other remaining studies, the skin was not treated physically or chemically prior to or concomitant with the application of the particulate formulations. However, the applied nanodispersion included some ingredients used in the synthesis of nanoparticles that could have an effect on the skin integrity, hence favoring particle penetration. For instance, some particles were coated with trimethylammonium hydroxide (skin corrosive) [53], docusate sodium (anionic surfactant) [53] or dispersed in absolute alcohol, 99% [65-66]. Even if the amounts used do not allow the skin penetration of nanoparticles, this should be regarded as a contributing factor. As a conclusion, it is very difficult to

dissect the single effect of bringing inorganic materials to the nano-range on their behavior with the skin barrier. This is presumably due to interplay of multivariate factors including the physicochemical attributes of the nanoparticles as well as the formulation, environmental and mechanical factors. The challenge would be to have a system which is tunable in size in the respective range of interest providing the same chemistry and hence the same properties regarding dispersibility and skin interaction.

1.7. Qualitative and quantitative analysis of inorganic nanoparticles in the skin

The rapid development of sensitive analytical techniques in the past decades has enabled researchers to monitor and accurately quantitate the amount of drugs present in the skin after penetration/permeation experiments and study the factors which either hinder or enhance their penetration. Among these techniques, HPLC provides a convenient method with a suitable limit of detection for accurate drug quantitation. On the other hand, quantitation of nanoparticles often represents a great analytical challenge; the scarce concentration of nanoparticles able to penetrate the skin with regard to the detection limit as well as the integrity of the particulate nature limits the available techniques or requires combination of at least two approaches of the available techniques. Table 1.2 lists the currently employed techniques with some examples from literature.

As shown from Table 1.2, so far monitoring skin penetration of nanoparticles is mostly based on qualitative microscopical visualization. This includes histology, SEM and TEM, fluorescence microscopy, confocal and multiphoton microscopy. Of all these methods, development of both confocal and multiphoton laser scanning microscopy was considered a great addition to the field allowing obtaining 3D information of the distribution of nanoparticles in different skin layers via optical sectioning. This would rather avoid artifacts due to mechanical sectioning and sample preparation. However, this is limited by the loss of laser power and the loss of resolution with depth inside the skin tissue [110-111].

Further attempts were made with the aim of establishing a quantitative approach which would allow for a better understanding of skin penetration of nanoparticles and provide a sound scientific basis for diverse biomedical applications and health risk assessment. This involves adopting quantitative analytical methods such as inductively-coupled plasma optical emission spectroscopy, inductively-coupled plasma mass spectroscopy and atomic absorption spectroscopy. However, these techniques suffer the disadvantage of not detecting the particles themselves but their elemental composition. This would raise doubts whether these analyzed atoms or ions originate from the nanoparticles themselves or from raw salts or chemical ingredients used in particle synthesis. This is in addition to possible interference with trace elements in biological materials, skin, such as zinc. Other approaches involved intensity measurement of fluorescence [89] and confocal [52] images or even manual counting of the number of fluorescent spots per field in confocal images [112].

This leads us to a side-question: what would be a good model for studying skin penetration of nanoparticles? From the analytical perspective, away from the clinical significance (mentioned earlier), inorganic nanoparticles especially quantum dots, gold and silver nanoparticles could be better tracked inside the skin rather than polymeric ones. This represents a further reason why most of the studies concerned with skin penetration of nanoparticles were conducted using inorganic particles rather polymeric ones. Other technical reason for that is the relative ease to prepare inorganic nanoparticles with respect to polymeric nanoparticles with a size smaller than 100 nm down to around 4 nm.

Table 1.2: Analytical methods used for monitoring particle penetration in the skin barrier.

Analytical method	Examples from literature	Comments
Microscopical visualization		
Light microscopy of stained skin samples	[82, 86]	Advantage: easy technique. Disadvantage: artifacts on staining and mechanical sectioning.

Background and Literature Survey

SEM	[53, 63, 78]	<p>Advantage: high resolution.</p> <p>Disadvantage: artifacts on mechanical sectioning.</p>
TEM	[45, 71, 76-77, 83-84, 87, 92]	<p>Advantage: high resolution for electron dense materials.</p> <p>Disadvantage: artifacts on mechanical sectioning.</p>
Fluorescence microscopy	[88-89]	<p>Advantage: higher selectivity, availability.</p> <p>Disadvantage: no depth information.</p>
Confocal laser scanning microscopy	[47, 52, 75-76, 87]	<p>Advantage: optical sectioning.</p> <p>Disadvantage: loss of laser power with depth in the skin specimen, expensive.</p>
Multiphoton laser scanning microscopy	[63, 85]	<p>Advantages: intrinsic optical sectioning, less scattering by the tissues and less phototoxicity than confocal.</p> <p>Disadvantage: loss of laser power with depth in the skin specimen, expensive.</p>
MPM-FLIM	[54, 67]	<p>Advantages: capability of studying the effect of nanoparticles on skin metabolism by measuring autofluorescence of the endogenous fluorophores without the need of extrinsic labels.</p> <p>Disadvantage: loss of laser power with depth in the skin specimen, more expensive.</p>
Nuclear imaging	[62, 113] [91]: Ion microscopy and autoradiography	<p>such as particle-induced X-ray emission, scanning transmission ion microscopy and Rutherford backscattering.</p> <p>Disadvantages: determination of the elemental composition of the particles, not the particle themselves thus an interference possibility.</p>

Other analytical techniques		
ICP-optical emission spectrometry	[44, 53]	Advantage: quantitative techniques. Disadvantage: determination of the elemental composition of the particles, not the particle themselves thus an interference possibility.
ICP-MS	[47, 60, 74, 78, 83]	
Atomic absorption spectroscopy	[46, 65-66, 81]	

1.8. Standpoint and recommendations for future directions

Applications of inorganic nanoparticles in pharmaceutical and biomedical fields have been established and are increasing progressively. Yet, their behavior with the skin barrier is still in question with several contradicting results reported in literature. In an attempt to solve this dilemma some points should be taken into consideration as recommendations for future investigations:

- Human skin should be used as the first choice “gold” standard skin model for *in vitro* penetration experiments. In parallel, more studies should be conducted on finding a correlation between *in vitro* and *in vivo* animal experiments and human studies with regard to penetration for several particles of different physicochemical parameters. This would allow better prediction of *in vitro* absorption when using these validated animal models.
- At the level of the experimental set-up, development of a more or less “universal” model with technical guidelines for testing skin penetration/permeation of nanoparticles is required. This also involves incubation times and concentration which are critical for sufficient and detectable penetration.
- Both the experimental conditions and the characteristics of the nanoparticles should be fully described; publications with missing information such as size were occasionally published.
- Formulation ingredients should be always addressed when discussing the results of the penetration/permeation experiments. Similarly, skin preparation prior to the experiment, such as shaving of the hair, should be considered as

critical parameter influencing the barrier function of the skin model and thus the results of the penetration/permeation experiment.

- Last but not least, data obtained should be well-presented to allow the reader to extract the same conclusion made by the authors. For instance, Upadhyay, P. [89] has reported penetration of diphtheria toxoid-QD conjugate through mouse skin *in vivo* using local thermia. However, only images captured by conventional fluorescence microscope were presented with no depth information. As another example, the FLIM-multiphoton images shown by Krishnan *et al.* [54] for AuNP in human epidermis are also somehow unclear. It is not stated by the authors whether these images do show depth information of AuNP in the SC and the underlying viable epidermal layers or not. This would unfortunately leave the reader in a state of uncertainty of the reported results.

Nevertheless, investigation of the skin penetration of nanoparticles, especially inorganic nanoparticles, for the aim of designing ideal transdermal carriers or for health risk analysis, is a very recent area of research that holds great promise especially on development of new analytical approaches and higher sensitivity techniques which allow tracking and quantitation of minute concentration of nanoparticles present in the skin. A further challenge facing future studies, however, could be the ability to dissect the “nano” effect on nanoparticle penetration through the skin barrier, since the resultant penetration indicated in several studies was not exclusively due to bringing the material into the nano-size range, but also due to other concomitant formulation and environmental factors, in addition to the barrier state of the skin.

2. Aim of the Thesis and Experimental Design

From the literature survey and the introductory part of the thesis, it can be concluded that studying nanoparticle interaction with the skin barrier is a topic of major importance that still needs further research efforts. This is on the level of basic research, as well as in the aim of designing potential topical and transdermal nanocarriers and biomedical diagnostic agents, in addition to health risk analysis. The main focus of the present thesis was to investigate the potential penetration of nanoparticles, using model gold nanoparticles, through human skin and studying the effect of the physicochemical properties of nanoparticles, namely size and surface properties, other formulation factors such as the vehicle of the nanodispersion, skin barrier conditions, etc., on their skin interaction.

- Excised human skin was the selected skin model for penetration experiments, being regarded as the “gold standard” for *in vitro* penetration experiments related to human dermal risk assessment [48].

- Gold nanoparticles (AuNP) were chosen as a good model for our study for the following reasons:
 - ✓ They have unique optical properties. They show distinctive extinction bands in the visible region, due to surface plasmon oscillation of free electrons [114]. This allows for visible, as well as spectrophotometric detection of particle aggregation. This is in addition to feasibility of detection in human skin on non-linear photon excitation.
 - ✓ They can be tailored in terms of size and surface chemistry offering a flexible system for studying the effect of physicochemical properties of nanoparticles on skin penetration.
 - ✓ Besides, AuNP have recently emerged as a delivery system of various payloads [23-24]. The payload could be a drug molecule [25-27] or a large biomolecule, such as protein [28], DNA [29-30], or RNA [31].
 - ✓ In addition, their physical properties could be exploited for clinical applications. AuNP cause local heating when they are irradiated with light in the range of 800-1200 nm. El-Sayed *et al.* [22] have showed the potential use of AuNP in photothermal destruction of tumors.

In summary, it was hypothesized that AuNP could serve as a good model for nanoparticle penetration of high pharmaceutical and clinical significance.

Penetration of AuNP through human skin was previously induced or enhanced by dermaportation using pulsed electromagnetic field [54] and dermabrasion [58]. Seto *et al.* [74] investigated the simultaneous application of ultrasound and sodium lauryl sulphate to pig skin as a synergistic mechanical and chemical approach to enhance the delivery of AuNP.

- Finally, multiphoton laser scanning microscopy was used for detection of gold nanoparticles in skin specimens. Multiphoton was found an efficient technique to track the penetration of nanoparticles in skin [85, 115].

In order to achieve the aimed research objectives (outlined in Figure 2.1), the work in this thesis passed through several stages:

Stage one: Development of a method for detection of gold nanoparticles in human skin using multiphoton microscopy. For a better understanding, this was followed by establishment of an experimental approach for semi-quantitation of gold nanoparticles in the different skin regions. The goals of this stage were met in “**Publication 3.1**”.

Stage two: Determination of the imaging parameters of multiphoton microscopy in skin in terms of the achievable detection depths and the resolution limit. Reconstructed human skin and excised human skin were employed for the study and the results were presented in “**Publication 3.2**”.

Stage three: Investigation of the behavior of the prepared gold nanoparticles, of different physicochemical and formulation parameters, when coming in contact with the skin barrier, as well as tracking possible penetration. The results of this stage were published in “**Publications 3.3 and 3.4**”.

Stage four: Enhancement of the skin penetration of gold nanoparticles using chemical penetration enhancers. This was in focus in “**Publication 3.5**”.

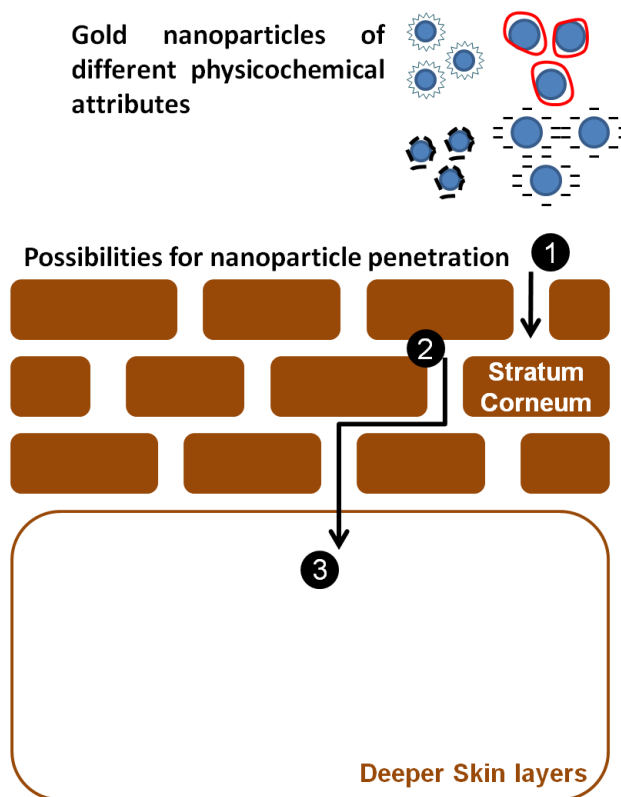


Figure 2.1: outline of the main research objective of the present thesis.

3. Publications

Publications are presented in the personal author form submitted to the journal, not the final version published in the journal, respecting the copyright terms indicated by the publishers.

3.1. Combined multiphoton imaging-pixel analysis for semiquantitation of skin penetration of gold nanoparticles

Hagar I. Labouta, Tobias Kraus, Labiba K. El-Khordagui and Marc Schneider

International Journal of Pharmaceutics

Vol. 413 (2011) 279– 282, DOI:10.1016/j.ijpharm.2011.03.067

Copyright © 2011 Elsevier B.V. All rights reserved.

International Journal of Pharmaceutics 413 (2011) 279–282



ELSEVIER

Contents lists available at ScienceDirect

International Journal of Pharmaceutics

journal homepage: www.elsevier.com/locate/ijpharm



Note

Combined multiphoton imaging-pixel analysis for semiquantitation of skin penetration of gold nanoparticles

Hagar I. Labouta^{a,b}, Tobias Kraus^c, Labiba K. El-Khordagui^b, Marc Schneider^{a,*}

^a Pharmaceutical Nanotechnology, Saarland University, Campus A4 1, D-66123 Saarbrücken, Germany
^b Department of Pharmaceutics, Faculty of Pharmacy, University of Alexandria, Egypt
^c Structure Formation Group, Leibniz Institute for New Materials (INM), Campus D2 2, 66123 Saarbrücken, Germany

The full text of this article is available online at:

<http://www.sciencedirect.com/science/article/pii/S0378517311003036>

Abstract

Interaction of nanoparticles with the skin barrier is a recent area of research that draws a lot of attention from the researchers. However, monitoring nanoparticles in or through the skin is mainly based on qualitative microscopical techniques. Yet, a quantitative approach is required for a better basic understanding. In response, a combined “multiphoton-pixel analysis” method was developed in this study for semiquantitation of gold nanoparticles penetration into different skin layers. The developed approach provides a useful tool for future studies focusing on skin penetration of nanoparticles for the aim of health risk assessment or for the design of topical and transdermal drug delivery systems.

Keywords: multiphoton imaging; semiquantitation nanoparticles skin penetration; gold nanoparticles.

Studying the skin penetration of nanoparticles is of great pharmaceutical importance for the design of potential topical and transdermal nanocarriers. Understanding the behavior of nanoparticles and their interaction with different skin layers would ultimately lead to the design of the “ideal” carrier [42]. Hence exploration of the relevant parameters of the nanoparticles, e.g. size, shape, surface chemistry, influencing skin penetration of nanoparticles is necessary. Furthermore, the amount of penetrating particles is crucial. Quantitative estimation of skin penetration of nanoparticles is however problematic due to detection limits of the available techniques with regard to the scarce concentrations of nanoparticles present in the skin in typical permeation-penetration experiments. The uncertainty whether penetration really occurs and the expected reduced diffusion rates of nanoparticles [42] are the key reasons for that. Therefore, monitoring skin penetration of nanoparticles has been based mainly on qualitative visualization by microscopy techniques. These include electron [77], fluorescence [88], confocal and multiphoton [115], Raman [116] and nuclear [113] microscopy. Other analytical methods including inductively-coupled plasma mass [86] and atomic absorption [46] spectroscopy do not detect the particles themselves. A quantitative approach based on nanoparticles' detection would allow a better understanding of skin penetration of nanoparticles and provide a sound scientific basis for diverse biomedical applications and health risk assessment.

We have established a method by multiphoton microscopy for investigating skin penetration of gold nanoparticles (AuNP) based on gold luminescence [56]. The objective of this study was to explore this method for semiquantification of AuNP penetrating into the stratum corneum (SC) and deeper skin layers (DSL). Pixel frequency was chosen as an indicator for the amount of AuNP avoiding the limitations of intensity measurement introduced previously [85].

Thiol-coated AuNP dispersion (diameter=6.00 ± 0.81 nm) were applied on human skin *in vitro* at $C_{\text{AuNP}} = 437 \mu\text{g/ml}$ in a vertical Franz diffusion set-up at 32°C for 24 h under occlusive conditions. Skin was then longitudinally cryo-sectioned, 10 μm thickness, at -20°C and subjected to two-photon excitation fluorescence microscopy (ZEISS_LSM_510_META system, Carl Zeiss, Jena, Germany). On sectioning, skin piece was not placed parallel to the cutting blade to avoid dislocation of the particles from outside into DSL or vice versa, but in a perpendicular position limiting

sectioning artifacts (Figure 3.1.1). Furthermore, imaging was done within the tissue and not on the surface of the cut. Longitudinal skin sections were used over full-thickness skin to reduce loss of laser power going deeper inside the skin. A wavelength of 800nm and energy of 0.485 and 0.647mW in the focal plane were used for both excitation of AuNP and scanning the skin, respectively. Signal due to gold luminescence and a light transmission image of the skin were simultaneously collected with no signal interference among tracks.

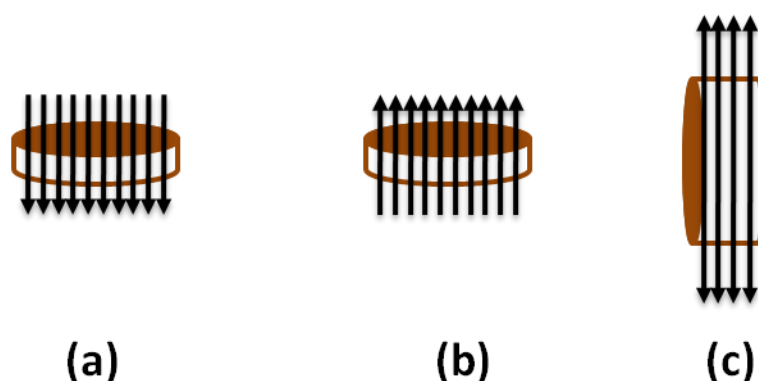


Figure 3.1.1: A schematic presentation showing different possibilities for longitudinal cryosectioning of a skin punch. The arrows indicate the direction of cutting. Placing the skin punch parallel to the cutting blade (a, b) results in possible dislocation of the particles on the surface into the DSL (a) or vice versa (b). On the other hand, placing the skin punch in a perpendicular position (c) (adopted cryosectioning method) avoids particle dislocation limiting sectioning artifacts.

Images of the longitudinal skin sections were then analyzed using ZEISS-LSM software, also feasible by any image analysis software. Semiquantitative data for the distribution of AuNP in different skin layers were extracted as follows: z-stacks, with optical layers 1 μ m thickness each, were adopted for analysis. The starting position (n=1) was defined as the first optical layer with detected signals in the AuNP track. Similarly, the end position (n=x) was the last optical layer showing AuNP. Each optical scan was composed of 512x512 pixel² and 71.4x71.4 μ m². For each layer, the intensity was first thresholded in order to remove the contribution of the background such as second harmonic generation from collagen [117]. The pixels due to gold luminescence were determined in the SC and in the DSL for this optical layer. Summing up these values for all the optical layers of the z-stack resulted in Σ pixel frequency (Σ Pixel) due to AuNP in the SC and in the DSL of this z-stack. Figure 3.1.2 illustrates the method used for semiquantitation.

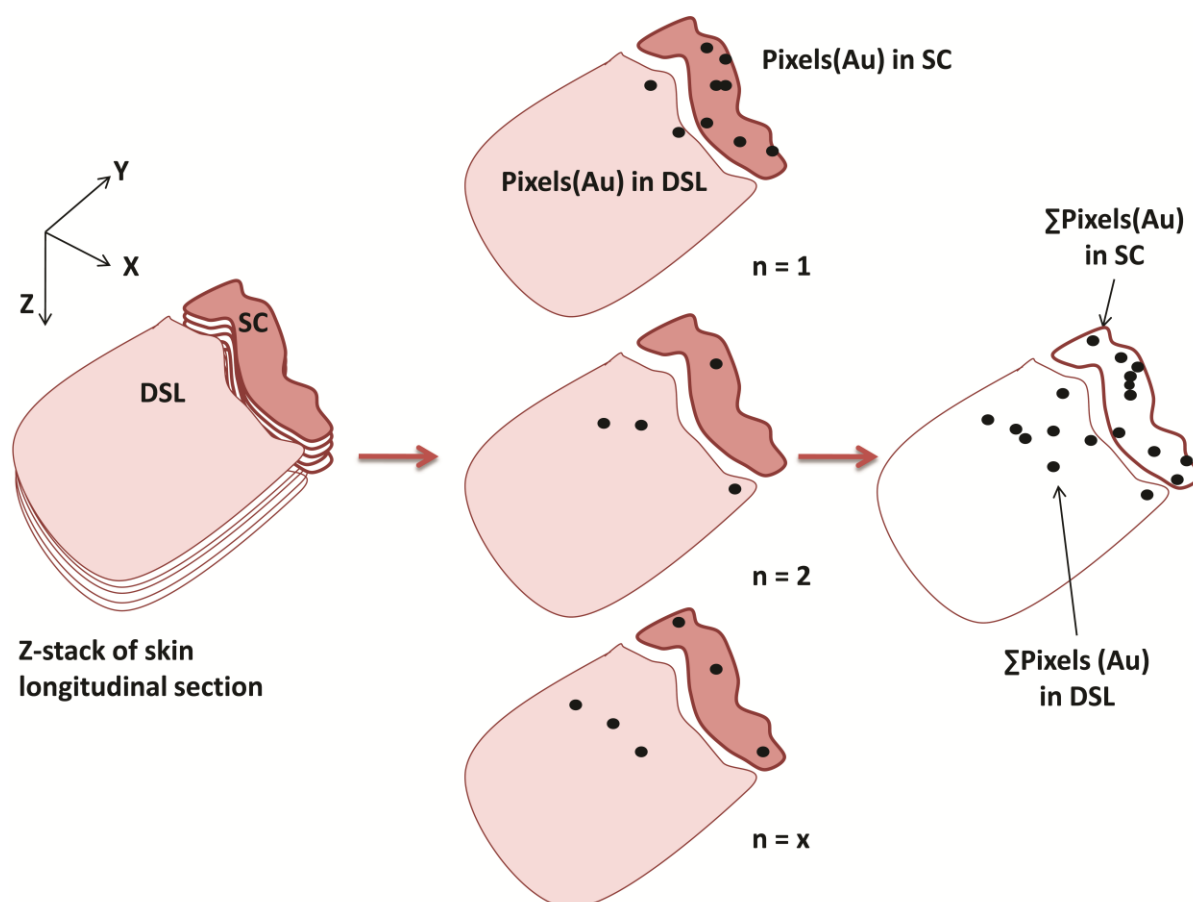


Figure 3.1.2: A schematic presentation of the experimental approach used for semiquantitation of the penetration of AuNP in a z-stack of a longitudinal skin section imaged by multiphoton microscopy. SC and DSL stand for the stratum corneum and the deeper skin layers, respectively.

Finally, $\sum \text{Pixel}$ of AuNP was normalized to determine the weighed number of particles (N_w) as follows: Considering an emission spectrum for AuNP of $\lambda \sim 530\text{-}640$ nm [118], the mean theoretical lateral resolution (r_{xy}) was calculated from Equation 3.1.1 [119] as ~ 0.341 μm , i.e. the area of a single diffraction-limited AuNP (A_{particle}) ~ 0.365 μm^2 .

$$r_{xy} = \frac{0.7\lambda}{NA} \quad (\text{Equation 3.1.1}),$$

where NA is the objective numerical aperture. Knowing the area of one pixel (A_{pixel}), 0.139×0.139 μm^2 in this study, N_w , the weighed number of nanoparticles, is calculated from:

$$N_w = \frac{\sum \text{Pixel} \times A_{\text{pixel}}}{A_{\text{particle}}} \quad (\text{Equation 3.1.2})$$

This method of analysis has the advantage of measuring the number of events not their intensity. Therefore, the gain settings of multiphoton imaging could be freely adjusted for each measurement individually according to the energy of the laser required to excite AuNP at different depths in the examined skin specimens reducing the limitations for typical comparative measurements. Only the objective (water immersion objective, 63X magnification, NA=1.2) and the image size should be kept the same throughout the measurements. This represents a great advantage over methods based on intensity measurement [85], where the gain settings have to be fixed for all experiments. This would rather limit the imaging capability of nanoparticles in deep positions of some imaged skin specimens resulting possibly in inaccurate results. This limitation was discussed by Gratieri *et al.* [52] when measuring the intensity of quantum dots as an indicator of their concentration in different skin layers using multiphoton microscopy. Our method overrides previous attempts involving manual counting of the number of fluorescent spots per field in confocal images [112]. Apart from human errors, adoption of the latter approach results in overlooking the area of the fluorescent spots if larger than the resolution limit. Moreover, a previous attempt to analyze fluorescence images [89] used only one image field of the examined skin for each experimental condition for analysis. However, as shown in Figure 3.1.3(i), one optical layer is not always descriptive for the overall penetration profile of nanoparticles. On the other hand, calculation of $\sum \text{Pixel}$ and N_w of AuNP in the SC and DSL in optical z-stacks of the examined longitudinal skin sections showed a depth-profile for AuNP concentrating more in the SC rather than in DSL (Figure 3.1.3(iii)).

In conclusion, a combined multiphoton imaging-pixel analysis approach was developed for semiquantitation of AuNP population in different skin locations in terms of pixels, from which the weighed number of particles could be calculated. These values could be used to determine the amount of AuNP penetrating into the SC and DSL in the same skin penetration experiment and correlate data among different experiments. The experimental approach described herein provides a valuable tool to advance our understanding of the interaction of nanoparticles with biological barriers, e.g. skin, and help identify various factors that enhance or limit their penetration. For future work, this method should be validated by the aid of analytical techniques such as inductively-coupled plasma mass and atomic absorption spectroscopy.

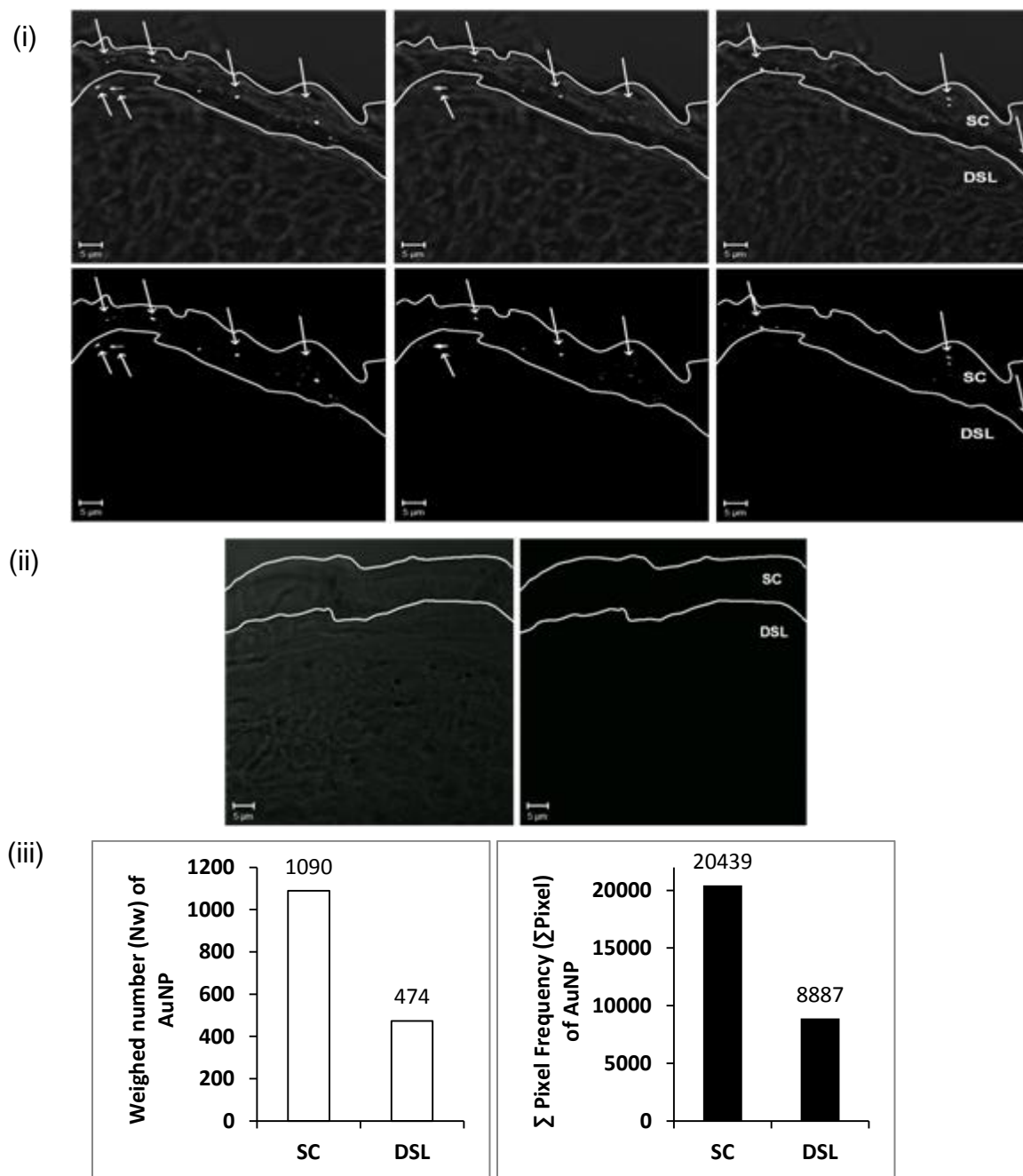


Figure 3.1.3: (i) Representative overlaid multiphoton/transmission images (upper panel) and the correspondent AuNP track (lower panel), each showing AuNP (indicated as white spots) at different optical layers of a z-stack of a longitudinal skin section, in which different amounts of AuNP in the SC (stratum corneum) and DSL (deeper skin layers) after 24 h of skin exposure were detected in each layer. A single layer is not descriptive for the overall penetration pattern. This is in comparison to (ii) an only vehicle-treated control skin specimen; the left image is an overlaid multiphoton/transmission image and the right image is the gold track only. (iii) Skin penetration of AuNP into the SC and DSL, expressed as Σ pixel frequency of AuNP (Σ Pixel) in all optical layers of the z-stack was determined and the respective weighed number of particles (N_w) were then calculated, as shown above, showing depth-profile for AuNP concentrating more in the SC rather than in DSL. Note that pixel values due to AuNP nanoparticles were recorded following thresholding of background intensity. Therefore, zero pixels were recorded for control skin specimens (not displayed).

3.2. Depth profiling of gold nanoparticles and characterization of point spread functions in reconstructed and human skin using multiphoton microscopy

Hagar I. Labouta, Martina Hampel, Sibylle Thude, Katharina Reutlinger, Karl-Heinz Kostka and Marc Schneider

Journal of Biophotonics

Vol. 5 (2011) 85-96, DOI:10.1002/jbio.201100069

Copyright© 2011Wiley Verlag-VCH GmbH&Co.KGaA, Weinheim. All rights reserved.

 Early View publication on
www.wileyonlinelibrary.com
(issue and page numbers not yet assigned;
citable using Digital Object Identifier – DOI)

J. Biophotonics 1–12 (2011) / DOI 10.1002/jbio.201100069

Journal of
BIOPHOTONICS

FULL ARTICLE

Depth profiling of gold nanoparticles and characterization of point spread functions in reconstructed and human skin using multiphoton microscopy

Hagar I. Labouta^{1,2}, *Martina Hampel*³, *Sibylle Thude*³, *Katharina Reutlinger*³,
*Karl-Heinz Kostka*⁴, and *Marc Schneider*^{*,1}

¹ Department of Pharmaceutical Nanotechnology, Saarland University, Campus A4 1, 66123 Saarbrücken, Germany

² Department of Pharmaceutics, Faculty of Pharmacy, University of Alexandria, Alexandria, Egypt

³ Fraunhofer Institute for Interfacial Engineering and Biotechnology (IGB), Stuttgart, Germany

⁴ Department of Plastic and Hand Surgery, Caritaskrankenhaus, 66822 Lebach, Germany

Received 8 August 2011, revised 18 August 2011, accepted 19 August 2011

Published online 10 October 2011

The full text of this article is available online at:

<http://onlinelibrary.wiley.com/doi/10.1002/jbio.201100069/abstract>

Supporting information for this article is available free of charge under:

[http://dx.doi.org/10.1002/jbio.\(DOI\)](http://dx.doi.org/10.1002/jbio.(DOI))

Abstract

Multiphoton microscopy has become popular in studying dermal nanoparticle penetration. This necessitates studying the imaging parameters of multiphoton microscopy in skin as an imaging medium, in terms of achievable detection depths and the resolution limit. This would simulate real-case scenarios rather than depending on theoretical values determined under ideal conditions. This study has focused on depth profiling of sub-resolution gold nanoparticles (AuNP) in reconstructed (fixed and unfixed) and human skin using multiphoton microscopy. Point spread functions (PSF) were determined for the used water-immersion objective of 63X/NA=1.2. Factors such as skin tissue compactness and the presence of wrinkles were found to deteriorate the accuracy of depth profiling. Broad range of AuNP detectable depths (20-100 μ m) in reconstructed skin was observed. AuNP could only be detected up to ~14 μ m depth in human skin. Mean lateral ($0.5\pm 0.1\mu$ m) and axial ($1.0\pm 0.3\mu$ m) PSF in reconstructed and human specimens were determined. Skin cells and intercellular components didn't degrade the PSF with depth. In summary, the imaging parameters of multiphoton microscopy in skin and practical limitations encountered in tracking nanoparticle penetration using this approach were investigated.

Keywords: multiphoton imaging; gold nanoparticles; skin nanoparticle penetration; point spread function; nanoparticle depth profiling.

3.2.1. Introduction

Optical techniques are of great importance as a non-destructive tool to study dermal penetration. Especially laser scanning microscopy (LSM) has shown its great potential. In confocal microscopy, a fluorophore is excited by the absorption of one photon of relatively high energy in the visible or ultraviolet spectrum. Multiphoton excitation, however, is a non-linear process in which a fluorophore is excited by two or more photons simultaneously of lower energy and longer wavelength in the infrared region [120]. Lower energy input, hence a reduced phototoxicity, and higher penetration of the excitation light are the distinct advantages over conventional LSM [121].

An important aspect for particle imaging is the ability to distinguish them from each other and to estimate if single or agglomerated particles are present. This ability is, however, limited by the resolution which is the minimal size when a sub-resolution light emitting object is imaged. Therefore, the imaging function, represented by the point spread function (PSF) needs to be known, to judge the image quality and for possible quantification of particle number. For biological systems the optical conditions are not well defined as scattering occurs when the refractive index changes e.g. due to mismatch of refractive index between the specimen and the objective or due to localized particles with refractive indices different from their surrounding imaging environment. This is clearly evident in imaging biological tissues with several scattering centers, cells and their organelles, different in size, shape and structure [122-124]. These effects limit and reduce the resolving power. Furthermore, absorption and scattering of excitation and emission radiations lead to signal attenuation with depth limiting the useful range of depth penetration [125-127]. Aberrations encountered on imaging biological samples are discussed in details by de Grauw et al. [124]. Skin represents a highly complex system due to its high optical density and complex structure, being composed of several skin layers different in physicochemical parameters of the cells in addition to the different inter- and intra-cellular components. As a consequence, experimental investigations are the only direct approach to determine reliable PSF in lateral and axial direction.

Two-photon excitation PSF was previously determined in water [128], glycerol [129] and in turbid media (gel and lipid emulsion) [130] containing fluorescent beads of diameter 100-220 nm. Interestingly, PSF was further determined in biological

specimens, lymph nodes [125], brain [125] and fixed kidney tissues [126] using sub-resolution fluorescent beads, showing strong dependence on tissue constitution and depth into the tissue. Possibly due to the great difficulty in inserting fluorescent nanoparticles inside the skin due to the barrier properties of the stratum corneum (SC), the early trial to measure PSF in skin was based on imaging beads placed on the top of skin samples of different thickness. This experimental setup, however, could not yield true PSF in the different skin layers [131]. Later, Guldbrand *et al.* [110-111] measured the PSF of fluorescent nanoparticles in human skin inserting them inside the skin specimen either by injection [110] or passive diffusion into the tissue after tape-stripping the SC [111]. However, both insertion methods did not assure homogenous distribution of the beads throughout the specimen and across the whole thickness.

Therefore, the objective of this study was the depth profiling of gold nanoparticles (AuNP) having sub-resolution dimensions in reconstructed skin specimens using two-photon excitation laser scanning microscopy, in addition to axial and lateral PSF determination at different depths from the skin surface. Reconstructed skin was grown from keratinocytes and fibroblasts together with AuNP in the culture medium. This would allow for the uniform particles distribution throughout the tissue. The compactness of the skin tissue was addressed by using fixed and non-fixed reconstructed skin specimens for examination. To complete the study, human skin injected with AuNP was also chosen for examination.

3.2.2. Materials and Methods

Preparation and characterization of AuNP. Ionically-stabilized, polar gold nanoparticles (AuNP) were prepared according to Turkevich method [25, 132]. Briefly, 70 ml solution of hydrogen tetrachloroaurate ($\text{HAuCl}_4 \cdot 3\text{H}_2\text{O}$, Sigma-Aldrich Chemie GmbH, Steinheim, Germany) containing about 100 $\mu\text{g}/\text{ml}$ was reduced by trisodium citrate dihydrate ($\text{Na}_3\text{C}_6\text{H}_5\text{O}_7 \cdot 2\text{H}_2\text{O}$, Sigma-Aldrich) containing 5-fold the molar concentration of the gold salt under reflux at 100°C.

The mean particle size of the gold core of the prepared nanodispersion was then determined by transmission electron microscopy (TEM) using a JOEL Model JEM 2010 instrument (JOEL GmbH, Eching, Germany) operated at an accelerating voltage of 120 kV. The hydrodynamic diameter and the polydispersity were

measured using Malvern Zetasizer Nano (Malvern Instruments, Malvern, UK) based on dynamic light scattering at 25°C. The surface charge was estimated by measuring the zeta potential based on the electrophoretic mobility using Malvern Zetasizer Nano (Malvern Instruments, Malvern, UK).

AuNP were sterilized by filtration then dispersed in Dulbecco's Modified Eagle's medium (DMEM) containing 10% fetal calf serum (FCS) under sterile conditions. Samples with two different concentrations, 97.4 and 487.1 µg/ml, in the culture medium were prepared. Under these conditions, colloidal gold dispersion was stable.

Growing a reconstructed skin from fibroblasts and keratinocytes together with the provided AuNP in the culture medium. A reconstructed skin equivalents were grown from human foreskin fibroblasts and keratinocytes in which AuNP were provided in the culture medium to be dispersed throughout the tissue according to the following protocol: Collagen gel containing human fibroblasts was pipetted on the top of a cell culture insert in a standard 24 well cell culture plate. The fibroblast-containing gel was cultured for 1 day at 37°C and 5% CO₂ under submersed conditions applying a total of 2.5 ml DMEM medium with 5% FCS per well and insert.

On the following day, 25 µl of the prepared AuNP dispersion in culture medium was added on each of the prepared gels, in either of the two concentrations of AuNP and incubated for 1 h at 37°C. A volume of 50 µl fibronectin solution (5 µg/ml) was then added and incubated again for 10 min at 37°C. Human foreskin keratinocytes in 100 µl KBM basal medium (Cambrex Bio Sciences) with 5% FCS were subsequently seeded on the top of the collagen gels. After 1 h incubation at 37°C, a total of 2.5 ml keratinocyte basal medium (KBM) containing FCS (5%), hEGF (0.1 µg/ 500 ml) and BPE (15 mg/ 500 ml) was added to each insert. While maintaining submersed culture conditions, medium was exchanged on day 3, 4 and 5, thereby gradually lowering the FCS concentration from 5% to 0%. At the end of the submersed culture period, inserts with the skin equivalents were transferred into 6 well cell culture plate. KBM medium with 1.88 mM CaCl₂ was filled into each well up to the level of the insert membrane (air-lift culture). The air-lift culture was performed for up to 13 days.

Treatment of human skin with AuNP. Human skin was obtained from female patients, who had undergone abdominal plastic surgery after approval of the ethic committee of Saarland, Germany (Ärzttekammer des Saarlandes, Dec. 2008). After excision, the skin was cut into pieces and the subcutaneous fatty tissue was removed from the skin specimen using a scalpel. The surface of each specimen was cleaned with water, dried, wrapped in aluminum foil and stored in polyethylene bags at -26°C until usage.

Human skin was exposed to AuNP under extreme conditions to assure distribution of the AuNP all over the tissue, but carefully so as not to damage the skin tissue. A punch of human skin, 8 mm in diameter, was injected with 1 ml of AuNP with a concentration $97.4\ \mu\text{g/ml}$ using a hypodermic needle, 0.3 mm in diameter (Sterican[®], absolute medical healthcare, Prague, Czech Republic). Injection sites were chosen on the top surface (SC), bottom surface (bottom layer of the viable deeper skin layers (DSL)) and from lateral sides of the skin punch. After injection, the skin turned red and was swollen in comparison to untreated skin punch (Supplementary 3.2.1). Human skin was, further, soaked in a dispersion of AuNP, $97.4\ \mu\text{g/ml}$, for 24 h.

Preparation of the skin specimens for examination using multiphoton microscopy.

i. Reconstructed skin

(a) Non-fixed (duplicate samples for each concentration of AuNP).

The culture media were carefully removed and freshly prepared phosphate buffer saline (pH 7.4) was added and specimens were then stored in an incubator (37°C , 5% CO_2) till further use. Specimens were stored under these conditions no longer than 1 day before usage. Specimens are either examined directly from the top by multiphoton microscopy or after longitudinal sectioning, $10\ \mu\text{m}$ thickness, at -26°C using a SLEE cryostat type mev (SLEE medical GmbH, Mainz, Germany).

(b) Fixed (duplicate samples for each concentration of AuNP)

The culture media were removed and skin specimens were fixed with 3.7% formalin in phosphate buffer saline for 2 h, followed by washing with phosphate buffer saline. Skin specimens were then treated as described above.

ii. Human skin

The treated skin specimen was frozen and 5 mm punch was taken for further examination. As mentioned before, the skin was examined from the top view and after longitudinal sectioning to examine the distribution of the particles throughout the skin tissue. Skin samples were then measured in duplicate using multiphoton microscopy as detailed below.

Multiphoton microscopy. Imaging was performed using an inverted confocal/two photon excitation fluorescence microscope (ZEISS LSM 510 META system, Carl Zeiss, Jena, Germany), equipped with a tunable Chameleon IR laser ($\lambda=720-930$ nm) for multiphoton laser microscopy, in addition to other conventional laser lines for confocal microscopy. A wavelength of 800 nm was used for both excitation of AuNP and the skin autofluorescence with a transmission energy of 0.467 and 0.485 mW, respectively, and a water immersion objective 63X (NA=1.2). The pulse width at the laser output was less than 140 femtosecond and the repetition frequency was 80 MHz. Only for longitudinal skin sections, a light transmission image of the skin was taken. The gain settings were adjusted for each measurement individually. No significant photobleaching was observed in our experiments under the conditions used for imaging AuNP in the different skin layers. z-stacks of the skin samples were acquired at 0.5 μm step. Each optical scan was composed of 512 x 512 pixel² or higher (2048 X 2048 pixel²).

z-stacks were subjected to analysis using the software of the supplier. Images were analyzed for depth profiling of AuNP in the imaged skin specimens and to determine the PSF of multiphoton microscopy in skin specimens at different depths from the surface in both XY (lateral resolution) and XZ (axial resolution) directions. Measurements were based on measurement of the mean intensity per pixel \pm standard deviation and pixel frequency. Prior to intensity and pixel measurements, the track of AuNP was only selected. The high background signals masking that from the particles were thresholded until only particles are selected. The threshold value was thus different from one case to another. Signals due to AuNP were then semiquantified in terms of pixels and intensity.

Data analysis. Generated data of PSF measurement were fitted to Gaussian function using Sigmaplot[®], version 11 (Systat Software GmBH, Germany) as follows:

$$f(x) = a \exp^{-0.5\left(\frac{x-\mu}{\sigma}\right)^2} \quad \text{Equation 3.2.1}$$

Where,

a: height of the curve's peak

μ : position of the peak

σ : standard deviation which controls the width of the peak

For each function, FWHM was then calculated using the following equation:

$$\text{FWHM} = 2\sigma\sqrt{2\ln 2} \quad \text{Equation 3.2.2}$$

Measuring FWHM of the central peak of PSF in XY and Z directions is a quite common experimental approach to determine lateral (r_{xy}) and axial (r_z) resolution. Practically-determined FWHM were compared to theoretically calculated lateral (r_{xy}) and axial resolution (r_z), determined based on Rayleigh criterion. Rayleigh criterion suggests that two point objects are resolved when the first minimum of one airy disc is aligned with the central maximum of the second airy disc. Therefore resolution, according to Rayleigh criterion, is defined as the distance between the central maximum and first minimum of the first airy disc and could be calculated from [119]:

$$r_{xy} = \frac{0.7\lambda}{\text{NA}} \quad \text{Equation 3.2.3}$$

$$r_z = \frac{2.3\lambda n}{\text{NA}^2} \quad \text{Equation 3.2.4}$$

where, λ is the wavelength of the emitted radiation, NA is the numerical aperture of the objective and n is the refractive index of the medium.

Lateral and axial PSF were determined for reconstructed skin specimens containing a concentration of 97.4 and 487.1 $\mu\text{g/ml}$ (fixed and non-fixed specimens) and for human skin specimens. For each of them, five z-stacks were analyzed for axial and lateral PSF at different depths from which the respective FWHM were determined.

Experimental FWHM in lateral and axial directions were compared to theoretical values calculated based on Rayleigh criterion according to Equations 3.2.3 and 3.2.4.

3.2.3. Results and discussion

The main objective of this study was to examine the imaging properties of multiphoton microscopy in skin specimens, reconstructed and human skin in which AuNP are distributed throughout the skin tissue. Therefore, AuNP with a size of (14.9 ± 1.8) nm for gold core and a hydrodynamic diameter of (15.3 ± 0.7) nm (polydispersity index 0.1 ± 0.0) and a zeta potential of (-35.1 ± 1.9) mV were prepared, sterilized by filtration, then redispersed in the culture medium together with keratinocytes and fibroblasts under sterile conditions to build up a reconstructed skin tissue in which AuNP are dispersed as shown in the protocol above. AuNP from the same batch were also used in treatment of human skin specimens.

On applying AuNP at the beginning of the growth phase of the reconstructed skin, the tissue could grow normally with a well distribution of AuNP throughout the tissue. This was shown from examination of the longitudinal sections (Figure 3.2.1). However, on examination of skin specimens from the top (Figure 3.2.2), AuNP could only be detected up to variable depths from the skin surface varying from around 20 to 100 μm (Table 3.2.1). Variable detection depths of the AuNP could be attributed to variable compactness of the examined tissues, with spaces of no particular pattern and of variable areas separating skin layers, where laser suffers much less scattering. Compact organization is not easy to obtain when the artificial organ is constructed *in vitro*, reconstructed skin in this case. However, the use of fixatives was found effective in structural preservation of reconstructed skin [133]. This could explain the limited variations in detection depths of AuNP in examined skin specimens after fixation with formalin, where AuNP could be detected up to a depth of around 20 μm , except for one replicate (~ 50 μm) which could be attributed to imaging round wrinkles, representing another problem of accurate determination of depth of nanoparticles in skin specimen examined from the top by means of multiphoton microscopy. In other words, the inaccurate definition of the skin surface would contribute in the variation of the maximum detectable depth for AuNP in skin

specimens. This would represent a problem when tracking skin penetration of nanoparticles, especially on detecting whether particles are located on the SC-viable epidermis border or have already penetrated into the viable tissue. This could be shown by imaging smaller skin areas (an optical image of $23.8 \times 23.8 \mu\text{m}^2$ rather than $47.6 \times 47.6 \mu\text{m}^2$, where AuNP could be only detected up to a depth of around $20 \mu\text{m}$ from the skin surface (Figure 3.2.2d). In Figure 3.2.2, the initial increase in the intensity per pixel values or the number of detected events for AuNP (pixel frequency) is mainly due to surface washing of skin specimen before examination. Note that intensity per pixel and pixel values shown in Figure 3.2.2 are thresholded values to eliminate the contribution of the background.

Table 3.2.1: Maximum depths for detected signals of AuNP in reconstructed skin specimens, grown from fibroblasts and keratinocytes examined from the top view by multiphoton laser scanning microscopy. The size of each optical scan of the z-stack was $47.62 \times 47.62 \mu\text{m}^2$.

Treatment of skin specimen	Un-fixed		Fixed	
AuNP concentration, $\mu\text{g}/\text{ml}$	97.4	487.1	97.4	487.1
Maximum detection depth, μm	~ 20	~ 50	~ 20	~ 20
(duplicate skin specimens)*	~ 90-100	~ 90	~ 20	~ 50

*For each skin specimen, the whole skin surface was roughly scanned for detection depth.

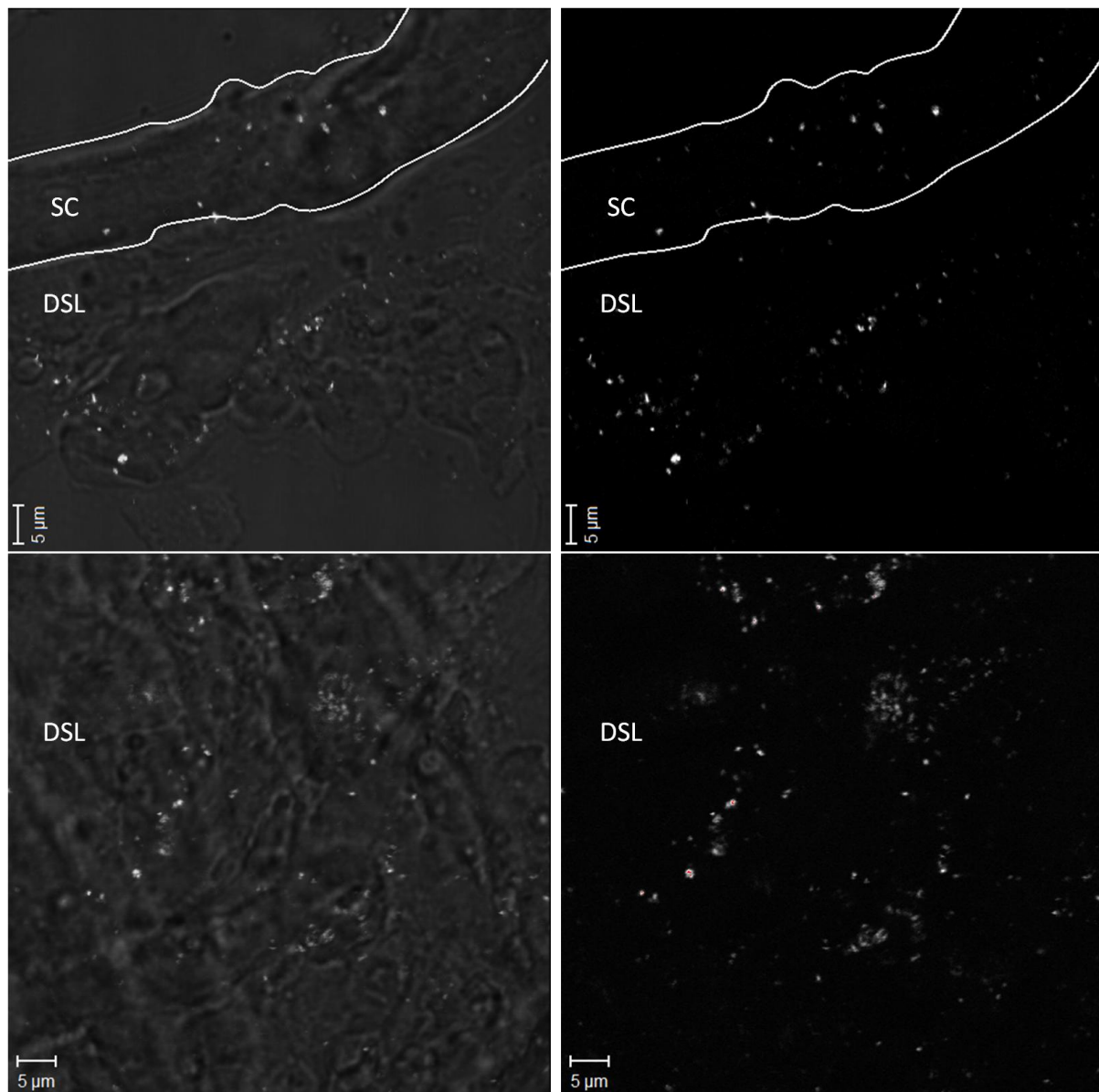


Figure 3.2.1: Representative images of AuNP (indicated as white spots) in longitudinal sections of reconstructed skin, grown from fibroblasts and keratinocytes together with AuNP at a concentration of 487.1 $\mu\text{g}/\text{ml}$, imaged by multiphoton laser scanning microscopy, showing distribution of AuNP in (a) the SC (stratum corneum) and DSL (deeper skin layers) and (b) even in much deeper layers inside the skin. The left panel is overlaid multiphoton/transmission images of AuNP in skin, while signals due to AuNP alone are shown in the right panel.

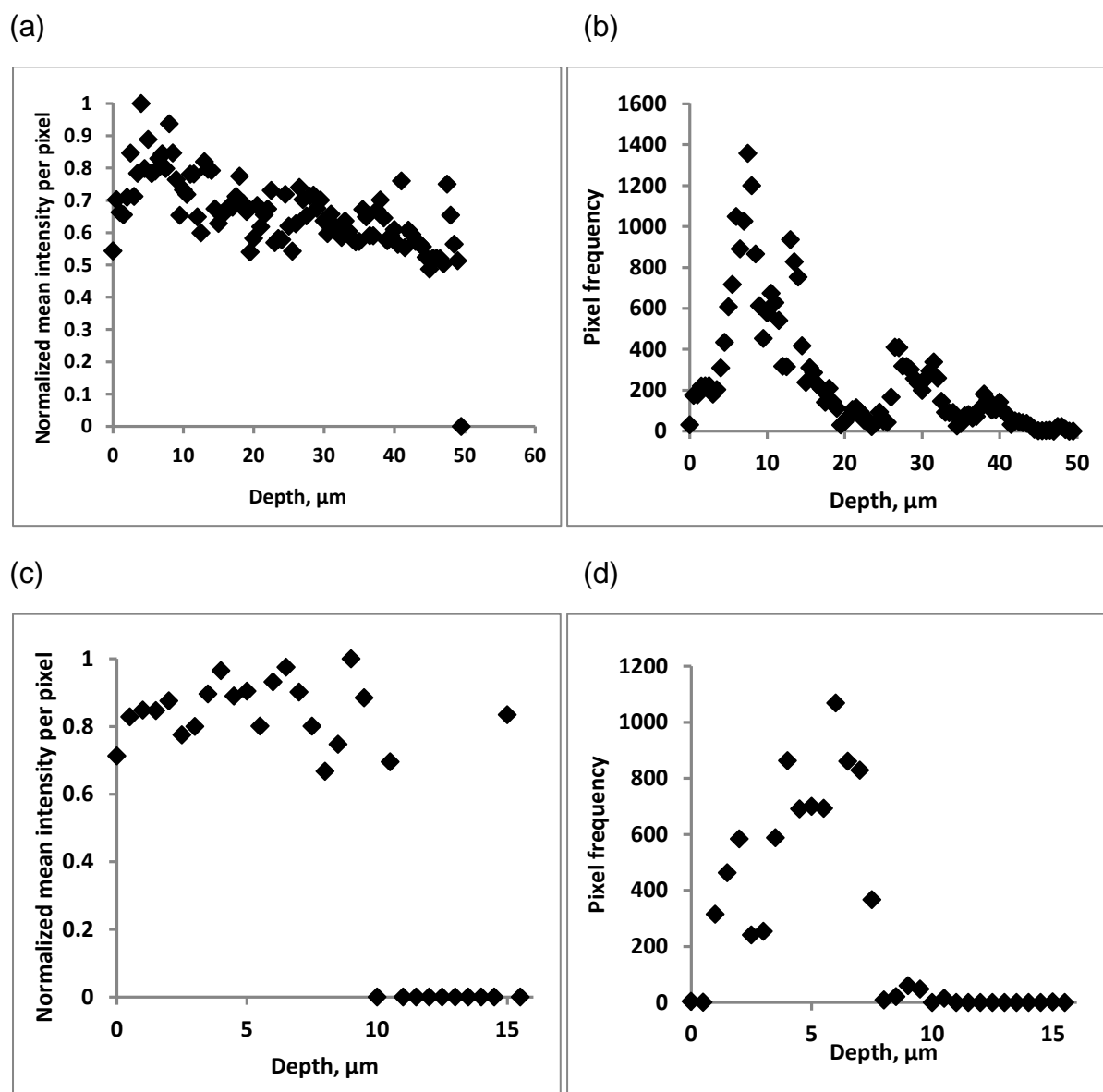


Figure 3.2.2: (a, c) Intensity-depth and (b, d) pixel-depth profiles of AuNP in z-stacks of a reconstructed skin specimen grown from fibroblasts and keratinocytes together with AuNP in a concentration of $487.1 \mu\text{g/ml}$ imaged by multiphoton laser scanning microscopy from the top. Profiles are generated based on z-stacks with an optical scan size of $47.6 \times 47.6 \mu\text{m}^2$ (a, b) and $23.8 \times 23.8 \mu\text{m}^2$ (c, d) The intensity and pixel frequency increase at the beginning then decrease going deeper inside the skin, however zero intensity and pixel values were reached at different depths from the skin surface. The presented intensity and pixel values were thresholded to eliminate the contribution of the background and skin autofluorescence.

Another aim of this study was to determine the PSF for multiphoton microscopy in skin as an imaging medium instead of water [128] and turbid liquids [130] already explored before. This would represent a more realistic condition when imaging ultra-small particles (particles with sub-resolution dimensions) in skin specimens for the purpose of resolution estimation, penetration estimation, etc. Determined PSF values could be useful to get more precise number of nanoparticles in skin specimens using multiphoton microscope, rather than depending on theoretical values [55, 134]. Lateral and axial PSF of multiphoton microscopy under these conditions were then determined by fitting the generated data to Gaussian function (Equation 3.2.1) then measuring the respective FWHM according to Equation 3.2.2 (Figure 3.2.3 and Figure 3.2.4). This was determined in reconstructed skin specimens grown from fibroblasts and keratinocytes together with AuNP in the culture medium at a concentration of 97.4 (fixed specimens) and 487.1 (non-fixed and fixed specimens) $\mu\text{g/ml}$ using a water immersion objective 63 X (NA = 1.2). At least five z-stacks were analyzed for each of them at different levels from the skin surface. Considering an objective NA of 1.2, a broad emission spectrum for AuNP of around 530-640 nm [118] and a refractive index for skin around 1.4 μm (1.443-1.448 μm and 1.378-1.396 μm for the epidermis and dermis, respectively) [135], theoretical lateral (r_{xy}) and axial resolution (r_z) could be calculated from Equations 3.2.3 and 3.2.4. The theoretical value of lateral resolution in both the epidermis and the dermis was calculated in the range of ~ 0.3 - 0.4 μm due to a broad emission spectrum. The theoretical axial resolution, however, should be in the range of ~ 1.2 - 1.5 μm and ~ 1.2 - 1.4 μm for the epidermis and dermis, respectively.

For PSF determination, the pixel size must be reduced sufficiently so that at least one pixel at a measurably lower intensity separates the objects of interest. Practically, a pixel 2.3 times smaller than the optical resolution limit of the system is required to digitally resolve that separation. This is known as the Nyquist criterion [136]. Therefore, on imaging, the pixel size was always kept 2.3 times below the theoretical values for lateral and axial resolution calculated from Equations 3.2.3 and 3.2.4, preventing undersampling for the aim of accurate determination of PSF experimentally. Sub-diffraction limited spots with individual out-of-focus rings (airy discs) not intersecting with out-of-focus rings from neighboring ones at different depths from the skin surface were chosen for PSF determination.

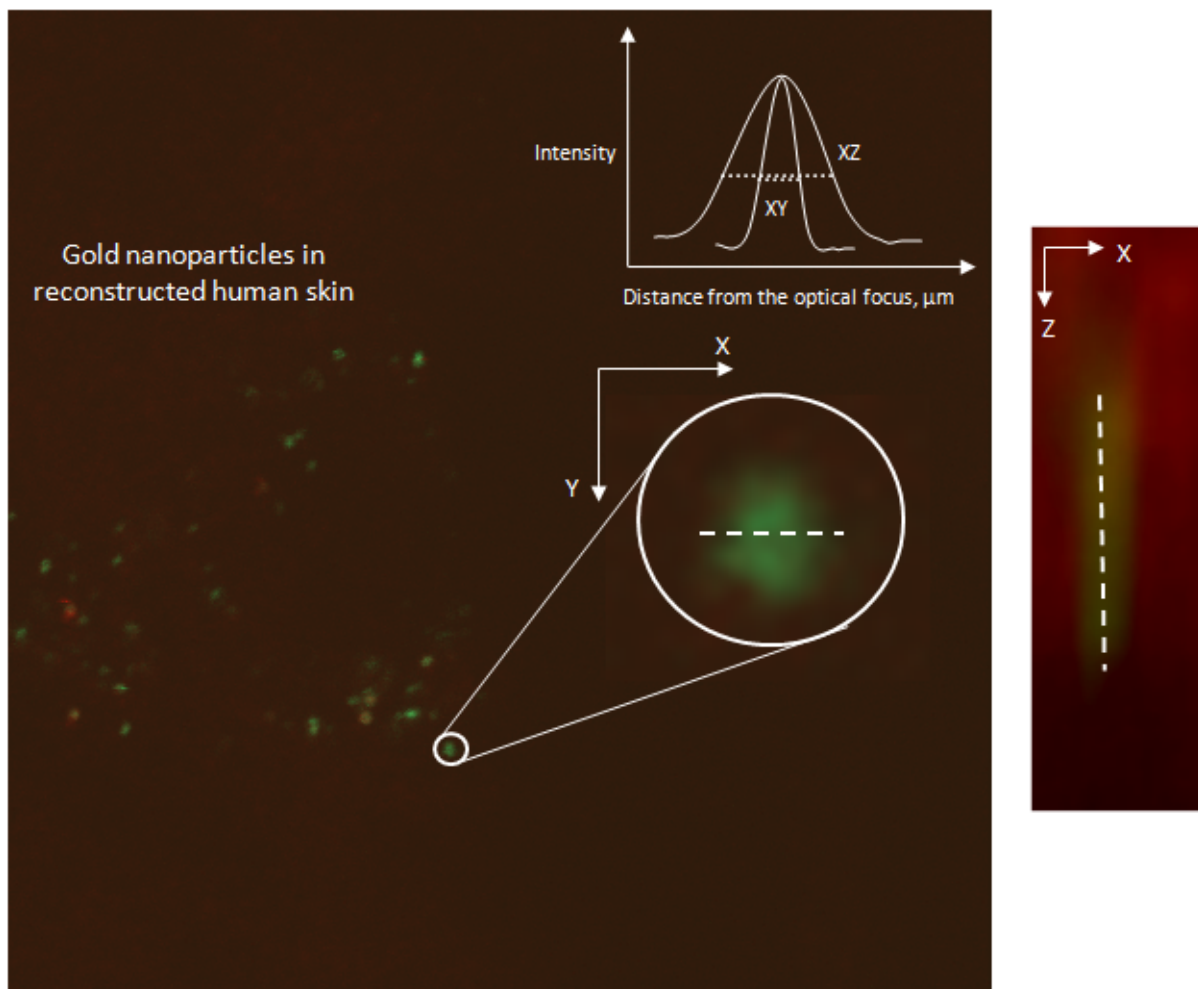


Figure 3.2.3: Multiphoton image of AuNP in reconstructed skin, grown from keratinocytes and fibroblasts together with AuNP at a concentration of $487.1 \mu\text{g/ml}$ at a depth of $5.5 \mu\text{m}$ from the skin surface. A single representative particle is viewed from lateral, denoted as XY, and axial, denoted as XZ, for calculation of FWHM (full-width half maxima) for the determination of lateral and axial point spread functions of the imaging system.

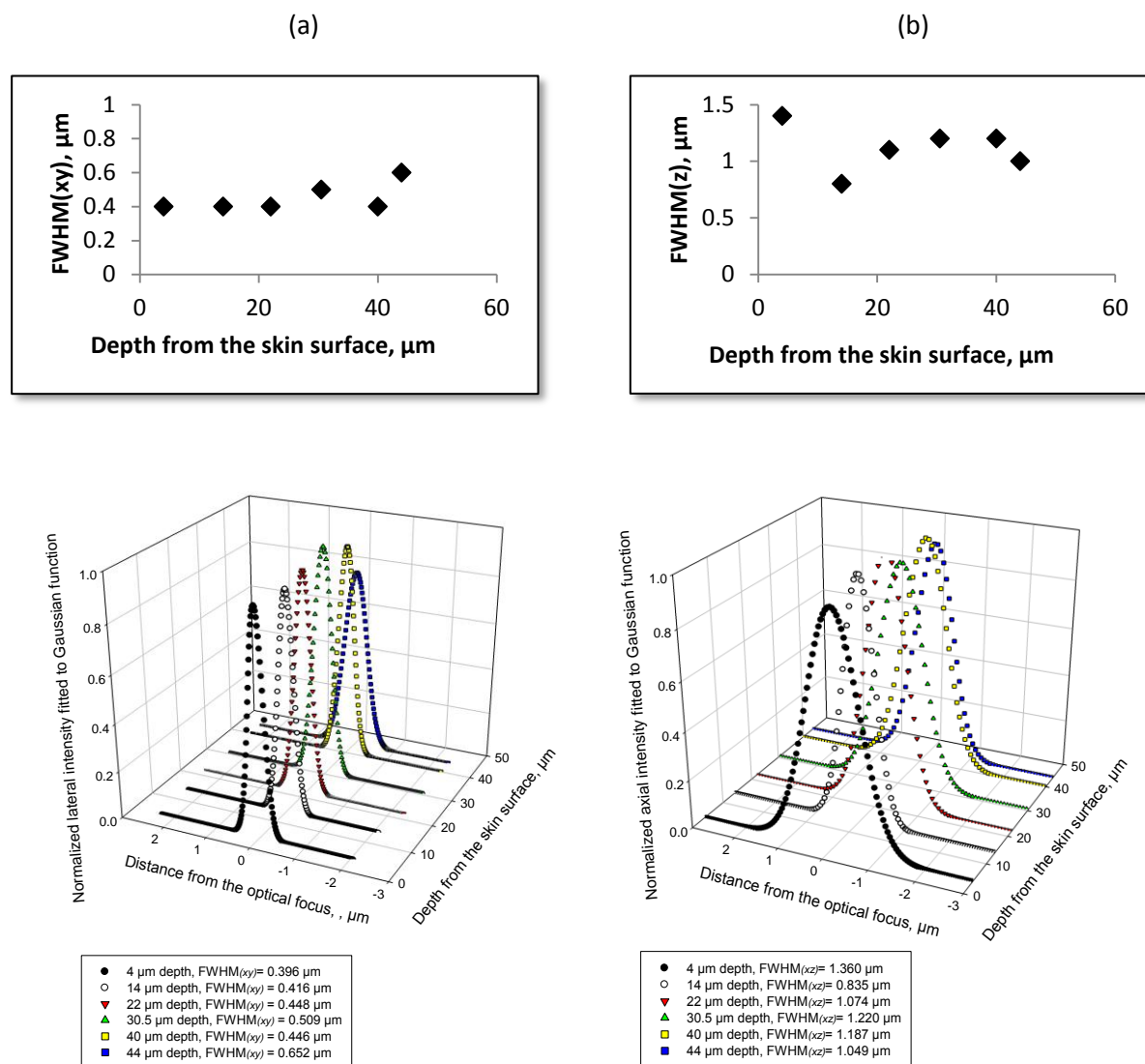


Figure 3.2.4: Point spread functions in lateral (a) and axial (b) directions in reconstructed skin grown from fibroblasts and keratinocytes together with AuNP at a concentration of 487.1 $\mu\text{g/ml}$ at variable depths from the skin surface (4-44 μm) fitted to Gaussian function showing independency of the lateral (XY) and axial (XZ) FWHM (full-width half maxima) on the depth from the skin surface.

The mean value of lateral PSF, determined in terms of FWHM, in all examined reconstructed skin specimens determined at different depths from the surface was $(0.50 \pm 0.1) \mu\text{m}$ and that for axial FWHM $(1.0 \pm 0.3) \mu\text{m}$. Both determined lateral and axial FWHM in skin specimens were higher than experimental values determined in water [128], glycerol [129] and turbid media [130] due to higher optical density of the skin as an imaging medium. On the other hand, only lateral FWHM values determined practically were higher than theoretical values calculated from Equations 3.2.3 and 3.2.4. However experimental axial FWHM values were in accordance with theoretical values. This could be attributed to the high refractive index of skin [135] and the consequent mismatch in refractive index of the skin specimen and the objective since theoretical lateral FWHM values were calculated independent of the refractive index of the skin (Equation 3.2.3). This calls for re-adaptation of the mathematical equation to include the refractive index of the medium as one of the determinants of lateral resolution, when imaging biological specimens. However for axial resolution, the refractive index of the medium is already considered (Equation 3.2.4) yielding closer values to the real case. Experimentally measured axial PSF were even slightly lower in some cases than theoretically computed ones. This could be due to the broad emission spectrum of AuNP on two-photon excitation [118]. It was also reported that axial FWHM is 10% lower than resolution determined based on Rayleigh criterion (Equation 3.2.4) [119].

No statistical significance ($p > 0.05$) was found between the resolution in fixed and non-fixed specimens. The mean values \pm SD are shown in Table 3.2.2. Though lateral and axial resolution were expected to get worse going deeper inside the skin due to scattering of incident radiation, this was not the case with no or slight variation ($p > 0.05$) among lateral and axial PSF values versus depth from the skin surface (Figure 3.2.4). This could be attributed to the poor compactness of the reconstructed skin, with spaces of no particular pattern and of variable areas separating various skin layers, where the laser suffers much less scattering. The same results were obtained for specimens with different concentration of AuNP (94.7 and 487.1 $\mu\text{g/ml}$). This would rather indicate that the determined values are for sub-resolution particles and not for aggregated population of particles; otherwise great variation among results would have been observed depending on the size of aggregates. Moreover, much higher values would have been generally expected on examining skin

specimens with higher concentration of AuNP in case of aggregation, since it is a phenomenon that is expected to increase on increasing concentration. All this eliminates the possibility of aggregation and insures that the measured values are essentially higher than the values reported in literature for lateral and axial resolution under ideal conditions, for instance ~ 0.2 and $0.7 \mu\text{m}$ [130], respectively due to the scattering phenomenon in the complex non-homogenous skin tissue.

Optical z-sectioning was further performed on longitudinal sections in different skin regions, SC and DSL, and lateral FWHM were determined, where nearly the same values were obtained (Table 3.2.2). Again, the lateral resolution did not change significantly going deeper inside the SC from the side view. Similarly, this could be due to the non-dense fibrous structure of the SC characterizing reconstructed skin. In DSL, a relatively denser part of the skin full of living cells, showed an increase in the lateral FWHM going deeper inside the tissue (Figure 3.2.5). This emphasizes the effect of tissue compactness on the imaging parameters by multiphoton microscopy.

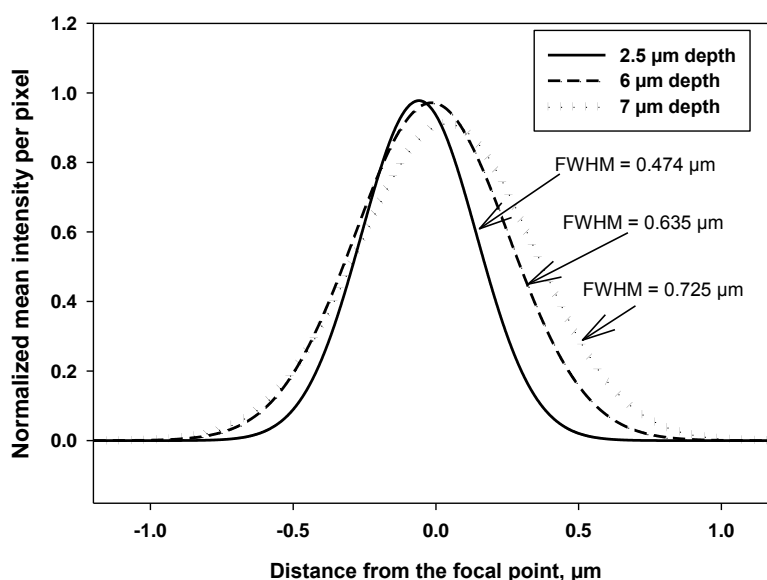


Figure 3.2.5: lateral point spread functions (fitted to Gaussian function) at different depths from the surface, 2.5, 6 and 7 μm in DSL (deeper skin layers) of a longitudinal section of reconstructed skin grown from fibroblasts and keratinocytes together with AuNP, at a concentration of 487.1 $\mu\text{g/ml}$. Determined values of FWHM are noted on the curves.

Table 3.2.2: (a) Summary of the results of determination of lateral and axial PSF of a multiphoton microscope using a water immersion objective of 63X, NA 1.2 in fixed and non-fixed specimens of reconstructed skin grown from fibroblasts and keratinocytes together with AuNP at a concentration of 94.7 and 487.1 $\mu\text{g/ml}$. (b) Mean values of lateral PSF in longitudinal sections of skin specimens grown with AuNP, 487.1 $\mu\text{g/ml}$, in the SC (stratum corneum) and DSL (deeper skin layers) measured at different depths from the surface (first layer of the side view).

(a)

	Lateral PSF, μm (mean \pm SD)	Axial PSF, μm (mean \pm SD)
All data	0.5 \pm 0.1	1.0 \pm 0.3
At a depth from the skin surface of *:		
1-15 μm :	0.5 \pm 0.1	0.9 \pm 0.3
15-20 μm :	0.5 \pm 0.1	1.0 \pm 0.3
>20 μm :	0.5 \pm 0.1	1.1 \pm 0.4
Fixed**	0.5 \pm 0.1	1.0 \pm 0.2
Non-fixed specimens with a concentration of AuNP ($\mu\text{g/ml}$) of:		
97.4	0.5 \pm 0.1	1.0 \pm 0.2
487.1	0.5 \pm 0.1	1.0 \pm 0.3

*For each depth from the skin surface, at least 3 particles were used for analysis for each AuNP concentration in fixed and unfixed skin specimens.

**AuNP concentration = 487.1 $\mu\text{g/ml}$.

(b)

Location in the longitudinal skin section	Lateral PSF, μm (mean \pm SD)
SC	0.6 \pm 0.1
DSL	0.6 \pm 0.1

AuNP Concentration = 487.1 $\mu\text{g/ml}$

A complementary part of the study was the depth profiling of the prepared AuNP in human skin and measuring the PSF in human skin instead. The results were then compared to that of reconstructed skin to further study the effect of the skin type and tissue compactness on imaging using multiphoton microscopy. Human skin is of more complex and denser structure. To assure distribution of AuNP all over the skin

thickness, human skin was exposed to AuNP, at a concentration of 97.4 $\mu\text{g/ml}$, under extreme conditions, as shown above. Longitudinal skin sections showed distribution of AuNP in almost all skin layers (Supplementary 3.2.2). On examination of the skin punch from the top view, however, AuNP could be detected up to a depth of only $\sim 14 \mu\text{m}$. Maximum detected depth was 23 μm . The latter was in an area of evident wrinkles on the skin surface, a parameter which contributes negatively to the accuracy of depth determination from the top view. A representative intensity-depth profile is shown in Figure 3.2.6a, where signal levels slowly attenuate with depth into the tissues reaching zero-intensity at a depth of 14.5 μm . Figure 3.2.6b shows a pixel-depth profile of this z-stack, where the number of events for AuNP detected signals initially increased followed by a subsequent decrease until 14.5 μm depth. Determined penetration depths were independent of the scan size (data not shown). Nevertheless, this again implies that the wide variations in detected penetration depths on z-optical sectioning of the examined reconstructed skin specimens could be due to its loose structure [133]. More important, our results in human skin show that nanoparticles could be tracked up to a shallow depth less than or equal to the average thickness of the SC due to scattering phenomenon in the heterogenous skin tissue with depth. This represents a major problem when tracking the penetration of nanoparticles into DSL. Different results were, however, obtained by Guldbrand *et al.* [110-111] detecting a signal due to their fluorescent particles up to a depth of 35-40 μm , implying an effect of the emission wavelength of the imaged fluorescent particles, 580 nm relative to a broad emission spectrum for AuNP 530-640 nm, as reported by Farrer *et al.* [118] and the high emission intensity. A second contributing factor would be the anatomical region of the excised skin, using breast skin versus abdominal skin used in our study. Moreover, in one approach they reported tissue damage on injecting their particles in the skin [110] and in another they stripped the SC before application of AuNP to allow for better penetration into the skin tissue [111]. This would certainly have an impact on the refractive index of the tissue; the epidermis has higher optical density than the dermis [135], and consequently on the spherical aberrations caused by the mismatch of the refractive index of the skin and the objective.

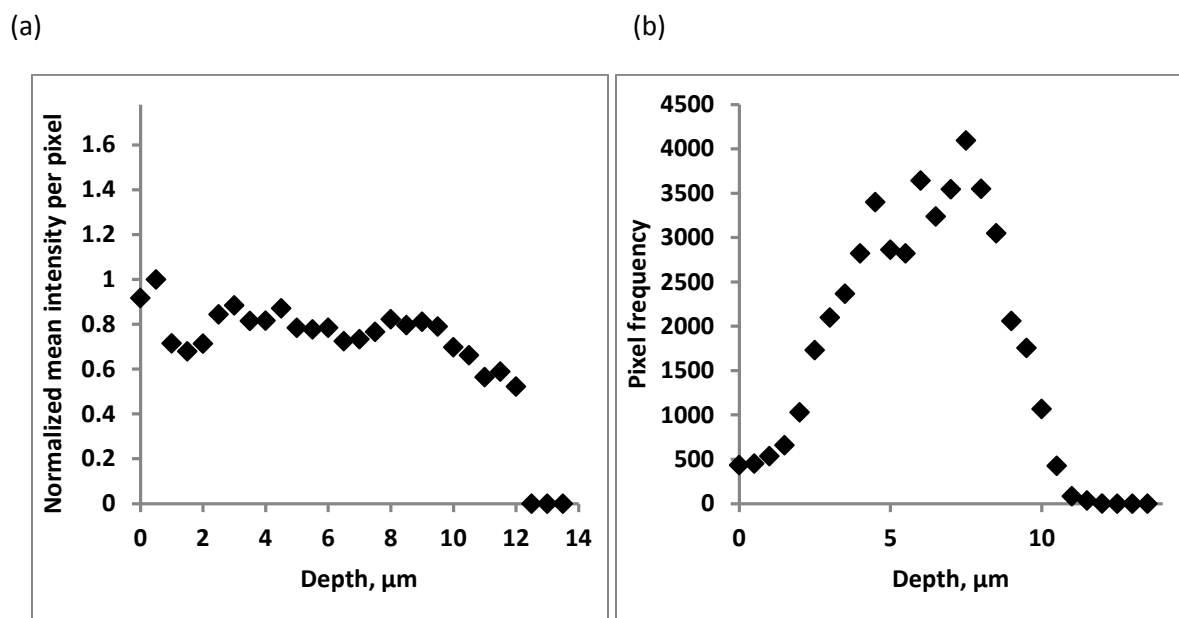


Figure 3.2.6: (a) Intensity-depth and (b) pixel-depth profiles of AuNP in a z-stack (optical scan size of $47.6 \times 47.6 \mu\text{m}^2$) of human skin treated with AuNP in a concentration of $97.4 \mu\text{g/ml}$ imaged by multiphoton laser scanning microscopy from the top. Both the intensity and pixel frequency increased at the beginning then decreased going deeper inside the skin. The presented intensity and pixel values were thresholded to eliminate the contribution of the background.

Table 3.2.3 shows the mean values of FWHM determined in human skin specimens from the top view and after longitudinal sectioning in the SC and DSL. Results of FWHM determination in human skin were comparable to our results in reconstructed skin with slightly higher values for human skin possibly due to the higher complexity and density of human skin compared to *in vitro* skin models grown from skin cell lines. These values are in line with previously determined FWHM by Guldbrand *et al.* [111] reporting a lateral resolution in the range of $\sim 0.4\text{-}0.6 \mu\text{m}$ and an axial resolution of $\sim 0.9\text{-}1.6 \mu\text{m}$. However, up to the limited imaging depth achievable in skin tissue by multiphoton microscopy, $\sim 14 \mu\text{m}$, scattering did not appear to significantly degrade the imaging PSF ($p > 0.05$) (Table 3.2.3). The same trend was recently reported by Guldbrand *et al.* [111], showing no influence of the imaging depth on the FWHM when imaging fluorescent beads in human skin. According to them, this was attributed to the higher influence of the distortions caused by the optical system.

Table 3.2.3: (a) Summary of the results of determination of lateral and axial PSF of a multiphoton microscope using a water immersion objective of 63X, NA 1.2 in human skin injected and soaked in AuNP at a concentration of 94.7 $\mu\text{g/ml}$. (b) Mean values of lateral PSF in longitudinal sections of human skin specimens injected and soaked in AuNP, 487.1 $\mu\text{g/ml}$, in the SC (stratum corneum) and DSL (deeper skin layers) measured at different depths from the surface (first layer of the side view).

(a)

	Lateral PSF, μm (mean \pm SD)	Axial PSF, μm (mean \pm SD)
All data	0.5 \pm 0.1	1.3 \pm 0.3
At a depth from the skin surface of *:		
1-6 μm :	0.5 \pm 0.1	1.3 \pm 0.2
6-10 μm :	0.6 \pm 0.0	1.1 \pm 0.3
10-20 μm :	0.5 \pm 0.1	1.3 \pm 0.5

*For each depth from the skin surface, at least 3 particles were used for analysis

(b)

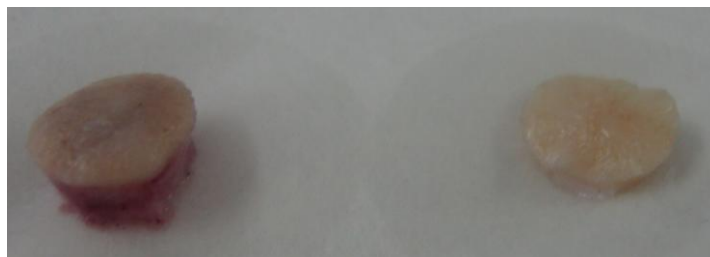
Location in the longitudinal skin section	Lateral PSF, μm (mean \pm SD)
SC	0.6 \pm 0.1
DSL	0.7 \pm 0.1

3.2.4. Conclusion

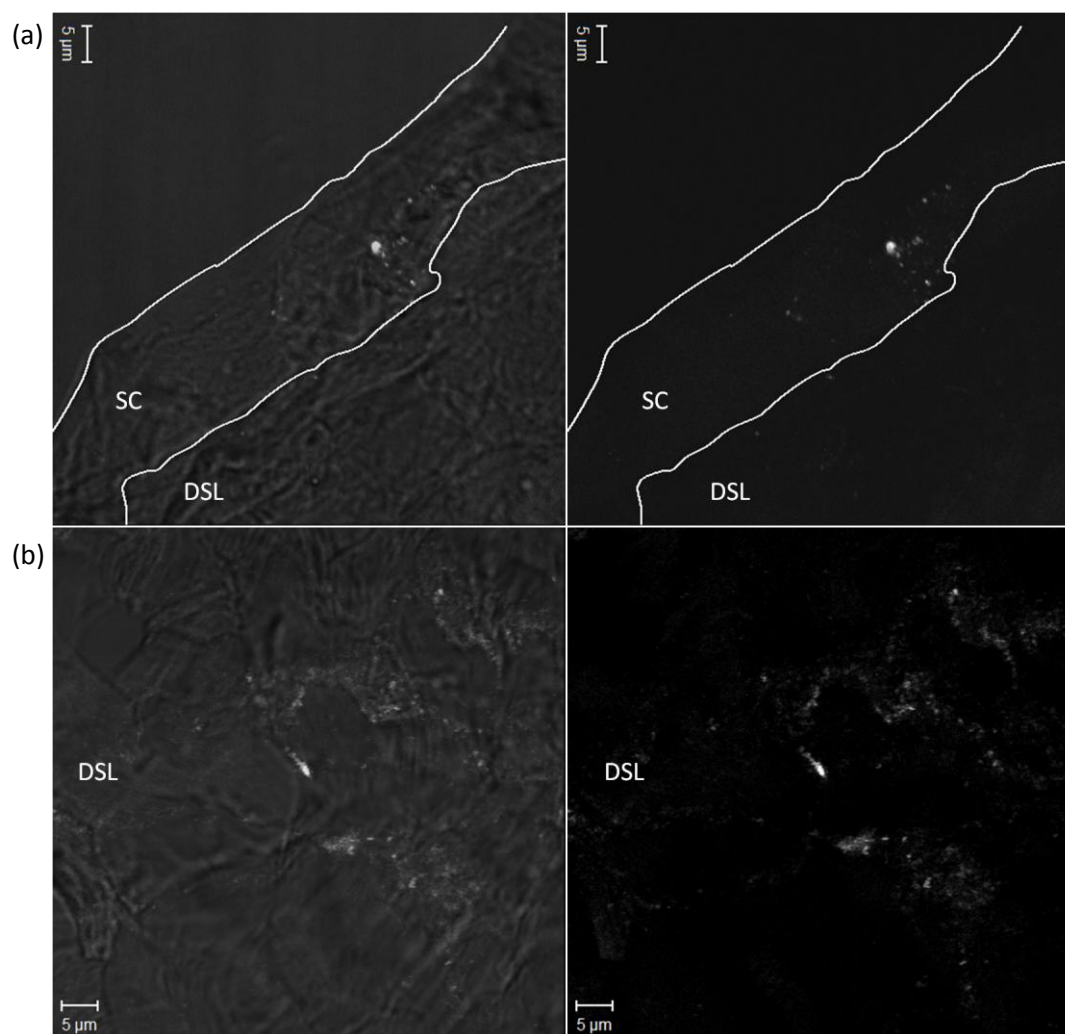
In conclusion, multiphoton laser scanning microscopy is a promising non-invasive technique in tracking skin penetration of nanoparticles. However, it suffers some limitations and thus results based on this technique should be interpreted with care. This was shown on depth profiling of AuNP in skin, where AuNP could be detected up to variable depths from the skin surface ranging from 14-100 μm , depending on the skin type (reconstructed skin and human skin), skin pretreatment (tissue fixation) and area of examination (presence or absence of wrinkles). Surprisingly, measured lateral and axial PSF were found not to degrade with depth, possibly due to the low tissue compactness, in case of reconstructed skin, or due to possible dominance of the distortions caused by the optical system along the relatively short detection depth for AuNP in human skin ($\sim 14 \mu\text{m}$). Another limitation which should also be taken into

consideration on depth profiling of nanoparticles in skin from the top is the variable thickness of the SC. Therefore, particles located at a depth more or less than 20 μm are not essentially in the DSL or yet in the SC, respectively. This means that examination of longitudinal skin sections, though suffering possible sectioning artifacts, still provides more accurate information on the status of skin penetration of nanoparticles rather than optical sectioning of skin specimens examined from the top.

Supplementary information



Supplementary 3.2.1: Human skin punch, 8 mm in diameter, injected with 1 ml AuNP at a concentration 97.4 µg/ml (left) in comparison to control non-treated skin punch (right).



Supplementary 3.2.2: Representative images of AuNP (indicated as white spots) in longitudinal sections of human skin treated with AuNP at a concentration of 97.4 µg/ml, imaged by multiphoton laser scanning microscopy, showing distribution of AuNP in (a) the SC (stratum corneum) and DSL (deeper skin layers) and (b) even in much deeper layers inside the skin. The left panel is overlaid multiphoton/transmission images of AuNP in skin, while signals due to AuNP alone are shown in the right panel.

3.3. Gold nanoparticle penetration and reduced metabolism in human skin by toluene

Hagar I. Labouta, David C. Liu, Lynlee L. Lin, Margaret K. Butler, Jeffrey E. Grice, Anthony P. Raphael, Tobias Kraus, Labiba K. El-Khordagui, H. Peter Soyer, Michael S. Roberts, Marc Schneider and Tarl W. Prow

Pharmaceutical Research

Volume **28** (11), 2931–2944, DOI: 10.1007/s11095-011-0561-z

Copyright © Springer Science+Business Media, LLC 2011

Pharm Res (2011) 28:2931–2944
DOI 10.1007/s11095-011-0561-z

RESEARCH PAPER

Gold Nanoparticle Penetration and Reduced Metabolism in Human Skin by Toluene

Hagar I. Labouta • David C. Liu • Lynlee L. Lin • Margaret K. Butler • Jeffrey E. Grice • Anthony P. Raphael • Tobias Kraus • Labiba K. El-Khordagui • H. Peter Soyer • Michael S. Roberts • Marc Schneider • Tarl W. Prow

Received: 23 April 2011 / Accepted: 3 August 2011 / Published online: 11 August 2011
© Springer Science+Business Media, LLC 2011

The full text of this article is available online at:

<http://www.springerlink.com/content/m3wg84un4112r770/>

Abstract

Purpose: To measure penetration and metabolic effects of ion-stabilized, polar, 15 nm gold nanoparticles in aqueous solution (AuNP-Aq) and sterically stabilized, non-polar, 6 nm gold nanoparticles in toluene (AuNP-TOL) on excised human skin.

Methods: Gold nanoparticles were characterized with dynamic light scattering and transmission electron microscopy (TEM). Skin penetration studies were done on frozen or fresh excised skin using static Franz diffusion cells. Viable treated skin was assessed by dermoscopy, reflectance confocal microscopy (RCM), multiphoton tomography (MPT) with fluorescence lifetime imaging microscopy (FLIM), and TEM.

Results: Dermoscopy and RCM showed large aggregates in the furrows of AuNP-Aq-treated skin. Treatment of thawed and viable skin only showed enhanced permeability to nanoparticles in the AuNP-TOL group with MPT and FLIM imaging to stratum spinosum of epidermis. TEM analysis revealed gold nanoparticles within AuNP-treated stratum corneum. FLIM analysis of NAD(P)H showed a significant decrease in total NAD(P)H in all toluene-treated groups.

Conclusions: Gold nanoparticles, 15 nm, in aqueous solution aggregated on the skin surface. Toluene treatment eliminated skin metabolism; skin treated with toluene/gold nanoparticles (6 nm) for 24 h, but not at 4 h, showed increased nanoparticle permeability. These results are of value to nanotoxicology.

Keywords: confocal reflectance microscopy; fluorescence lifetime; multiphoton microscopy; nanoparticle; skin.

Abbreviations

ANOVA: analysis of variance

AuNP: gold nanoparticle(s)

AuNP-Aq: gold nanoparticle in aqueous solution

AuNP-TOL: gold nanoparticle in toluene

BP: band pass filter

EDXS: energy-dispersed X-ray spectroscopy

FLIM: fluorescence lifetime imaging microscopy

HFT KP: dichroic low pass filter

ICP: inductively coupled plasma

MPT: multiphoton tomography

MPT-FLIM: multiphoton tomography with fluorescence lifetime imaging microscopy

NA: numerical aperture

NAD(P)H: nicotinamide adenine dinucleotide and nicotinamide adenine dinucleotide phosphate

RCM: reflectance confocal microscopy

SB: stratum basale

SC: stratum corneum

SG: stratum granulosum

SS: stratum spinosum

TEM: transmission electron microscopy

TEWL: trans-epidermal water loss

VE: viable epidermis

3.3.1. Introduction

Penetration and adverse effects of topical nanoparticle exposure is an important issue for public health, regulatory agencies, and industry [42, 137-138]. Our skin is exposed to a number of nanoparticles from natural and manmade sources. Nanoparticulates, such as zinc oxide and titanium dioxide, are useful sunscreens found in cosmetics. The penetration and nanotoxicology in skin is a debated topic in academia, from small interest groups and regulatory agencies [139-140]. The capacity of nanoparticles to overcome the SC and reach the viable skin is dependent on the model, barrier integrity, nanoparticle (size, shape, surface properties, and charge) and nanoparticle degradation kinetics [137, 141-142]. Tape stripping [143], mechanical flexion [144], UV exposure [87], sonophoresis [76], and microneedles [145] have all been shown to increase nanoparticle penetration in skin. However, there is a gap in the literature with regard to nanoparticle studies done in human skin with a focus on workplace exposure. Yet, there are several toxicity studies based on cell-culture experiments as well as skin penetration studies to evaluate the safety of topical application of nanoparticles. These studies were previously reviewed by Crosera *et al.* [146], Cevc and Vierl [41], Prow *et al.* [142], Schneider *et al.* [42], and others.

Nanoparticle skin exposure can come from topical products, but, importantly, workplace exposure is a critical area of nanotoxicology without a significant knowledge base [141, 147-148]. Solvents are commonly used in the workplace [149] and in the synthesis of nanomaterials [150]. While solvent effects on drug penetration kinetics have been studied extensively [151-152], very few studies exist on penetration and toxic effects of solvent/nanoparticle in topical exposure scenarios [148].

Beyond the workplace, separating solvent and nanoparticle effects is critical for estimating toxicity. One example is the case of colloidal fullerene nanoparticles reported to be toxic in a variety of tests, where the toxicity is now being attributed to the solvent, tetrahydrofuran, and not the nanoparticle [153]. We hypothesised that AuNP could serve as model nanoparticles for examining the combined effects of topical nanoparticles and solvents. This is the first report to simultaneously quantify

nanoparticle penetration and metabolic effects of toluene and nanoparticles in human skin.

Xia *et al.* (2010) reported on the penetration of small fullerene nanoparticles, 1 nm, in four solvents—toluene, cyclohexane, chloroform, and mineral oil—on Yorkshire weanling pigs [148]. Chloroform, cyclohexane, and toluene increased nanoparticle penetration into deeper layers of the SC. Toluene was the second solvent after chloroform promoting fullerene penetration into SC. Xia *et al.* proposed that the mechanism of action was not wholly due to the solubility of the nanoparticle in the solvent. Further, two other mechanisms were proposed including solvent flux and solvent evaporation-induced supersaturation [148]. Our goal was to evaluate the solvent and nanoparticle combination. We chose AuNP as a model nanoparticle because of the inert nature of gold and the capacity to track these particles by two-photon luminescence [118, 134].

Noble metal photoluminescence was described in 1969 [137] and two-photon luminescence reported in 1986 [154]. The optical and photonic properties of AuNP are favorable for biomedical imaging, in part because of enhanced light absorption to 1.4×10^7 and $3.7 \times 10^8 \text{ M}^{-1} \text{ cm}^{-1}$ for 5 nm and 15 nm particles, respectively. However, the body of literature in the field of dermatology is limited with regard to topical AuNP application. There are several reports on AuNP effects on cultures of skin-derived cell lines [155-157]. However, there are no reports on the metabolic consequences of topical AuNP application on skin or any reports measuring penetration depth of nanoparticles less than 12 nm in human skin. Sonavane *et al.* (2008), showed penetration of 15 nm AuNP through excised rat skin after 24 h [45]. These data show that there is potential for small AuNP to penetrate deep enough through skin to reach the circulatory system in the dermis; thus, there may be some risk of systemic nanoparticle exposure. A recent report by Larese Filon *et al.* (2011) supports the earlier findings of Sonavane. They found similar results when evaluating AuNP penetration (12.9 nm) in thawed human skin [58]. AuNP were detected in the receiving solution of the Franz cells after 24 h of skin exposure. The authors also investigated the effects of skin abrasion on AuNP penetration.

The objectives of this study include an in-depth investigation of the consequences of topical exposure to two AuNP formulations, with different size, charge, surface

chemistry, and vehicle, in terms of penetration and metabolic changes in human skin using multiphoton tomography (MPT), TEM, reflectance confocal microscopy (RCM), dermoscopy, and fluorescence lifetime imaging microscopy (FLIM). Our data suggest that toluene, a common industrial solvent, is associated with increased nanoparticle penetration through viable human skin, but only after long-term exposure.

3.3.2. Materials and methods

AuNP-Aq synthesis. Ionically-stabilized polar AuNP were prepared using the Turkevich method [132]. A 100 µg/ml solution of hydrogen tetrachloroaurate (70 ml, $\text{HAuCl}_4 \cdot 3\text{H}_2\text{O}$, Sigma-Aldrich Chemie GmbH, Steinheim, Germany) was heated to 100°C under stirring at 440 rpm and then reduced by adding a solution of trisodium citrate dihydrate ($\text{Na}_3\text{C}_6\text{H}_5\text{O}_7 \cdot 2\text{H}_2\text{O}$, Sigma-Aldrich) containing 5-fold molar concentration of gold salt. After the gold colloid had formed, the temperature was lowered to 25°C. The colloid was then stored at 4°C in the dark.

AuNP-TOL synthesis. Sterically stabilized apolar AuNP were synthesized as described by Zheng *et al.* [158]. AuNP were formed upon gold reduction by an amine-borane complex in the presence of an alkyl thiol. In a typical synthesis, 0.31 g chlorotriphenylphosphine gold (purity 98%, ABCR, Karlsruhe, Germany) was dissolved in 50 ml of benzene (purity >99.5%, Riedel-de Haen, Germany), forming a colorless solution. A mixture of 0.53 g tert-butylamineborane (purity, 97%, Fluka, Germany) and 0.31 ml dodecanethiol (purity >98%, Fluka, Germany) was added to the formed solution and left to react at 55°C for 1 h. Upon completion of the reduction reaction, the red solution was cooled to room temperature, precipitated by the addition of ethanol and washed by centrifugation and subsequent resuspension in toluene. Finally, the resuspended particles were stored at room temperature away from light.

Nanoparticle characterization. The optical properties of the AuNP were recorded using a UV/Vis spectrophotometer (lambda 35, Perkin Elmer LAS, Germany) in the range of 400–800 nm. Mean particle size of the gold core (n=30) and morphology were determined by transmission electron microscopy (TEM) using a JOEL Model

JEM 2010 instrument (JOEL GmbH, Echting, Germany) operated at an accelerating voltage of 120 kV. Samples for TEM analysis were prepared by placing 12 μl of dispersed nanoparticles on carbon-coated 400 mesh copper grids. The solvent was allowed to evaporate at room temperature. The nanoparticle hydrodynamic radius was measured using a Malvern Zetasizer Nano (Malvern Instruments, Malvern, UK) based on dynamic light scattering at 25°C. The surface charge of AuNP-Aq was estimated by measuring the zeta potential based on the electrophoretic mobility (Zetasizer Nano, Malvern Instruments, Malvern, UK) in water. The samples (1.5 ml) were run in triplicate using disposable folded capillary cells that contained the electrodes.

Excised human skin preparation. Human skin was obtained from abdominoplasty patients with the approval of either the Research Ethic Committee of Saarland, Germany (Ärztchamber des Saarlandes, Dec. 2008) (thawed skin experiments) or Princess Alexandra Hospital Research Ethics Committee (No. 1997/097), Australia (viable skin experiments). All volunteers had previously signed informed consent forms. Eleven skin donors were used in this study. The subcutaneous fatty tissue was immediately removed from the skin. The surface of each specimen was cleaned with water. For thawed skin experiments, skin specimens were wrapped in aluminum foil and stored in polyethylene bags at 4°C or -26°C for less than 6 months before further usage. Previous investigations have shown that there is no change in the penetration characteristics of drugs through thawed skin stored frozen for 6 months [159].

Skin discs, 25 mm in diameter, were cut, thawed, cleaned with deionized water/Ringer solution, and transferred into the Franz diffusion cells. Transepidermal water loss (TEWL) was measured with a Biox AquaFlux Condenser Chamber unit (model AF200) to assess barrier integrity before and after 24 h treatment.

Skin penetration studies. *Ex vivo* penetration experiments were carried out in static Franz diffusion cells with previously frozen and viable skin. Skin was mounted in Franz cells with a diffusion area of 1.8 cm^2 and 1.1 cm^2 and receptor compartment volumes of 12 ml and 3.2 ml volume for frozen and viable skin experiments, respectively. Receptor solution was phosphate-buffered saline, pH 7.4, magnetically stirred at 500 rpm. Nanoparticle-containing solutions in their original dispersion

medium, 500 μ l at 90 μ g/ml, were topically applied in the donor cell. Diffusion cells were maintained at 32°C throughout the 4 and 24 h exposure experiments. Following treatment, the excess nanoparticle solution was drained, and the skin was removed.

Cryosectioning. Skin was fixed, embedded, and sectioned as previously described [138]. Skin was fixed in 2% paraformaldehyde in 0.1 M phosphate buffer pH 7.4 for 2 h at room temperature. Skin sections (10–50 μ m thick) were cut at –20°C using a SLEE cryostat type mev (SLEE medical GmbH, Mainz, Germany) or Leica CM1850 cryostat (Leica microsystems, Heidelberg, Nussloch, Germany). The sections were mounted in Prolong Gold (Invitrogen, Mulgrave, Victoria, Australia) or FluorSave™ (Calbiochem, San Diego, USA) prior to microscopic analysis. On cryosectioning, placement of the skin punch was not parallel to the cutting blade of the cryotome to avoid dislocation of the particles from outside into the deeper skin layers or vice versa, but in a perpendicular position limiting sectioning artifacts [134].

Dermoscopy and reflectance confocal microscopy (RCM). Treated skin was visualized using RCM (Vivascope 1500, Lucid Inc., Henrietta, NY) with an in-built dermascope used for visualization of treated skin surface and localization of nanoparticle aggregates on and within skin. Color dermoscopy images were taken to 6x6 mm² at 1000x1000 px². RCM carried out at 830 nm with an optical power between the range of 3–6.9 mW was used to take 500x500 μ m images at 30X magnification.

A z-stack was taken with images taken every 2 μ m from the skin surface to a depth of 100 μ m. ImageJ (National Institutes of Health, Bethesda, Washington, D.C., USA) was used to analyse the mean intensity of AuNP in the SC of furrow depth using a threshold of 240–255 to identify highly reflective areas and to render RCM images in 3D.

Thawed skin MPT. MPT imaging was performed using an inverted confocal/two-photon excitation fluorescence microscope (Zeiss LSM 510 META system, Carl Zeiss, Jena, Germany), equipped with a Chameleon infrared laser (λ =710–930 nm). The objective was a water immersion lens 63X NA=1.2; an excitation wavelength of 800 nm, dichroic beam splitters HFT KP 700/488 nm, and an emission filter BP 560–615 nm filter were used. Transmission light images of the skin sections were also

taken simultaneously and shown as overlays with the nanoparticle luminescence. Z-stacks were taken with steps every 1 μm until there was no detectable signal. An excitation radiation with transmission energy of 0.6 and 0.5 mW was used for skin and nanoparticle tracks, respectively.

Viable skin MPT and FLIM. A multiphoton tomograph (DermalInspect[®], JenLab GmbH, Jena, Germany) equipped with a time-correlated single photon counting detectors, FLIM system (Becker and Hickl, Berlin, Germany) was used to simultaneously image nanoparticles and endogenous NAD(P)H as described previously [142]. A tuneable laser (Mai Tai, Spectra physics, Mountain View, USA) with a range of 710–920 nm was used as the excitation source and ultra-short pulse width (65 fs) in pulsed mode-locked at 80 MHz. Treated skin was optically sectioned using MPT-FLIM with a 740 nm excitation wavelength from SC to SB in 5 μm increments using 40X objective lens with an image size of 210 \times 210 μm^2 . The emission was filtered with a 350–650 nm band pass filter (BG39), a <700 nm short pass optical filter, and a 350–450 nm band pass filter. A constant excitation power of 30 mW at the rear of the objective was used. At least three biological replicates were analysed at 4 and 24 h of treatment for each group.

Resulting FLIM data were analyzed with SPC 830 2.9 Image software (Becker and Hickl) to generate fluorescence lifetime decay and photon contribution curves from NAD(P)H autofluorescence and gold luminescence. The instrument response function of each FLIM image was calibrated to a sucrose crystal standard (Ajax Finechem Pty Ltd.). The fluorescence decay curve was fitted with a double exponential model, $N(t) = \alpha_1 e^{-t/\tau_1} + \alpha_2 e^{-t/\tau_2}$, that defines the short and long lifetime/amplitude values. NAD(P)H-related metabolic rate and AuNP luminescence were quantified as previously described [142, 160]. NAD(P)H autofluorescence was isolated using $\alpha_1\%$ from 45–85, and AuNP luminescence was isolated from NAD(P)H using $\alpha_1\%$ from 90–100. The $\alpha_1\%$ is the proportion of the emission photons that return to the detector during the short lifetime phase of the decay curve, and the $\alpha_2\%$ represents the proportion of long lifetime photons. Although fluorescence lifetime changes with changes in the microenvironment, the $\alpha_1\%$ does not. This allows the AuNP luminescence positive pixels to be separated from skin autofluorescence.

Transmission electron microscopy. A high resolution TEM microscope, fitted with EDXS and selected area electron diffraction, was used to visualize AuNP in treated skin samples. High pressure freezing was used to preserve the skin ultrastructure using a Leica EM PACT2 system. Skin was placed in a 1.5x0.2 mm well with a membrane carrier coated with 1-hexadecene and filled with 1-hexadecene and then rapidly frozen. Samples were then stored in liquid nitrogen and transferred to vials containing 1% osmium tetroxide (OsO₄), 0.5% uranyl acetate, and 5% H₂O in acetone. Samples were then cryosubstituted at -85°C for two days before being gradually warmed to room temperature. After cryosubstitution, the sample was removed from the membrane carrier, washed in acetone, and infiltrated in Epon resin with the use of a microwave (3x40 s, 250 W, no vacuum). Infiltration was gradually carried out with Epon in steps of 1:3, 1:2, 1:1, 2:1, 3:1, 100% and 100% Epon:acetone steps (2x3 min, 250 W, vacuum) using a microwave (Biowave, Pelco) at 60°C. Ultrathin sections (60 nm thickness) were cut from the polymerised block, collected on Formvar-coated 200 mesh copper grids, and examined using a JOEL 2010 transmission electron microscope with 80 kV power.

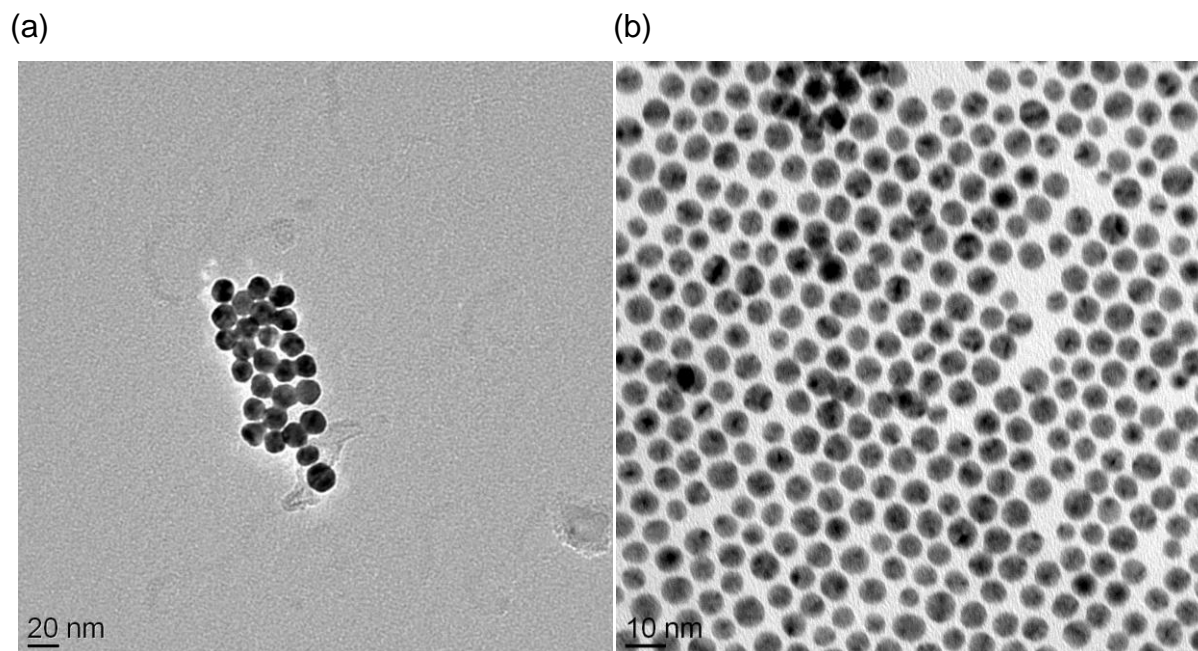
Statistical analysis. Differences in measured macroscopic parameters of treated and control groups were tested applying the non-parametric Mann-Whitney t-test. Two-way ANOVA analysis was used to determine significance within multiple groups. Level of significance was accepted at $p \leq 0.05$.

3.3.3. Results

Characterization of AuNP. Dynamic light scattering was used to assess physical properties of two nanoparticles formulations (Table 3.3.1). Both nanoparticles were monodisperse as shown by TEM. Nanoparticle diameters were confirmed with TEM (Figure 3.3.1). Zeta potential measurements showed that the AuNP-Aq were negatively charged and the AuNP-TOL were uncharged. Both prepared AuNP dispersions showed physical stability and no aggregation. Aggregation of AuNP would be indicated by a large red-shift of the spectral peak and/or strong peak broadening [161].

Table 3.3.1: Characteristics of the Prepared AuNP Dispersion

AuNP-code	Surface chemistry	Size of gold core, nm	DLS diameter, nm	Zeta potential, mV	Vehicle
AuNP-Aq	Citrate ions	14.9±1.8	15.3±0.7	-35.1±1.87	Water
AuNP-TOL	Dodecanethiol	6.0±0.8	7.2±0.9	Uncharged	Toluene

**Figure 3.3.1:** (a) Citrate-stabilized AuNP-Aq and (b) thiol-coated AuNP-TOL imaged with TEM.

Excised human skin barrier integrity. Transepidermal water loss was used as an indicator of barrier integrity. After receipt, skin was cut into circular pieces and mounted in Franz cells. We then evaluated TEWL in specimens before and after 24 h of treatment. The mean±SE of TEWL was 26±1, 25±1, 25±2 and 27±1 g/(m²h) for the aqueous, toluene, AuNP-Aq, and AuNP-TOL groups before treatment. After 24 h, TEWL had increased to double for all groups. There was no statistical significance between any two groups within a single time point, and there was significant TEWL increase in all groups after 24 h treatment to $p < 0.0001$.

Dermoscopy of AuNP-treated skin. After 24 h treatment, skin surface of AuNP-treated and vehicle-only skin samples was visualized using dermoscopy (Figure 3.3.2a–d). Fine purple lines corresponding to the furrows can be seen in AuNP-treated skin (Figure 3.3.2c–d). The color is reminiscent of AuNP aggregates. There was more intense and bluer color associated with the AuNP-Aq treated skin

compared to the AuNP-TOL group, pointing towards increased aggregation with the aqueous-formulated AuNP.

RCM of AuNP-treated skin. The resolution of RCM enables visualization of cellular morphology and large, reflective nanoparticle aggregates [142]. Treated skin was imaged with RCM after 24 h treatment. With RCM we observed distinct morphological changes that suggested toxicity in toluene-treated skin (Figure 3.3.2f, h) but not in skin treated with aqueous dispersions (Figure 2e, g). Highly reflective aggregates were seen in both nanoparticle treated groups (Figure 2g, h) but not in vehicle-only controls (Figure 3.3.2e, f). Aggregates were most prominent in the AuNP-Aq group, supporting the hypothesis that the AuNP-Aq were highly aggregated on the skin surface (Figure 3.3.2c, g). As in the dermoscopy images, there were fewer AuNP-TOL aggregates than observed in the AuNP-Aq group (Figure 3.3.2g, h). Aggregates were only observed on and within the upper SC in nanoparticle-treated groups. The dermoscopy and *en face* RCM images showed that there were AuNP aggregates within the skin furrows. A 3D reconstruction of the RCM z-stacks confirmed the presence of large aggregates within the furrows of AuNP-Aq treated groups and the absence of these aggregates in all other groups (Figure 3.3.3). Figure 3.3.3 shows treated skin from a cross-sectional point of view. The dotted line highlights the surface of the skin; the arrowhead in Figure 3.3.3b indicates a representative cluster deep within a furrow.

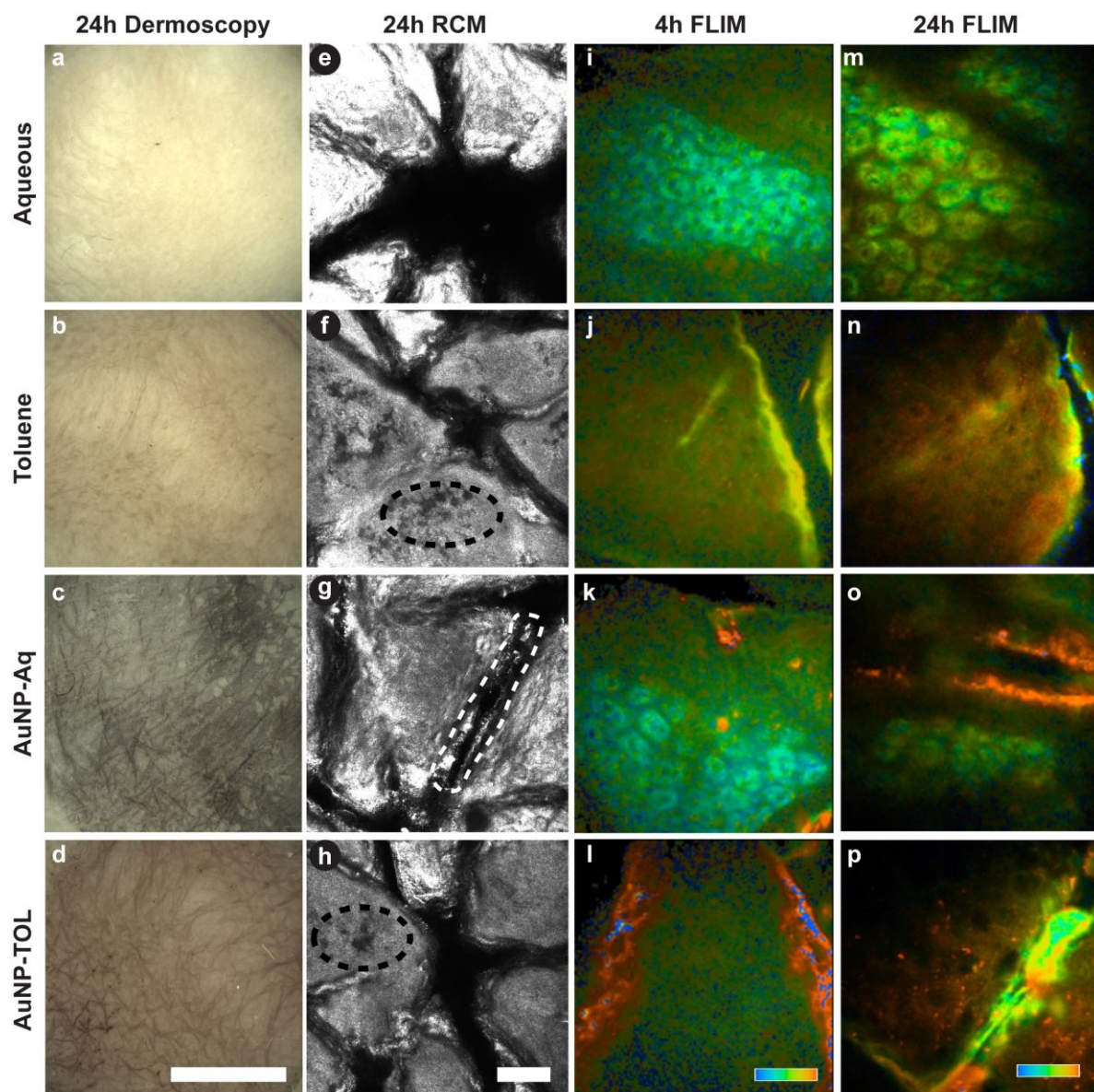


Figure 3.3.2: Dermoscopy, RCM and MPT-FLIM images of treated human skin. Dermoscopy and RCM images showing the surface of skin specimens treated with aqueous solution, toluene, AuNP-Aq, and AuNP-TOL for 24 h for dermoscopy (a–d) and for RCM images (e–h). Black dashed line indicates abnormal reflectance structure within the toluene treated skin (f, h); white dashed line shows highly reflective particles on the surface of the skin (g). FLIM images from the stratum granulosum layer of the epidermis from skin treated for 4 (i–l) and 24 h (m–p). Scale bars: 4 mm (d); 50 μ m (h, l, p); pseudocolored MPT-FLIM images are $\alpha_1\%$ 50–100 from blue to red. Blue-green coloration indicates cellular autofluorescence, i.e. NAD(P)H, and gold nanoparticle luminescence is orange to red (k, l, o, p).

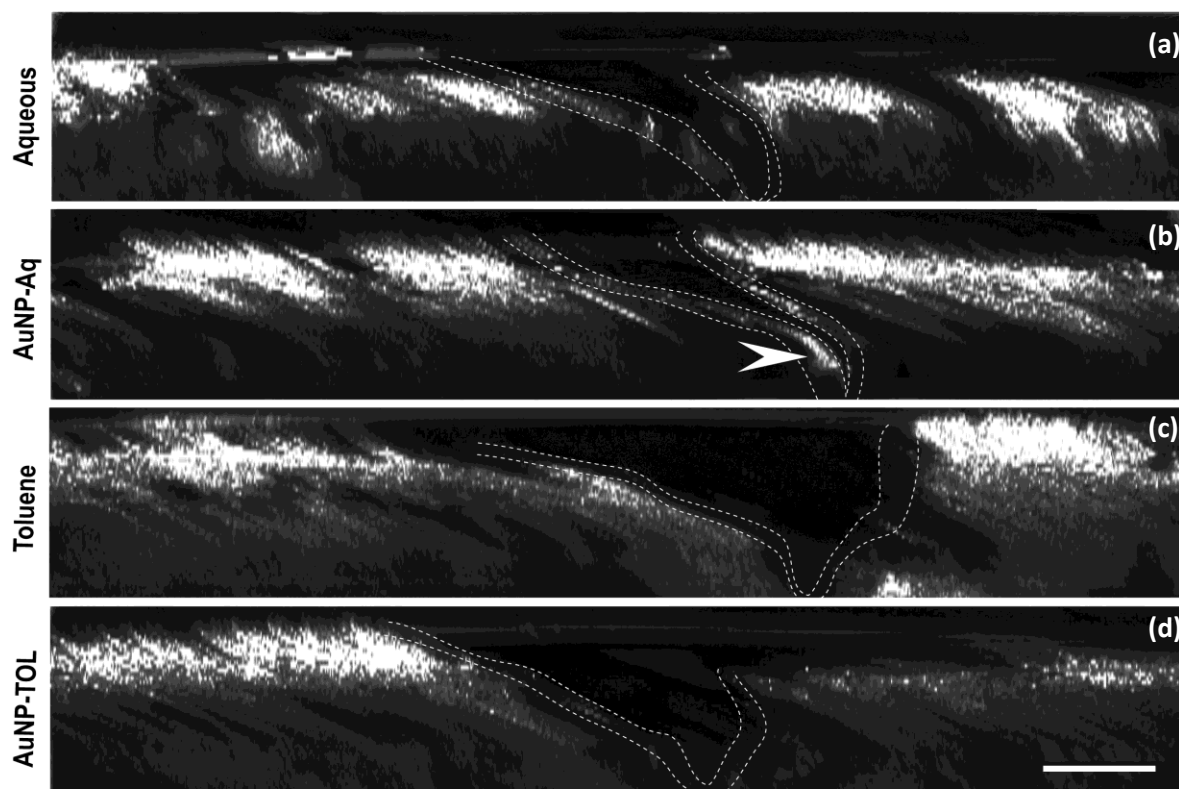


Figure 3.3.3: 3D reconstructed RCM images rendered in cross section. 3D reconstructed RCM images of skin specimens treated with aqueous solution, AuNP-Aq, toluene and AuNP-TOL. The stratum corneum within the furrows is highlighted with dotted lines. The arrowhead indicates gold nanoparticle aggregates deep within the furrow. Scale bar: 50 μm .

En Face MPT-FLIM analysis of viable skin treated for 4 and 24 hours. The fluorescence lifetime decay curve contains a short and a long component in this context. The short component represents the photons that return to the detectors quickly, i.e. in the ultrafast multiphoton excited photoluminescence that results from metal nanoparticles and second harmonic generation from collagen. The lifetime is usually reported in picosecond or nanosecond units. Fluorescence lifetimes can change with the microenvironment and are thus not optimal for separating AuNP and NAD(P)H. The $\alpha\%$ is the proportion of photons that have short or long lifetimes; this proportion does not change with changes in the microenvironment or concentration. Therefore, we use $\alpha\%$ ranges to separate AuNP and NAD(P)H, where intensity changes represent changes in concentration. Skin treated for 4 and 24 h was subjected to MPT-FLIM analysis. The images shown in Figure 3.3.2i–p are from the SG layer and are pseudocolored at $\alpha_1\%$ 50–100% (blue to red). The autofluorescent components of living skin, i.e. NAD(P)H and keratin, can be seen in Figure 3.3.2i, m, k, o in green and blue. AuNP luminescence is shown in orange to red in Figure

3.3.2k, l, o, p. AuNP signal can be seen primarily in the furrows of nanoparticle treated skin. Skin treated with aqueous formulations shows clear keratinocyte morphology due to NAD(P)H, found primarily in active mitochondria. Toluene-treated skin shows an absence of NAD(P)H autofluorescence. Skin treated for 24 h with AuNP-TOL revealed AuNP signals from the SG suggesting some nanoparticle penetration. This phenomenon was not observed in any other group.

Cross-section analysis of nanoparticle penetration with TEM, MPT, and MPT-FLIM. Frozen sections of thawed skin treated with nanoparticle formulations for 24 h showed AuNP luminescence within the epidermis in AuNP-TOL but not in AuNP-Aq treated samples (Figure 3.3.4). We then used TEM to assess nanoparticle penetration and tissue ultrastructure in viable human skin. Skin treated for 24 h was subject to high pressure freezing for TEM or cryopreservation for MPT-FLIM (Figure 3.3.5). TEM imaging showed ultrastructure indications of toxicity in toluene-treated skin. SC showed some delamination, but there were significant signs of toxicity in the viable epidermis. Cell membranes were severely disrupted, including mitochondria and cell junctions (Figure 3.3.5b, d). The electron-dense nature of AuNP results in increased electron scattering of the incident electrons and thus appears as dark spots in TEM images. AuNP were found on the skin surface and up to two cell layers deep in SC of AuNP-Aq-treated skin (Figure 3.3.5g). AuNP were found up to ten cell layers deep in the AuNP-TOL-treated skin, but could not be identified within the viable epidermal layers. This may be due to increased particulate background from the staining solution binding to particulates associated with toluene-damaged tissue (Figure 3.3.5c, d).

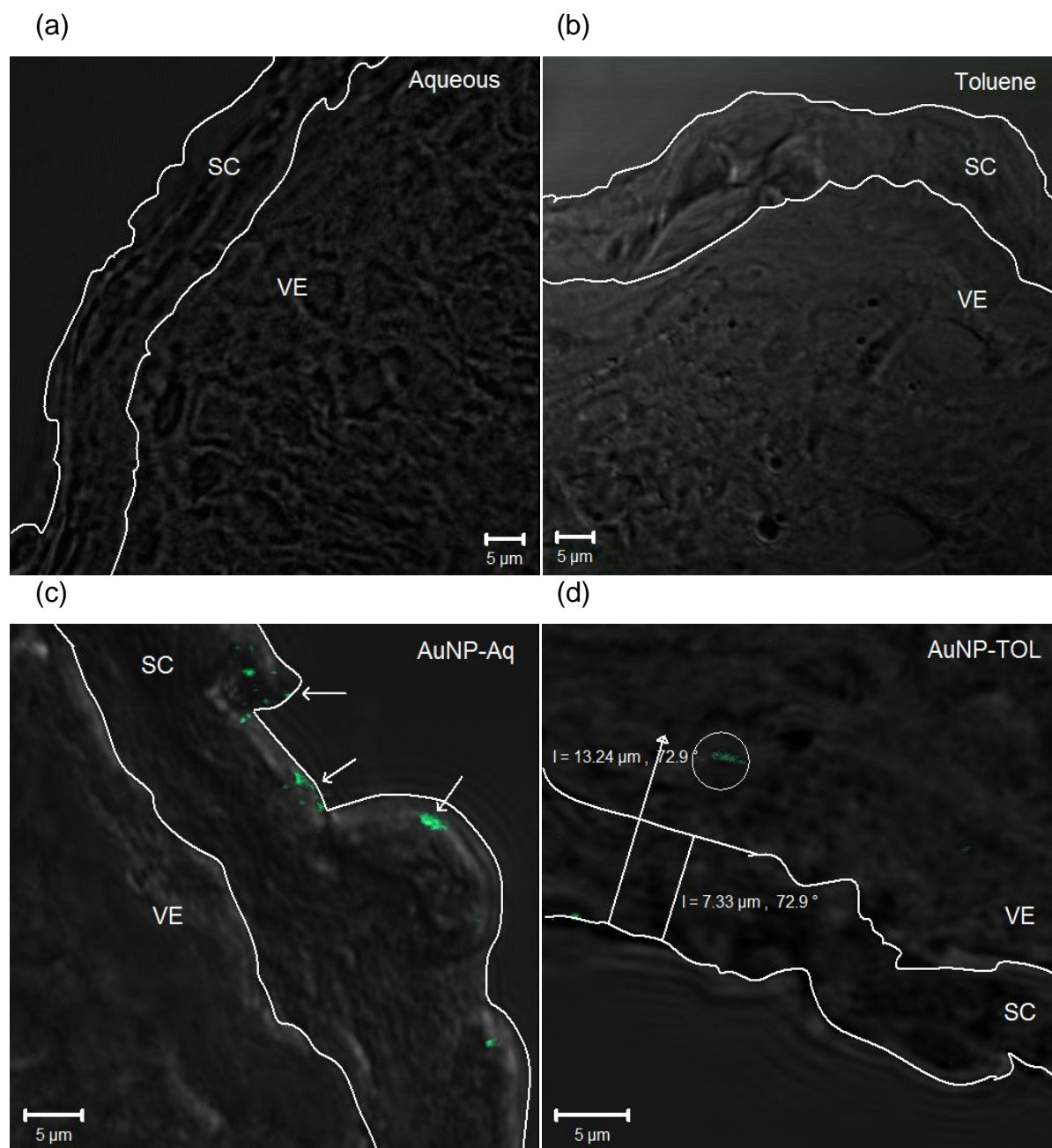


Figure 3.3.4: MPT of thawed skin treated for 24 h. (a–d) 10 μm-thick cryosectioned skin from aqueous, toluene, AuNP-Aq, and AuNP-TOL groups. The images are overlays of light transmission and gold luminescence images. The stratum corneum and viable epidermis are labelled SC and VE; the SC is outlined in white. The white arrows indicate AuNP in the AuNP-Aq image and the circle indicates AuNP in the AuNP-TOL image that is 13 μm deep.

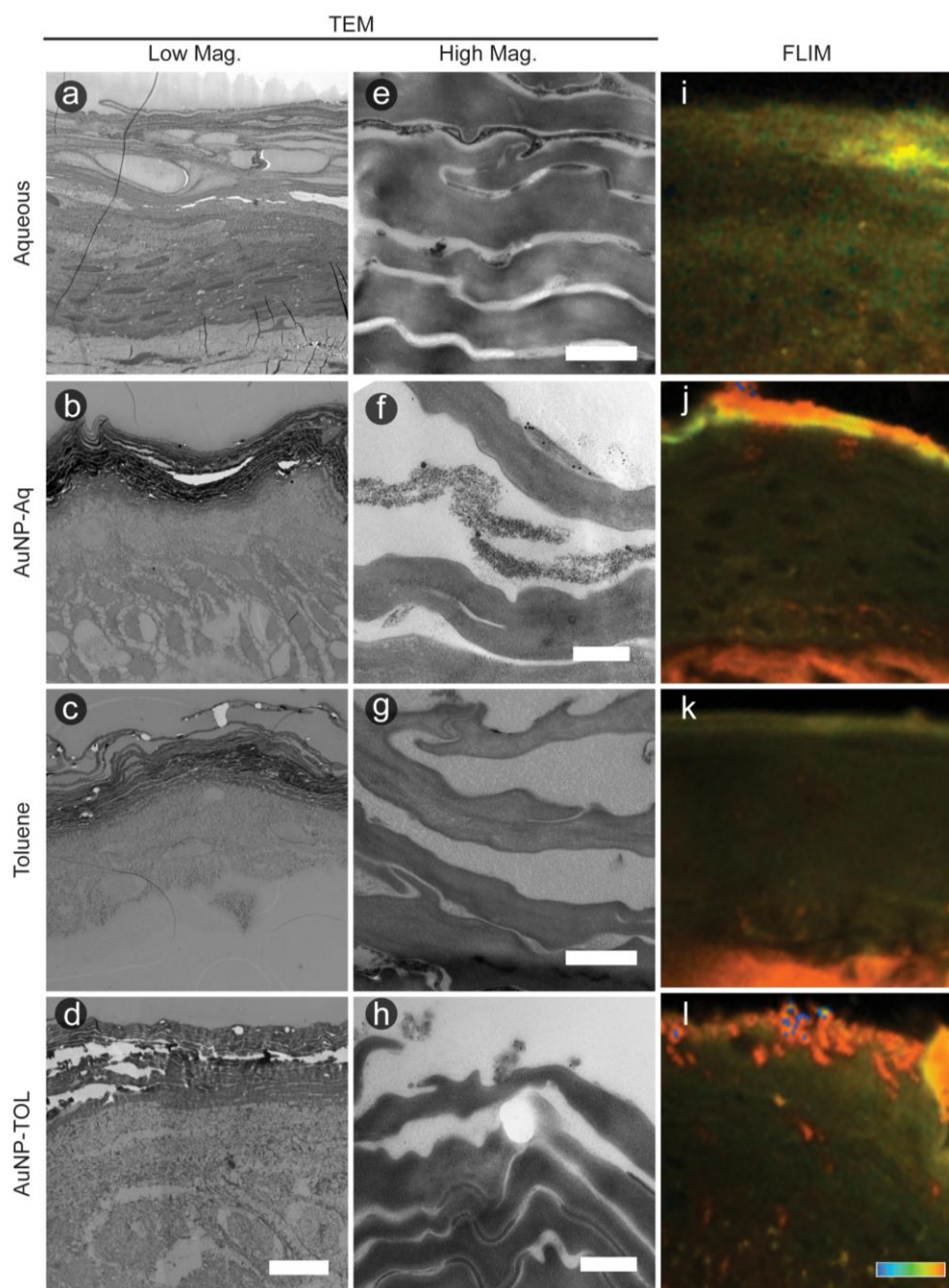


Figure 3.3.5: Gold nanoparticle penetration in cross-sections using TEM and MPT-FLIM. Low and high magnification images of the epidermis and superficial stratum corneum from each of the treatment groups (a–h). Scale bars: 1 μm (a–d); 200 nm (e, f); 500 nm (g, h). Pseudocolored MPT-FLIM images (i–l) show the penetration pattern of gold nanoparticles (orange to red). MPT-FLIM imaging with a 740 nm excitation wavelength and emission was filtered with a 350–650 nm band pass filter (BG39). (i–l) Scale bar: 50 μm ; pseudocolored MPT-FLIM images are $\alpha\%$ 50–100 from blue to red.

Quantification of multiphoton images was conducted. Representative optical z-stacks, 1 μm nominal step width, for examined thawed skin cross-sections were then quantified, according to a method we developed and recently published elsewhere [134]. Briefly, the method of quantification is based on calculation of Σ pixel frequency due to AuNP in the SC and DSL, from which weighed number of particles were calculated. No particles were quantified in DSL of thawed skin specimens treated with AuNP-Aq. On the other hand, results showed depth-profile for AuNP-TOL having higher numbers of AuNP in the upper skin layer, SC (1082 nanoparticles) rather than viable epidermis (470 nanoparticles) [134].

We used MPT-FLIM to separate cellular autofluorescence from AuNP luminescence. In Figure 3.3.5i, j, cryosections of treated skin are shown with MPT-FLIM and are pseudocolored from blue to red for α_1 % 50–100%. Cellular autofluorescence is shown in green to yellow; AuNP luminescence is shown in orange to red. These colors correspond to relatively slow autofluorescence lifetime and relatively instantaneous nature of AuNP luminescence. Images are oriented so the SC is at the top and dermis is towards the bottom. Aqueous-treated samples (Figure 3.3.5i, j) show an even green signal through the viable epidermis with dark ellipsoids suggestive of nuclei in position, size, and absence of NAD(P)H signals. These morphological queues are not prominent in toluene-treated skin (Figure 3.3.5k, l), suggesting a lack of the usual membranes that partition NAD(P)H out of the nucleus. The orange signal at the bottom of Figure 3.3.5j, k is likely to be collagen second harmonic generation, where the green-orange interface is the dermal epidermal junction. The second harmonic signal from collagen has overlapping lifetime characteristics with gold luminescence, resulting in an indistinguishable lifetime signature that limits identifying AuNP signals to the epidermis. Only AuNP-treated groups show strong signals at the skin surface (Figure 3.3.5k, l). The key difference between the AuNP-Aq and AuNP-TOL images was the presence of punctuate AuNP signals with a depth-dependent decrease in number from within the viable epidermis in the AuNP-TOL (Figure 3.3.5l), but not in the AuNP-Aq-treated skin (Figure 3.3.5j). These data indicate that AuNP penetrated deeper within human skin in presence of toluene for 24 h. Importantly, these images were taken from the centre of thick (50 μm) cryosections to minimize potential edge contamination effects, and the punctuate signal pattern was not observed in any of the other treatment groups, including toluene-only control.

En Face MPT-FLIM intensity measurement of AuNP luminescence in human skin. Penetration profiles of AuNP luminescence signals are shown for 4 and 24 h treatment groups in Figure 3.3.6a, b. Depth stacks of MPT-FLIM images were taken of treated human skin; AuNP luminescence signal was quantified using a stringent range of $\alpha_1\%$ 90–100 to exclude skin autofluorescence. Significantly more AuNP signal was detected deep in the SC in the AuNP-TOL group at 4 h ($p < 0.001$), but not in the other 4-hour treatment groups (Figure 3.3.6a). AuNP luminescence signals were found within the SC in both AuNP treatment groups after 24 h treatment, but not in vehicle-only groups (Figure 3.3.6b). AuNP luminescence signals were found significantly deeper in the AuNP-TOL-treated group than AuNP-Aq group at 24 h ($p < 0.05$), supporting the histological findings above. Intensity of gold aggregate reflectance signal in furrows was quantified from RCM analysis (Figure 3.3.6c). These data show the presence of significantly more highly reflective aggregates deep within the furrows of AuNP-Aq-treated skin ($p < 0.0001$), compared to all other groups.

MPT-FLIM analysis of NAD(P)H at 4 and 24 hours post-treatment. MPT-FLIM analysis of NAD(P)H was carried out in epidermis of excised human skin. FLIM data were taken via a depth series of *en face* images that were processed to quantify total NAD(P)H intensity and α_1/α_2 ratio. The α_1/α_2 ratio is inversely related to the metabolic rate [162]. Toluene-treated skin, including toluene alone and AuNP-TOL, at both 4 and 24 h showed low NAD(P)H signals similar to those seen in non-viable skin (Figure 3.3.2j, n, l, p; Figure 3.3.7a, b) [163]. Total NAD(P)H signal in toluene-treated groups was significantly depressed when compared to the aqueous groups, $p < 0.001$. After 4-hour treatment with AuNP-Aq, total NAD(P)H levels were significantly lower than aqueous-only controls, $p < 0.01$. α_1/α_2 data mirrored the total NAD(P)H results with a significant increase in the ratio of toluene-treated groups compared to the aqueous groups ($p < 0.001$) (Figure 3.3.7c, d). At 24-hour treatment, differences in α_1/α_2 ratio were less pronounced than in total NAD(P)H analysis. This may be due to natural skin necrosis after removal from the donor, as we have previously reported [163]. Unlike the total NAD(P)H data, the α_1/α_2 ratio data showed no differences between the aqueous groups.

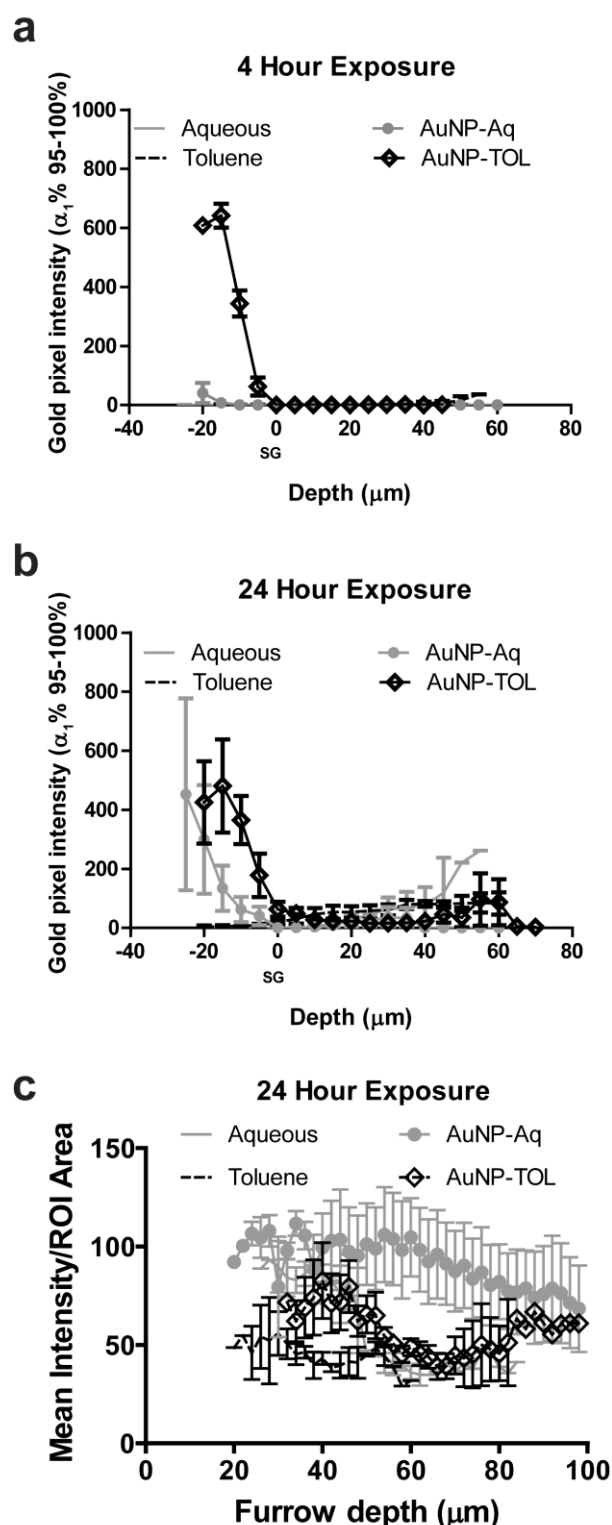


Figure 3.3.6: Gold nanoparticle luminescence and reflectance skin profiles. Data from MPT-FLIM depth series (SG indicates the stratum granulosum) were processed to identify gold nanoparticle luminescence intensity as a function of depth in non-furrow-containing regions. Data are shown for both 4 and 24 h treatment groups (a, b). Furrow reflectance intensity was derived from the stratum corneum and outer surface of furrow areas; the top of the skin is at 0 μm (c). These data were gathered from a depth series of *en face* images.

3.3.4. Discussion

Nanoparticle skin penetration is a multi-factorial and multistep process that is affected by a number of factors, including the skin type, barrier damage, and inherent physicochemical attributes (size, shape, surface charge, etc.) and vehicle of the applied colloids. Measuring nanoparticle penetration and NAD(P)H effects in excised human skin was the focus of this microscopy study. Human skin was chosen, being regarded as the “gold standard” and most reliable set-up for *in vitro* skin penetration studies, especially in human dermal risk assessment [48]. The public could come in contact with nanoparticles non-intentionally in daily life via handling of several products such as cleaning agents, sport clothes, paints, etc., in addition to environmental exposure to water and air contaminated with nanoparticles.

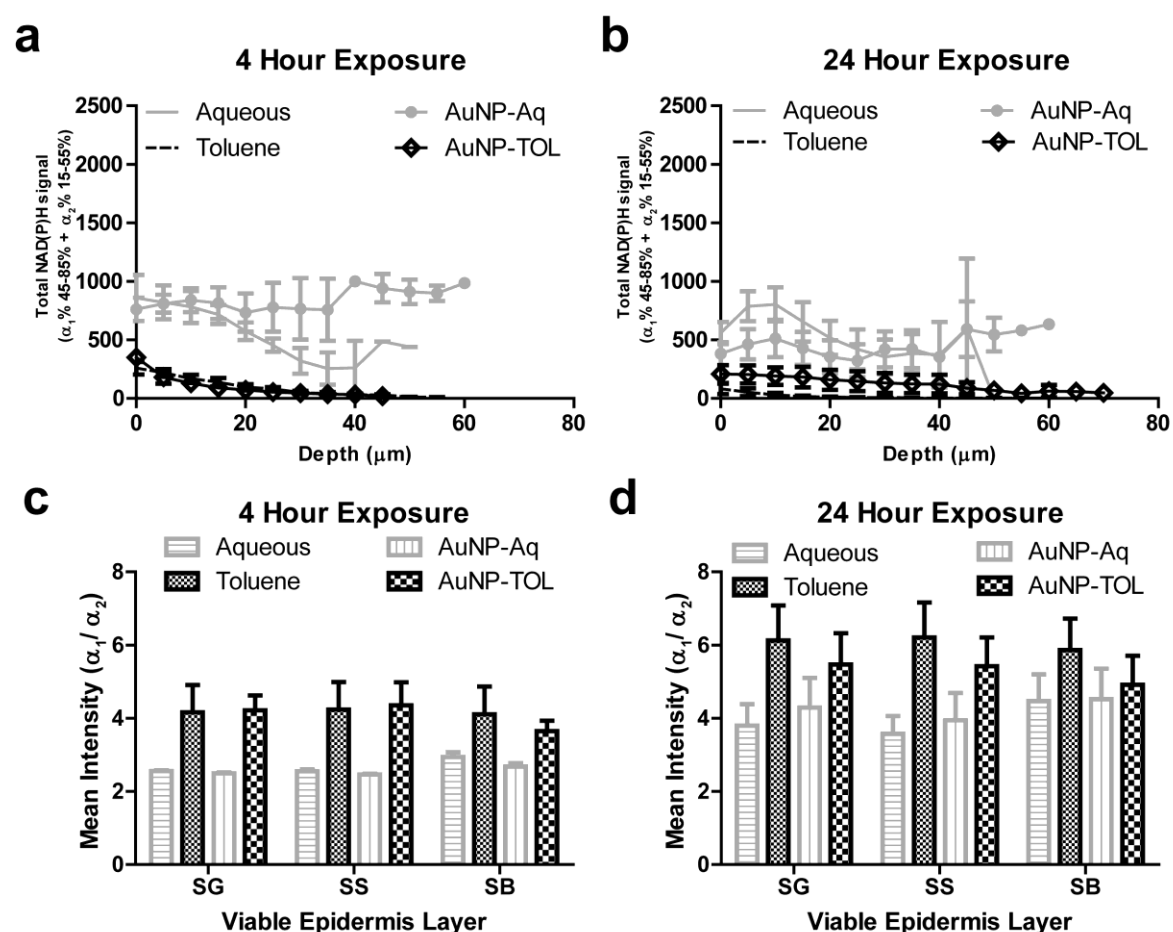


Figure 3.3.7: NAD(P)H effects from MTP-FLIM imaging. NAD(P)H signals were separated from gold nanoparticle luminescence by selecting $\alpha_1\%$ 45–85. NAD(P)H intensity with depth in non-furrow areas (SG (stratum granulosum), SS (stratum spinosum) and SB (stratum basale)) from skin treated for 4 and 24 h (a, b). The α_1/α_2 ratio is inversely related to the metabolic rate and was calculated for each of the treatment groups at 4 and 24 h (c, d).

Last but not least, the safety of personnel working in industry and research handling nanoparticles was not in focus. Though nanotechnology is finding a lot of applications in pharmaceutical industry, safety issues should be further studied, highlighting the importance of this study. Aside from occupational health issues, studying the behavior of nanoparticles with the skin barrier is a very important basic research approach for later application in designing topical drug delivery systems with optimal parameters. This is especially true when solvents like terpenes are used in topical formulations [164]. Our experimental design was congruent with previous gold nanoparticle skin penetration studies with similar exposure times and use of static Franz cells. Our study design was unique because we evaluated viable human skin and utilized clinical dermoscopy, RCM and MPT-FLIM. Therefore, our results can be directly compared to future clinical studies because our assessment technologies can be applied *in vivo*.

Sonavane *et al.* (2008) showed that 15-nm AuNP in aqueous solution were capable of penetrating through full thickness rat skin over 24 h using spectrophotometry and TEM [45]. Similarly, Larese Filon *et al.* (2011) showed AuNP penetration after 24 h using ICP to detect gold ions in the receptor [58]. Our study showed penetration into SC but not beyond using 14.9-nm AuNP in aqueous solution with TEM, MPT-FLIM, and RCM. This incongruity with the rat skin study by Sonovane *et al.* and thawed human skin by Larese Filon *et al.* might be due to the type of skin used. Viable rat skin is thinner and more permeable to nanoparticles than viable human skin [73, 142]. Thawed human skin is non-viable [163] and, therefore, is likely to be more permeable to nanoparticles than viable human skin. The use of MPT-FLIM to detect luminescent nanoparticles eliminates the possibility of solubilized nanoparticle residues from our analysis because luminescence only occurs in the presence of the intact particle, thus eliminating potentially confounding factors like soluble or endogenous ions, as can occur with ICP analysis. The inability of the 15-nm AuNP-Aq to cross skin barrier could be also attributed to their surface aggregation, as observed by dermoscopy. This could be attributed to the exchange of the citrate ions on the AuNP surface with skin proteins or lipids, as shown in other biological environments [165-166].

There were substantial similarities between our results with nanoparticles in toluene and the study by Xia *et al.* (2010) [148]. They showed increased nanoparticle penetration in the presence of solvents that included toluene. As pig skin is more

similar to human skin and this study was done *in vivo* using Yorkshire weanling pigs, it is a more relevant comparison to our study than rat skin or thawed human skin. The expected similarities in nanoparticle penetration between human and porcine skin are based on similar solute fluxes previously observed [167-168].

Our TEM data showed widespread disruption of the epidermal ultrastructure in toluene-treated samples. These TEM images showed discontinuous cell membranes and particulates throughout the samples that were not present in aqueous-treated groups. Disruption of lipid barriers by toluene could have directly led to the increased nanoparticle penetration we observed in the AuNP-TOL-treated skin. We observed dramatic decreases in total NAD(P)H autofluorescence with toluene treatment. These data were similar to those from necrotic skin we previously published [163]. Therefore, we hypothesize that toluene-treated skin was metabolically disrupted within 4 h of treatment by chemically induced necrosis. TEWL measurements indicate the integrity of the skin specimens with general increase in values after 24 h of occlusive conditions due to over-hydration of the skin. Regarding nanoparticle penetration only, long-term incubation revealed some penetration, indicating that skin barrier was not completely disrupted. Skin treated with AuNP in aqueous solution revealed lower total NAD(P)H signal, but metabolic rate appeared unchanged. We have observed decreases in the metabolic rate of silver nanoparticle-treated human skin [142], so we hypothesize that the unchanged metabolic rate data from AuNP treatments suggest that the total NAD(P)H signal may have been reduced by AuNP light scattering and not metabolic effects.

3.3.5. Conclusion

Our data showed that 15-nm AuNP in aqueous solution tended to aggregate on the superficial SC after 24 h exposure, while 6-nm AuNP in toluene penetrated through SC and into epidermal layers of human skin. Our NAD(P)H imaging data showed that epidermis was not viable at 4 and 24 h post-toluene treatment regardless of the presence of AuNP. Nevertheless, an exclusive role of the size or solvent on skin penetration should not be the conclusion of this research work. A more in-depth study of the single size and solvent effects is therefore in need. The results of this paper, however, should raise public awareness regarding the environmental exposure to nanoparticles, especially for personnel in research and industry. In the

future, similar studies are needed characterizing the impact of different physicochemical properties of nanoparticles with regard to penetration and metabolic effect on the skin.

3.4. Mechanism and determinants of nanoparticle penetration through human skin

Hagar I. Labouta, Labiba K. El-Khordagui, Tobias Kraus and Marc Schneider

Nanoscale

Vol. 3 (2011), 4989-4999, DOI:10.1039/C1NR11109D.

Copyright © The Royal Society of Chemistry (2011). All rights reserved.



Abstract

The ability of nanoparticles to penetrate the stratum corneum was the focus of several studies. Yet, there are controversial issues available for particle penetration due to different experimental setups. Meanwhile, there is little known about the mechanism and determinants of their penetration. In this paper the penetration of four model AuNP, of diameter 6 and 15 nm differing in surface polarity and the vehicle nature through human skin was studied using multiphoton microscopy. This is in an attempt to profoundly investigate the parameters governing particle penetration through human skin. Our results imply that nanoparticles at this size range permeate the stratum corneum in a similar manner to drug molecules, mainly through the intercellular pathways. However, due to their particulate nature, permeation is also dependent on the complex microstructure of the stratum corneum with its tortuous aqueous and lipidic channels, as shown from our experiments performed using skin of different grades of barrier integrity. The vehicle (toluene-versus-water) had a minimal effect on skin penetration of gold nanoparticles. Other considerations in setting-up a penetration experiment for nanoparticles were also studied. Results obtained are very important for designing a new transdermal carrier and for the basic understanding of skin-nanoparticles interaction.

3.4.1. Introduction

The potential ability of nanoparticles to overcome the barrier function of the stratum corneum (SC) has been recently the target of several studies. Nevertheless, there is a controversy among researchers whether nanoparticles do penetrate the SC into the viable tissue [50, 75] or not [60, 62, 115]. The different results are mainly due to different experimental setups, in terms of the skin type, skin surface area, exposure time and type and concentration of applied nanoparticles. A great deal of the recent work was mainly focused on treating the skin physically, e.g., tape stripping [73, 90], mechanical flexion [144], UV exposure [87], sonophoresis [76], microneedles [145] or chemically using penetration enhancers [85] to cause or enhance the penetration of nanoparticles into the deeper skin layers (DSL). In this study, however, a well-designed skin penetration experiment, using excised human skin as the gold standard for *ex vivo* skin penetration is considered crucial in regard to the extensive studies on animal skin [45, 75, 90, 144, 148]. The physicochemical parameters, size, surface polarity, physical state of the nanoparticles, in addition to the effect of vehicle were in focus.

Surface polarity of nanoparticles and the vehicle nature are expected to play a role in skin penetration of nanoparticles. Yet, to our knowledge, only three studies investigated the effect of surface charge of nanoparticles on skin penetration, though they were also controversial in terms of the surface charge which leads to higher affinity of the particles to porcine skin [75, 169-170]. Senzui *et al.* [78] studied the penetration of 35 nm titanium dioxide nanoparticles, uncoated and coated with alumina/silica/silicon, through porcine skin. However, no penetration was reported for both particles.

Apart from the size factor, the effect of surface polarity of nanoparticles, having the same size diameter, on skin penetration was not the scope of any investigation so far. On the other hand, the only evidence for the effect of solvents on the skin penetration of nanomaterials was recently reported by Xia *et al.* [148] for pristine fullerenes of 1 nm in diameter. Several industrial organic solvents: chloroform, toluene, cyclohexane and mineral oil were examined. Porcine skin biopsies showed penetration of particles for all of the tested solvents except for mineral oil, with much higher penetration in case of chloroform. Baroli *et al.* [53], however, compared the effect of nanoparticle formulation to blank solutions on human skin resistivity and

concluded a minor effect of the vehicle on their results. Finally, the physical stability of nanoparticles when coming in contact with the skin and its effect on skin penetration, though not studied so far, is an important parameter that could partly explain the disagreement of results reported by different researchers concerning the penetration of nanoparticles of the same size range [60, 75]. Hence, a more systematic study on the penetration of nanoparticles through human skin taking into account that all the mentioned relevant physicochemical parameters together has not been done so far.

Several nanoparticles, polymeric or inorganic nanoparticles, were investigated for possible skin penetration [42]. Among these particles, gold nanoparticles (AuNP) are considered a good model for studying skin penetration of nanoparticles [58, 86, 134]. They have unique optical properties. They show distinctive extinction bands in the visible region, due to surface plasmon oscillation of free electrons [114]. This property allows for tracking the physical state of the particles under different conditions throughout the experiment and for their detection in human skin. AuNP have also high clinical significance due to their ability to deliver various payloads [5, 23-24] such as drug molecules [25], large biomolecules, such as proteins [28], DNA [29-30], or RNA [31]. Moreover, AuNP cause local heating when they are irradiated with light in the visible range allowing for the potential use of AuNP in photothermal destruction of tumors [22].

In an earlier study, we reported on the consequences of topical exposure to two selected polar and apolar gold nanoparticles in regard to their effect on skin metabolism and penetration into deeper layers of human skin using multiphoton tomography and fluorescence lifetime imaging [55]. The present work, however, is a mechanistic study of the penetration of nanoparticles into human skin using a full matrix of particles of different surface polarity, size and vehicle. In addition, concentration of applied nanoparticles, skin exposure time, physical state of the particles on skin exposure and skin integrity were investigated.

3.4.2. Materials and Methods

Preparation of AuNP. Sterically stabilized, apolar gold nanoparticles (AuNP1) were synthesized from an organometallic precursor. The synthetic procedure was adapted from Zheng *et al.* [158]. Gold nanoparticles were formed upon reduction of the gold

source by an amine-borane complex in the presence of an alkyl thiol. In a typical synthesis, 0.31 g chlorotriphenylphosphine gold (purity 98%, ABCR, Karlsruhe, Germany) was dissolved in 50 ml of benzene (purity >99.5%, Riedel-de Haen, Germany) forming a colorless solution. A mixture of 0.53 g tert-butylamineborane (purity, 97%, Fluka, Germany) and 0.31 ml dodecanethiol (purity >98%, Fluka, Germany) were added to the formed solution and left to react at 55°C for 1 hour. Upon completion of the reduction reaction, the red solution was cooled to room temperature, precipitated by the addition of ethanol and washed by centrifugation and subsequent resuspension in toluene. Finally, the particles were resuspended in toluene and stored at room temperature protected from light.

Phase transfer of apolar AuNP1 into water. AuNP1 were transferred into water using an emulsification method. A solution of 10 g lecithin (Pure lecithine (98% phospholipids), Boma-Lecithin GmbH, Otter, Germany) in 400 ml water was prepared and stirred overnight to ensure complete dissolution. About 40 ml of the AuNP dispersion in toluene was added to the solution and the mixture was shaken and further emulsified at the maximum energy of an ultrasonic bath (Elmasonic S100H, Elma GmbH & Co KG, Singen, Germany) for 5 min and at half its maximum energy for 15 min, followed by heating it to 90°C under stirring for 1 h. This procedure was repeated several times to ensure emulsification and toluene evaporation. Unemulsified parts of the AuNP dispersion were separated from the mixture and emulsified separately using additional sonication steps. Finally, AuNP2 dispersion with hydrophilized surface was stirred at 90°C until all toluene had evaporated leaving a clear red aqueous solution.

Ionically-stabilized, polar gold nanoparticles (AuNP3) were prepared according to Turkevich method [132]. Briefly, 70 ml solution of hydrogen tetrachloroaurate ($\text{HAuCl}_4 \cdot 3\text{H}_2\text{O}$, Sigma-Aldrich Chemie GmbH, Steinheim, Germany) containing about 100 $\mu\text{g/ml}$ gold was first heated to boiling at 100°C under magnetic stirring at about 440 rpm and then reduced by a solution of trisodium citrate dihydrate ($\text{Na}_3\text{C}_6\text{H}_5\text{O}_7 \cdot 2\text{H}_2\text{O}$, Sigma-Aldrich) containing 5-fold the molar concentration of the gold salt. All solutions were used without filtration. After the gold colloid had formed, the temperature was lowered to about 25°C. The colloid was then transferred into a suitable glass container and stored in the refrigerator protected from light.

Phase transfer of polar AuNP3 into toluene. The method of phase transfer followed the protocol published by Zhu *et al.* [171] after several modifications. Practically, a volume of thioglycolic acid (TGA) ($C_2H_4O_2S$, 99%, Sigma-Aldrich Chemie GmbH, Steinheim, Germany) equivalent to 1.29×10^{-3} moles was added to 2 ml of AuNP dispersion, with a concentration of 99.05 $\mu\text{g/ml}$ gold and stirred until the solution gets purple, indicating chemical bonding of $-SH$ group of TGA onto the surface of AuNP. N-cetyl-N,N,N-trimethylammonium bromide (cetrimide) ($C_{19}H_{42}BrN$, Merck KGaA, Darmstadt, Germany) was then introduced to the AuNP dispersion portionwise while stirring. The molar ratio between TGA and cetrimide is 2:1. Stirring was continued for 30 min to allow for the adsorption of surfactant molecules through electrostatic interaction between TGA and cetrimide. A volume of 2 ml toluene was then mixed with the dispersion for 10 min, resulting in O/W emulsion. Finally, 2 ml ethanol, containing 0.21 M cetrimide, was added to break the emulsion, in addition to 3 ml toluene for better extraction of AuNP with hydrophobized surface. The whole two-phase system was vigorously shaken for 20 min. Ethanol is miscible with water, thus the dissolved cetrimide further coat AuNP that are still in the aqueous phase resulting in more particles transferred into toluene. Extracted AuNP in toluene were further treated with cetrimide. A weight of cetrimide equivalent to 6.86×10^{-6} moles is required for each 1 ml of prepared AuNP4 dispersion to keep it stable over a prolonged period of time.

Characterization of the optical and colloidal properties for the prepared AuNP.

The optical properties of prepared AuNP were checked using a UV/Vis Spectrophotometer (lambda 35, Perkin Elmer, Rodgau-Jürgesheim, Germany) in the range of 400-800 nm. The mean particle size and the morphology of the gold core were determined by transmission electron microscopy (TEM) using a JOEL Model JEM 2010 instrument (JOEL GmbH, Eching, Germany) operated at an accelerating voltage of 120 kV. Core diameters determined by TEM were used as particle size facilitating comparison of particle diameters as hydrodynamic radius is only available in aqueous solution. Samples for TEM analysis were prepared by placing 12 μL drop of dispersed nanoparticles in water on carbon-coated 400 mesh copper grid. The solvent was allowed to evaporate slowly at room temperature. Finally, the surface charge of AuNP2 and AuNP3 was estimated by measuring the zeta potential based

on the electrophoretic mobility (Zetasizer Nano, Malvern Instruments, Malvern, UK). The prepared dispersions (1.5ml) were directly measured (solvent is water) in triplicate using disposable folded capillary cells that contained the electrodes. Measurements were done at room temperature. Since particle dispersion in the non-polar solvent, toluene, in case of AuNP1 and AuNP4, would not allow for development of surface charge (though a value near zero could be measured by zetasizer), this was denoted as “uncharged” in Table 3.4.1.

Table 3.4.1: Characteristics of the prepared AuNP dispersions.

AuNP code	Surface chemistry	Diameter of gold core* [nm]	Zeta potential** [mV]	Vehicle
AuNP1	Dodecanethiol	6.00 ± 0.81	Uncharged	Toluene
AuNP2	Lecithin	”	-53.5 ± 1.44	Water
AuNP3	Citrate ions	14.90 ± 1.76	-35.1 ± 1.87	Water
AuNP4	cetrimide	”	Uncharged	Toluene

* measured by TEM (n is more than 30).

** given as a criterion indicating surface charge.

Study of the penetration of AuNP through Human Skin.

Skin preparation. Human skin was obtained from female patients aged 30 to 57 years, who had undergone abdominal plastic surgery after approval of the ethic committee of Saarland, Germany (Ärzttekammer des Saarlandes, Dec. 2008); three skin donors were used in the study. Adequate health and no medical history of dermatological disease were required. Immediately after excision, the skin was cut into pieces and the subcutaneous fatty tissue was removed from the skin specimen using a scalpel. Afterwards the surface of each specimen was cleaned with water, wrapped in aluminium foil and stored in polyethylene bags at -26°C until used. Previous investigations have shown that no change in the penetration characteristics occurs during the storage time of 6 months [159].

Skin discs, 25 mm in diameter, were punched out from frozen skin, thawed, cleaned with deionized water and transferred into the Franz diffusion model.

Skin penetration study. *In vitro* penetration experiments were run in static Franz diffusion cells having a diffusion area of 1.76 cm² and a receptor compartment of 12

ml volume. The prepared human skin was fastened carefully between the donor and receptor compartments, with the SC side up and held in place with a clamp. The dermal side of the chamber contained a receptor solution of phosphate buffer saline, pH 7.4 magnetically stirred at 500 rpm. A volume of 500 μ l of the prepared AuNP dispersion was placed on the skin then the donor compartment was occluded. The diffusion cells were maintained at 32°C throughout the experiment. Following exposure, the skin was removed and the skin surface was gently cleaned with cotton. Collected skin was examined after longitudinal cryo-sectioning and the donor solution was analyzed directly by UV/Vis spectroscopy to determine the physical state of the particles following skin contact.

Additional penetration experiments involved skin pre-exposure to toluene (vehicle) or chloroform/methanol mixture (discussed later) or tape-stripping of the stratum corneum before application of particle dispersion. Infrared densitometry was used for determining the endpoint of tape-stripping, i.e. complete SC removal, a method described by Hahn *et al.* [172].

Longitudinal skin cryo-sectioning. Cross-sections of \sim 10 μ m thickness were performed at -20°C using a SLEE cryostat type mev (SLEE medical GmbH, Mainz, Germany). It is important to note here that on sectioning, the skin piece should not be placed tangential to the blade to avoid dislocation of the particles from outside into DSL or vice versa, but in a perpendicular direction to the cutting blade limiting sectioning artifacts. Skin sections were placed on microscopical slides and were stored at -20°C until imaged by multiphoton laser scanning microscopy. Before examination, specimens were mounted by an aqueous mounting medium (FluorSaveTM reagent, Calbiochem, San Diego, USA) and covered with glass cover slips. At least 20 cuts were used for microscopical examination.

Multiphoton laser scanning microscopy. Fluorescence imaging was performed using an inverted confocal/two photon excitation fluorescence microscope (ZEISS LSM 510 META, Carl Zeiss, Jena, Germany), equipped with a tunable pulsed IR laser ($\lambda=720-930$ nm) (Chameleon, Coherent, Dieburg, Germany) for multiphoton laser microscopy, in addition to other conventional laser lines for confocal microscopy. The objective used was water immersion lens 63X (NA=1.2). A wavelength of 800 nm was used for both excitation of AuNP and scanning the skin using a transmission

energy of 0.485 and 0.647 mW in the focal plane, respectively. The optical settings, discussed in detail earlier [55], allowed for the separation of both signals with no signal interference among tracks. Z-stacks of the skin samples were taken with steps every 1 μm . Each optical scan is composed of 512 x 512 pixels² and a size of 0.14 x 0.14 μm^2 . The gain settings were adjusted for each measurement individually. No significant photobleaching has been observed in our experiments under the conditions used to quantify penetration.

Data analysis. Multiphoton images of the longitudinal skin sections were then analyzed using the software by the supplier. Semiquantitative data for the distribution of AuNP in different skin layers were extracted as published earlier. Shortly, z-stacks were adopted for analysis. For each optical layer, the intensity was first thresholded in order to remove the background. Pixels due to luminescence of AuNP were determined in the SC and in the DSL for this optical layer. Summing up these values in all the optical layers of the z-stack ends up with \sum_{pixel} frequency due to AuNP in the SC and in DSL of this z-stack, from which the weighed number of particles were calculated according to Equation 3.4.1, where $A_{\text{pixel}} = 0.139 \times 0.139 \mu\text{m}^2$ and A_{particle} (area of diffraction-limited AuNP) $\approx 0.365 \mu\text{m}^2$ for the optical settings used in this study as detailed elsewhere [134]. It should be noted here that the summed value developed by data analysis is regarded as a semi-quantitative index to compare penetration into the SC and DSL under the same conditions as well as for different formulations and conditions. Summed values were found more informative than mean values ($\pm\text{SD}$) due to the non-homogeneous distribution of the particles throughout the diffusion area. In other words, a summed value on analysis of x number of image fields offers a relatively more rigid and resistant parameter to the great variability of particle localization.

$$N_w = \frac{\sum \text{Pixel} \times A_{\text{pixel}}}{A_{\text{particle}}} \quad \text{Equation 3.4.1 [134],}$$

Finally, maximum penetration depths could be also determined for these skin experiments.

Study of the vehicle effect on skin penetration of AuNP.

i. Gravimetric analysis

(a) Preparation of epidermal sheets.

Heat-separated human epidermal sheets were prepared from specimens of full thickness human skin of 15 or 25 mm diameter according to Kligman and Christophers [173]. Shortly, full thickness human skin was immersed in water of 60°C for 90 seconds. The epidermis was then carefully peeled off the dermis using forceps.

(b) Determination of the wet and dry weights of the epidermis.

Heat-separated epidermal sheets are then carefully dried using a filter paper and weighed on Teflon sheets. This represents the wet weight of the epidermis. Epidermal sheets were then dried for two days in a desiccator at room temperature then weighed once more to obtain the dry weight of the epidermis.

(c) Determination of lipid amount extracted by toluene.

Epidermal sheets, prepared from 25 mm skin punches, were fitted in static vertical Franz diffusion cells having a diffusion area of 1.76 cm² and a receptor compartment of 12 ml volume. The receptor compartment was filled with phosphate buffer saline, pH 7.4 and magnetically stirred at 500 rpm. A volume of 500 µL toluene was used as a donor solution for 0.5, 2, 6 and 24 h and the donor compartment was occluded. At the end of the skin exposure time, the donor solution was filtered and dried under nitrogen. Dried lipid extracted by the donor solution was then placed in a desiccator overnight and weighed for the lipid amount.

(d) Determination of the total epidermal lipid content.

Another set of epidermal sheets, prepared from 15 mm skin punches, were used to determine the total amount of lipid present in the epidermis of this skin donor having

the same diffusion area as in Franz diffusion experiment. Each epidermal sheet was extracted with 5 ml chloroform/methanol, 2: 1 in well-closed test tubes for 24 h under mild shaking. As described above, solutions were filtered, dried and lipid amounts were weighed.

ii. High performance thin layer chromatography (HPTLC)

Dried lipid extracts of 2 h skin exposure were then redispersed in 100 μ l toluene or chloroform /methanol, 2: 1 and a volume of 1-5 μ l of the lipid extract was spotted on silica gel 60-HPTLC plates (Merck KGaA, Darmstadt, Germany) along with 1 μ l spots of standard solutions containing serial concentrations of cholesterol, cholesteryl oleate, glyceryl trioleate, oleic acid and ceramide NP (a ceramide consisting of a nonhydroxy N-acyl fatty acid and phytosphingosine). A maximum of 8 spots are applied on each plate of 20 x 10 cm dimensions. Plates are then separated into two groups according to the developing system. The first group was developed using the following sequential development system: (1) n-Hexane: diethyl ether: acetic acid (80:20:10) for a distance of 12 cm from the spotting level, (2) n-hexane for 14 cm distance, for separation of cholesterol, oleic acid, triglycerides and cholesteryl ester. The plates were allowed to dry before the second development step. The second group of plates were developed using chloroform: methanol: acetic acid (95:4.5:0.5) for separation of skin ceramides. All plates were then dried and sprayed with a solution 10% CuSO_4 in 8.5% H_3PO_4 under nitrogen flow. The plates were then placed on a thermoplate of preadjusted temperature of 110°C and heated until 160°C. Separated lipid fractions were then quantified using IR densitometry using Image J (version 1.43, available as freeware from <http://rsbweb.nih.gov/ij/>). Area under the curve was calculated for all the separated spots and quantification was based on the known quantities of the co-migrated standards used to develop a calibration curve.

3.4.3. Results and Discussion

Monodisperse gold nanoparticles, AuNP1 and AuNP3, with ~ 6 and 15 nm diameter, respectively, were successfully prepared. AuNP1 were uncharged, thiol coated and

dispersed in toluene. On the contrary, AuNP3 were negatively charged due to stabilization with citrate ions and dispersed in water. In order to study the effect of surface polarity, vehicle nature, in addition to size of nanoparticles on their skin penetration, each of the prepared AuNP1 and AuNP3 were transferred into water and toluene, respectively, using a suitable phase transfer agent, as indicated in the experimental section. The surface chemistry was therefore changed accordingly keeping the core size unchanged hence having same-sized particles of different surface polarity and different vehicle stability. All AuNP were fully characterized. The characteristics of the prepared AuNP are summarized in Table 3.4.1 and their TEM images are shown in Figure 3.4.1.

Prepared and characterized AuNP were then applied to excised human skin at different concentrations and skin exposure times (Table 3.4.2). After skin penetration experiment, skin punches were longitudinally sectioned and analyzed using multiphoton microscopy (Figure 3.4.2), an efficient technique to track the penetration of nanoparticles in skin [55, 85, 115, 134, 174]. All AuNP formulations could penetrate the SC into the DSL after 24 h of skin exposure, except for AuNP3. It should be noted here that though penetration of AuNP was observed not being homogenous throughout the examined longitudinal sections, conclusion was made based on repetitive observation as indicated in the methodology section. Representative optical z-stacks, 1 μm nominal step width, for all examined longitudinal skin sections were then quantified by calculation of signal pixel frequency due to AuNP in the stratum corneum (SC) and deeper skin layers (DSL) for each optical layer. Finally a summed value of pixels ($\sum\text{pixel}$) due to AuNP in each the SC and DSL were calculated. From this parameter the weighed number of particles was calculated [134]. Therefore this method takes into account the non-homogeneous distribution of AuNP all over the diffusion area and is not depending on one image field only. Results showed depth-profiles for AuNP having higher values in the upper skin layer, SC, decreasing reaching DSL (Figure 3.4.3). The following factors were found critical in skin penetration of nanoparticles.

Table 3.4.2: Conditions of skin penetration experiments for the prepared AuNP dispersions.

AuNP code	Concentration [$\mu\text{g/ml}$]	Time of skin exposure [h]
AuNP1	90	0.5, 2, 6 and 24
	437	0.5, 2, 6 and 24
AuNP2	90	24
AuNP3	90	24
AuNP4	90	24

Effect of size and surface polarity of AuNP. The physicochemical attributes of nanoparticles are key factors governing their skin penetration and permeation. Overlaid multiphoton/transmission microscopy images of longitudinal sections from skin specimens after 24 h exposure to 90 $\mu\text{g/ml}$ concentration of AuNP1-4, different in size and surface chemistry are shown in Figure 3.4.2. Only hydrophilic, citrate-stabilized, 15 nm diameter AuNP3 were shown not to penetrate the SC into DSL [55].

Interestingly, surface modification of AuNP3 using thioglycolic acid and cetrimide, resulted in AuNP4 with hydrophobic surface showing skin penetration into deeper layers. A similar pattern was observed for the smaller particles, AuNP1 and AuNP2. Surface modification of hydrophobic AuNP1 using lecithin yielded hydrophilic AuNP2 with lower skin penetration ability under the experimental conditions, as indicated by the number of AuNP in the SC and DSL in representative optical z-stacks of the respective 10 μm thickness longitudinal skin sections examined by multiphoton microscopy (Figure 3.4.3a). Therefore, nanoparticles with more hydrophobic character, AuNP1 and AuNP4, were more favorable for skin penetration. This indicates that nanoparticles, in this size range, follow the same penetration pathways postulated for the penetration of drug molecules. However their particulate nature will reduce the speed of diffusion [42] through the intercellular route dominated mainly by fluid lipidic pores [175].

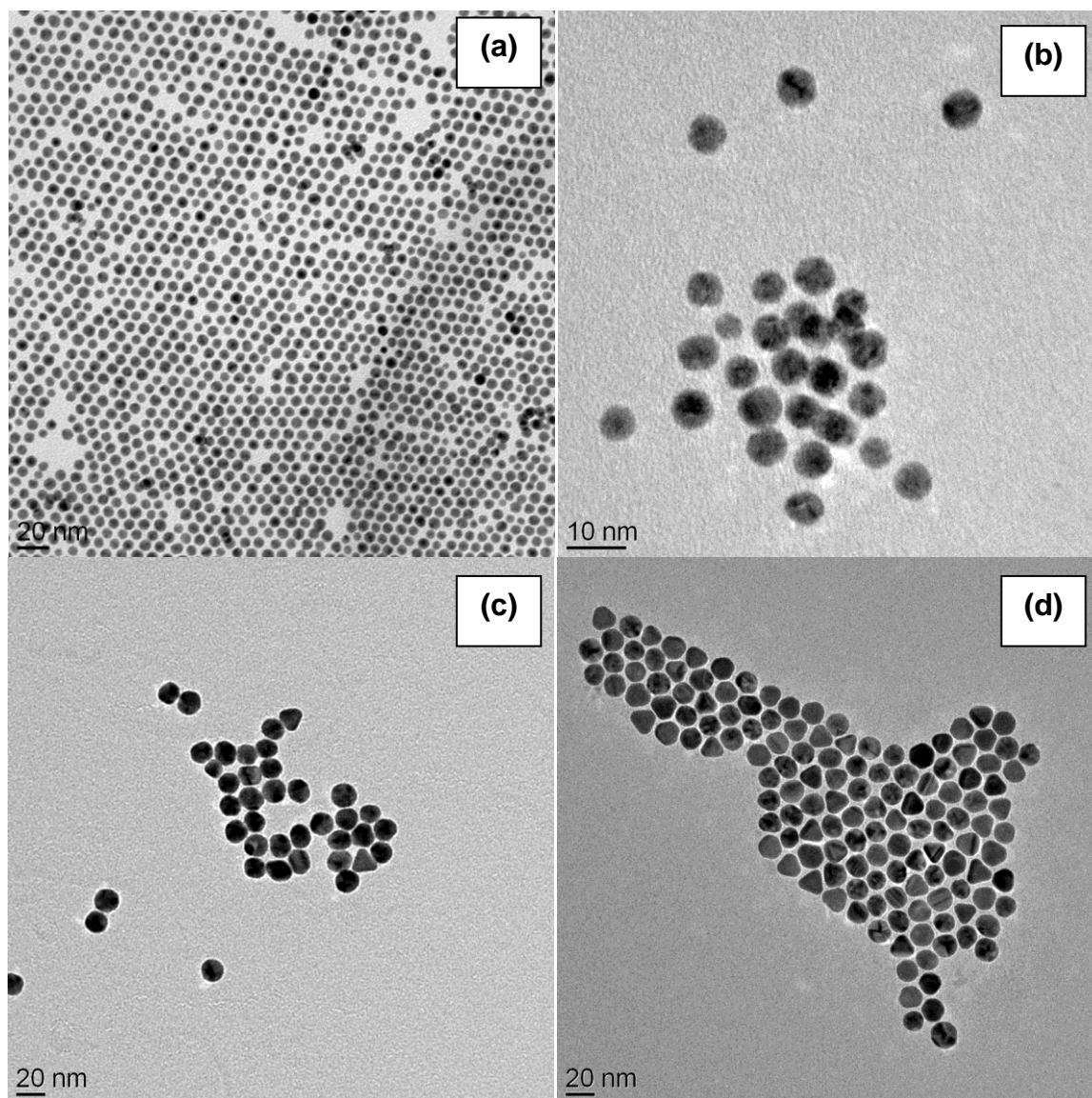


Figure 3.4.1: TEM images of prepared (a) AuNP1 (6 nm thiol-coated AuNP, dispersed in toluene), (b) AuNP2 (6 nm lecithin-coated AuNP, dispersed in water), (c) AuNP3 (15 nm citrate-stabilized AuNP, dispersed in water) and (d) AuNP4 (15 nm cetrimide-coated AuNP, dispersed in toluene).

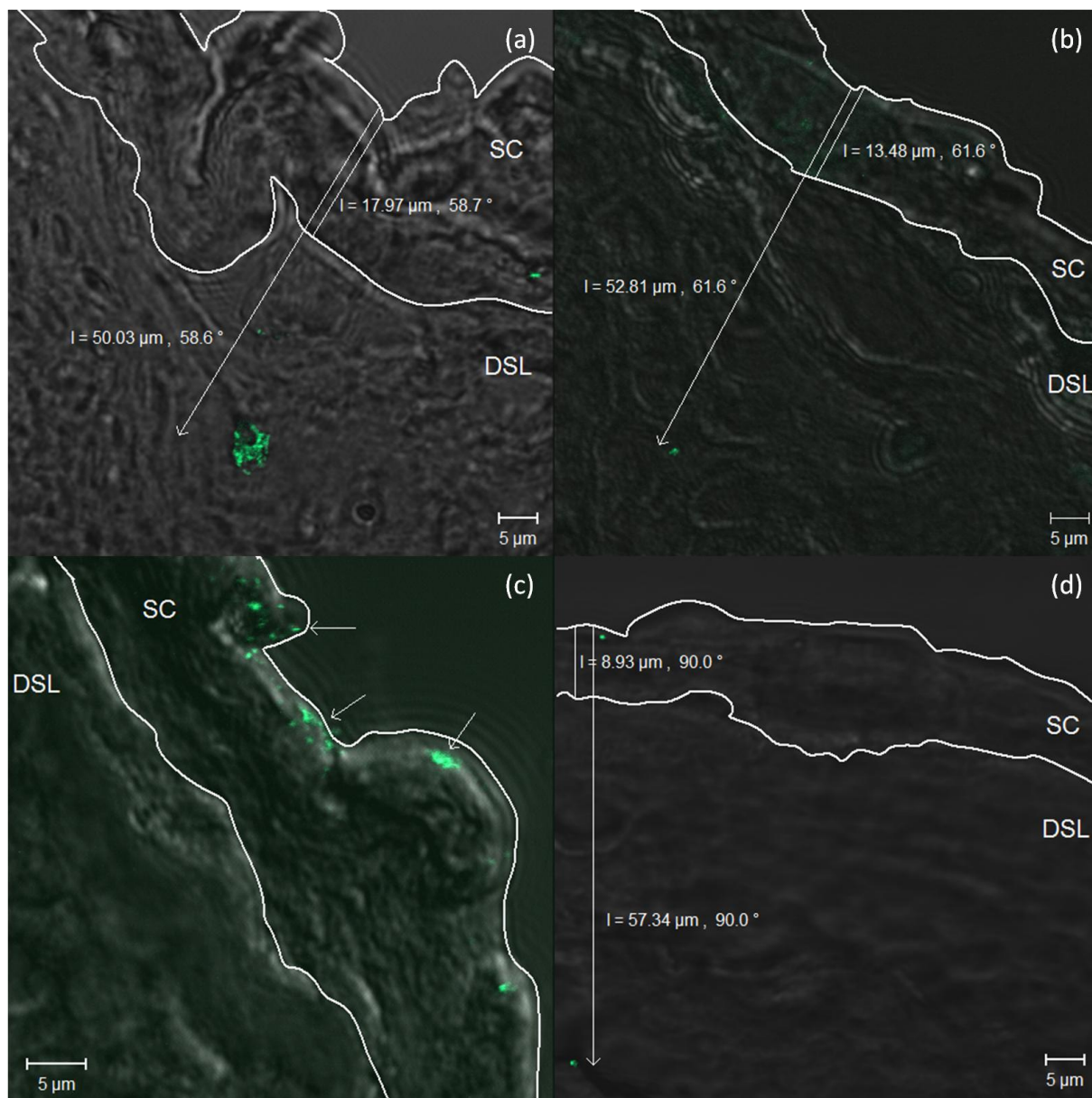


Figure 3.4.2: Selected overlaid multiphoton/transmission images of AuNP (indicated as green pseudo-colored spots) in longitudinal skin sections in which the stratum corneum (SC) is outlined by a white line to separate it from the deeper skin layers (DSL). Skin sections were obtained from skin punches exposed for 24 h to (a) AuNP1 (6 nm thiol-coated AuNP, dispersed in toluene), (b) AuNP2 (6 nm lecithin-coated AuNP, dispersed in water), (c), AuNP3 (15 nm citrate-stabilized AuNP, dispersed in water) and (d) AuNP4 (15 nm cetrimide-coated AuNP, dispersed in toluene). As indicated in the figure, exclusive localization of nanoparticles in the SC for AuNP3 and penetration of AuNP1, AuNP2 and AuNP4 into the DSL at variable penetration depths were observed.

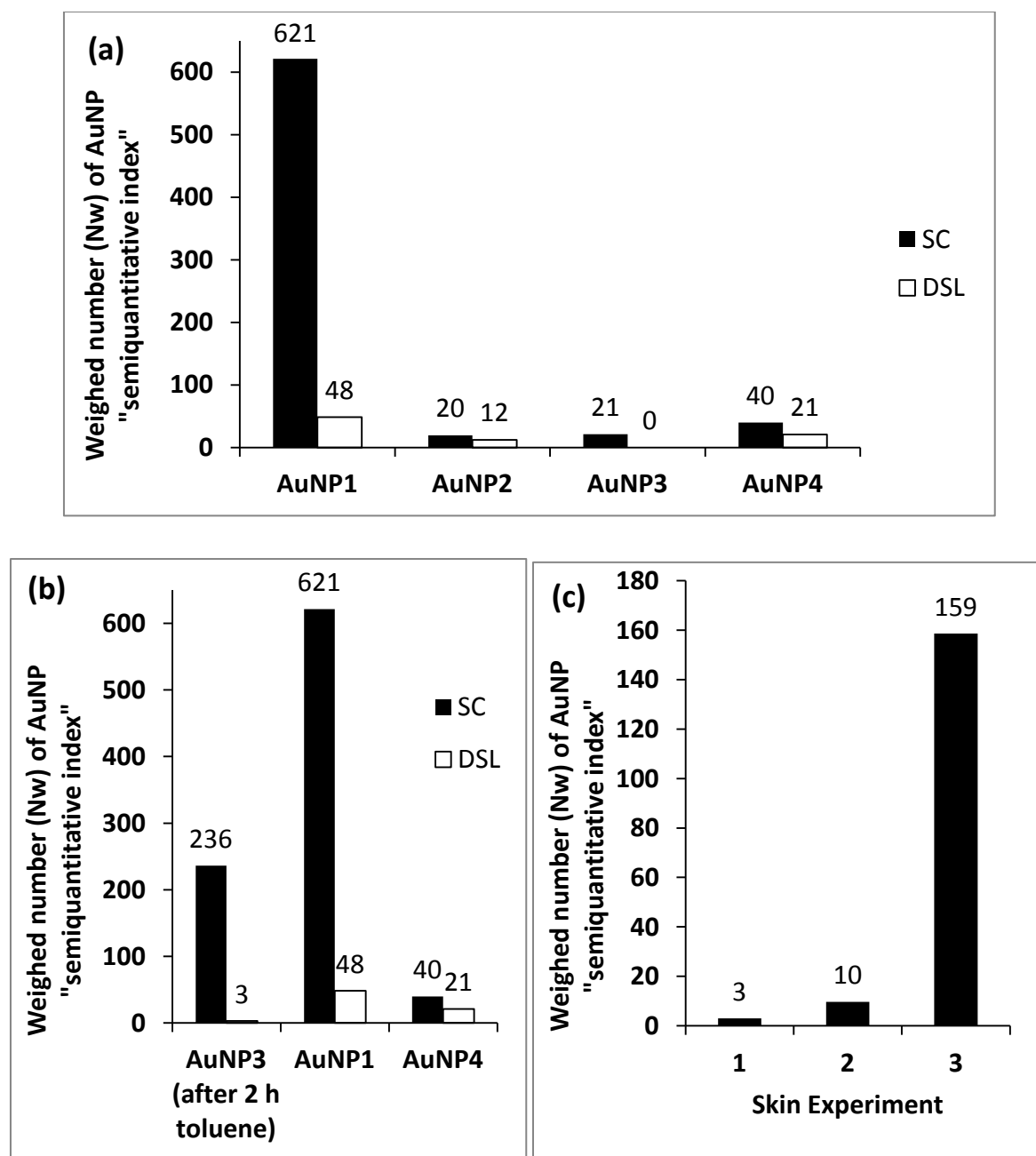


Figure 3.4.3: The effect of the physicochemical parameters of nanoparticles, the vehicle and skin integrity on skin penetration of AuNP as extracted from optical layers of z-stacks (1 µm step width) of longitudinal skin sections imaged by multiphoton microscopy. (a) Skin penetration of AuNP1 (6 nm thiol-coated AuNP, dispersed in toluene), AuNP2 (6 nm lecithin-coated AuNP, dispersed in water), AuNP4 (15 nm cetrimide-coated AuNP, dispersed in toluene) at a concentration of 90 µg/ml of gold after 24 h of skin exposure. (b) Skin penetration of AuNP3 (15 nm citrate-stabilized AuNP, dispersed in water) on 22 h skin exposure following 2 h pre-exposure to toluene in comparison to skin penetration of AuNP1 and AuNP4 dispersed in toluene into the SC and DSL after 24 h of skin exposure. (c) Effect of 2 h pre-exposure to toluene "1" in comparison to removal of skin lipids using chloroform/methanol mixture, 2:1 "2" and to complete removal of the SC by tape stripping "3" on skin penetration of AuNP3 into DSL after 22 h of skin exposure.

Smaller sized AuNP1 and AuNP2, 6nm in diameter, showed higher skin penetration than 15 nm AuNP3 (no penetration into DSL) and AuNP4, as shown in Figure 3.4.3a. A similar pattern was also reported for drug penetration where high molecular weight compounds could penetrate the SC to a less extent than small molecules [176]. Though our results are partly contrary to the findings of Sonavane *et al.* [45] who showed skin permeation of AuNP, 15 nm in diameter after only 1 h (they used rat skin of different histology than human skin in our study), their results also indicated size-dependent skin permeation. According to them, higher permeation for 15nm AuNP compared to 102 nm and 198 nm AuNP was indicated and the permeability coefficient was reported to decrease on increasing the particle size. Another report also indicated skin penetration of latex nanoparticles of 50, 100, 200 and 500 nm diameter in a size-dependent manner [170].

Effect of the physical state of AuNP dispersion. The physical state of the applied nanodispersion, whether composed of individual particles or aggregated ones, is considered critical and should be analyzed carefully in parallel with skin penetration study. This is to avoid any misinterpretation of the results in regard to the significance of particle size as a determinant of skin penetration. Here AuNP serve as a good model whose Plasmon band provides precise and easily accessible information on the aggregation state of the colloidal gold. Aggregation is indicated by a big red-shift of the spectral peak and/or strong peak broadening [161]. Therefore, it was important to analyze the applied AuNP dispersion spectrophotometrically before and after skin penetration experiment (Figure 3.4.4). At the beginning of the skin experiment, all applied AuNP dispersions showed physical stability. No significant red-shift was observed for the test nanodispersions AuNP1, AuNP2 and AuNP4, applied at a concentration of 90 $\mu\text{g/ml}$, after 24 h of skin contact. However, after 24 h of skin exposure, aggregation was observed for AuNP3 (hydrophilic, citrate-stabilized and 15 nm in diameter) as evident from peak broadening (Figure 3.4.4c). The zeta potential also increased by about 2-fold. Aggregation of AuNP3 could be attributed to the exchange of citrate ions on the surface of gold nanoparticles with skin proteins or lipids, as shown in other biological environments [166, 177]. This could be also due limited citrate ionization in the slightly acidic pH of the skin surface. This overnight aggregation further decreased the availability of single

dispersed particles of higher probability to penetrate the SC into DSL (Figure 3.4.2). On the other hand, all other particles (AuNP1, AuNP2 and AuNP4), penetrating the SC (Figure 3.4.2), showed no significant aggregation following skin contact (Figure 3.4.4a, b, d).

Effect of the vehicle of AuNP dispersion. Away from the physicochemical properties of nanoparticles, the vehicle is known to influence skin penetration profiles. Hence this effect also should hold true for nanoparticle penetration. Unfortunately, this effect of the vehicle was usually disregarded in skin penetration studies of nanoparticles. Here, however, the effect of the vehicle was in the focus of this study. AuNP1 and AuNP4 were dispersed and applied in toluene, in comparison to AuNP2 and AuNP3 (water). Therefore, the effect of toluene under the applied experimental conditions on the intercellular lipids of the SC, providing the main barrier function [175], was investigated. The percentages of lipid extracted from heat separated epidermal sheets on applying toluene for exposure times between 0.5 - 24 h, relative to the dry weight of the epidermis were determined by gravimetry (Table 3.4.3). These values were compared (as a percentage) to the total lipid content in the equivalent epidermal area for this skin donor (extracted by chloroform/methanol mixture, 2:1 after 24 h incubation), also calculated with respect to the dry weight of the epidermis. As shown in Table 3.4.3, a percentage of about 8 – 17% of the total epidermal lipid content was extracted by toluene. However, a closer look to the standard deviation values, one could conclude that the amount of lipid extracted by toluene is time-independent, i.e. the amount of lipid extracted after 0.5 h is not significantly different than that after 24 h.

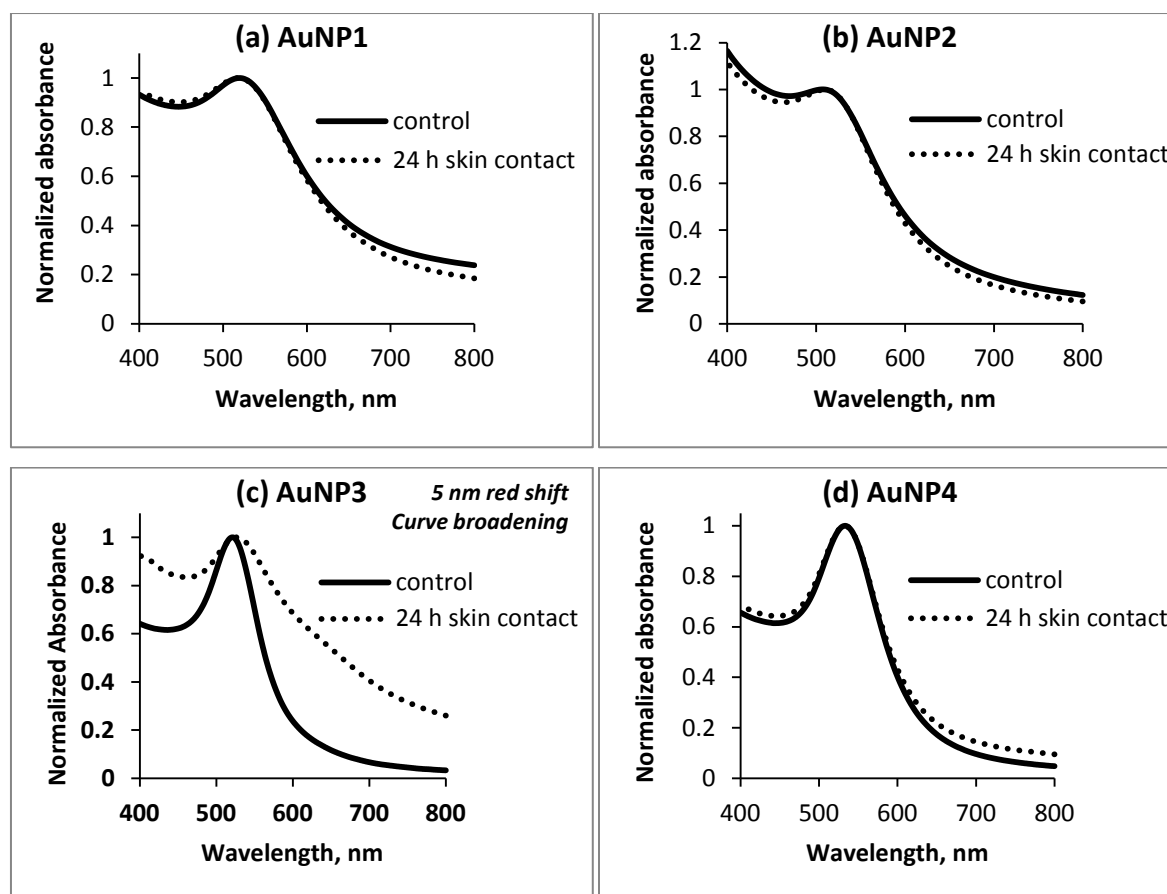


Figure 3.4.4: UV/Vis spectra of (a) AuNP1 (6 nm thiol-coated AuNP, dispersed in toluene), (b) AuNP2 (6 nm lecithin-coated AuNP, dispersed in water), (c) AuNP3 (15 nm citrate-stabilized AuNP, dispersed in water) and (d) AuNP4 (15 nm cetrimide-coated AuNP, dispersed in toluene) at a concentration of 90 $\mu\text{g/ml}$ of gold, showing particle stability before and after 24 h of skin contact.

Table 3.4.3: Gravimetric analysis of toluene lipid extract of heat separated epidermis after 0.5, 2, 6 and 24 h exposure time versus total epidermal lipids.

Incubation time [h]	% lipid extracted with respect to dry skin wt	% lipid extracted with respect to total epidermal lipids
0.5	2.43 \pm 0.08	7.82 \pm 0.26
2	3.20 \pm 1.25	10.29 \pm 4.02
6	2.79 \pm 1.89	8.97 \pm 6.08
24	5.32 \pm 3.29	17.08 \pm 10.60
Control (total epidermal lipids) ^[a]	31.13 \pm 3.55	

^[a] determined by shaking the epidermal sheets with chloroform/methanol mixture, 2:1 for 24 h)

Furthermore, the barrier function of the SC depends not only on the lipid quantity in the SC but also on the lipid composition. The main lipid classes in the SC are ceramides, cholesterol and fatty acids. Detection of triglycerides in the SC has been explained in literature either by contamination with sebum glycerides or by extraction of subcutaneous fat. Other lipid ingredients present in minute amount include cholesterol esters [175, 178]. The quantitative composition of the SC lipids differs depending on the extraction method [179] and inter- and intraindividual variations. Among all the lipid members, ceramides are known to be the most important component of the SC multilamellar lipid structure with defined physicochemical properties necessary for the barrier function of the skin [178]. After 2 h of skin exposure, epidermal lipid members extracted by toluene or chloroform/methanol mixture (total lipid extract) were quantified using HPTLC versus increasing serial concentrations of standard lipid mixture. The lipid composition of each extract was then determined by densitometric analysis and the results are shown in Figure 3.4.5. Toluene could extract the surface lipids, however the structural lipids of the SC, ceramides, were not extracted by toluene. In contrast ceramides were found in the total lipid extract of this skin donor.

Nevertheless, it could be concluded so far that toluene has an effect on the barrier function of the SC through lipid extraction. However, a drastic structural change in the skin barrier on toluene application is not likely, evident by the absence of ceramides in the toluene extract. Afterwards, it was important at this stage to determine whether the penetration of AuNP1 and AuNP4, dispersed in toluene, was mainly due to the effect of toluene on the barrier function of the skin, or this is only a contributing factor. Therefore, further skin penetration experiments were conducted, preincubating the skin with 500 μ l toluene for 2 h, followed by application of non-penetrating AuNP3, dispersed in water. The number of AuNP penetrating into the SC and DSL in a representative z-stack of a 10 μ m thickness skin section was semiquantified according to a method we published recently [134] and the result was compared to that due to application of AuNP1 and AuNP4, dispersed in toluene, at a concentration of 90 μ g/ml for 24 h (Figure 3.4.3b). It was found, however, that the number of AuNP penetrating into DSL was 16- and 7-fold higher for AuNP1 and AuNP4, respectively. This indicates that penetration of nanoparticles did not depend mainly on the vehicle, toluene. Yet, it is a complex mechanism depending on several parameters; and removal of SC lipids enhances the penetration ability.

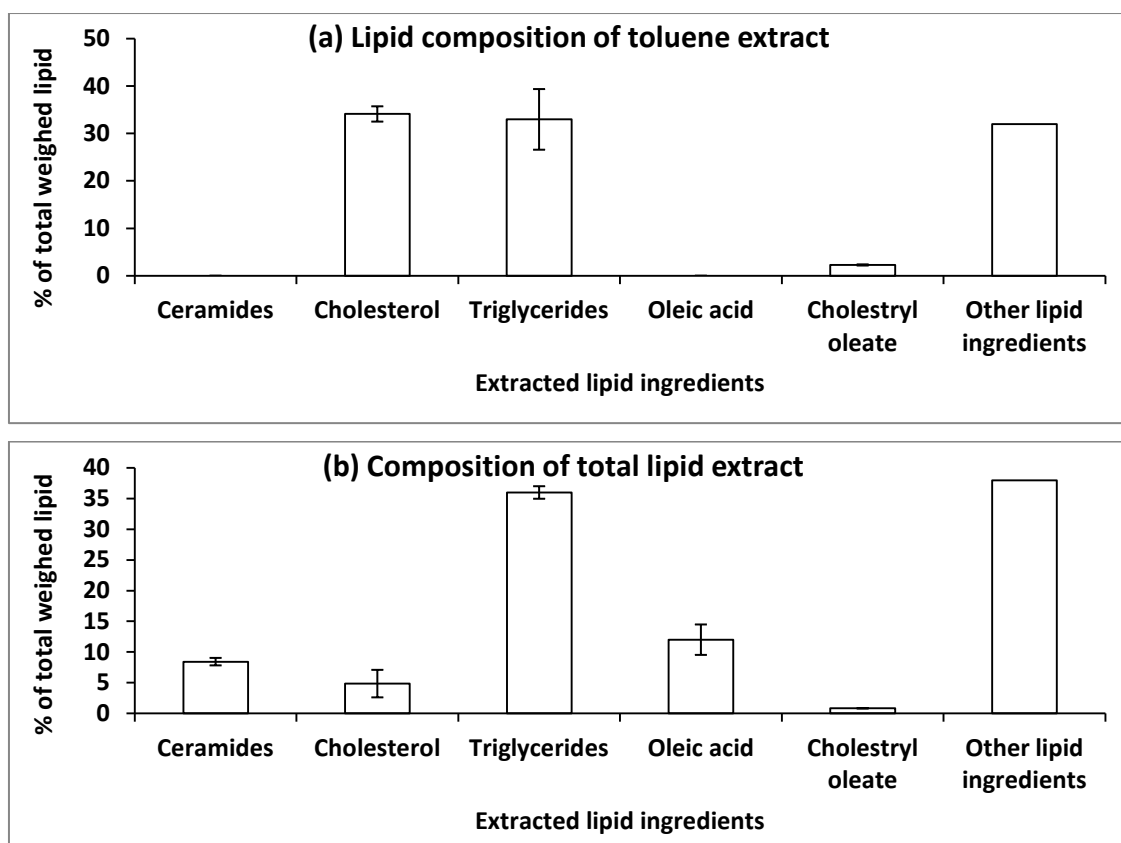


Figure 3.4.5: Lipid composition of toluene extract of heat separated epidermis after 2 h of skin exposure time (a) versus total lipid extract using chloroform/ methanol mixture, 2: 1 (b).

Effect of formulation ingredients. Skin penetration of nanoparticles should not be studied without considering formulation factors. Ingredients used in synthesis of nanoparticles could have an influence on their interaction with the skin when present in the dispersion. However, previous studies did not always take these factors into account when discussing nanoparticles penetration. This raises a question, whether nanoparticles do passively penetrate the SC due to their small size or this is a result of the physicochemical attributes of the nanoparticles as well as formulation, environmental and mechanical factors. In this study, chemicals used in particle synthesis could affect the skin hence possibly favoring more skin penetration including dodecanethiol and tert-butylamineborane (AuNP1), and thioglycolic acid (AuNP4). Furthermore, lecithin and cetrimide used in the preparation of AuNP2 and AuNP4, respectively are considered as penetration enhancers [104]. However, based on the amounts used relative to those described in literature [104, 180-181], they are assumed not to contribute much in skin penetration of nanoparticles. Yet, this is only an assumption and possibility for contribution is not discarded.

Effect of deteriorating the barrier function of the SC. In general, damaged skin is assumed to facilitate penetration. Hence, additional experiments were carried out to determine the effect of deteriorating the skin barrier function (i.e., the SC) on penetration of nanoparticles. AuNP3, shown not to penetrate the SC, were chosen for these experiments. The results were compared to skin penetration of AuNP3 after 2 h skin pre-exposure to toluene.

(1) Skin lipids were removed by treating the skin surface with 1 ml of chloroform/methanol mixture, 2: 1 for 22 h. HPTLC of the applied mixture showed extraction of the epidermal lipids: ceramides, cholesterol, fatty acids (oleic acid), triglycerides and cholesteryl ester (cholesteryl oleate) (data not shown). Removal of epidermal lipids was then followed by application of AuNP3 for further 22 h. However, it should be noted here that in order to set-up such an experiment a total of 44 h skin treatment was required (22 h for removal of epidermal lipids, followed by 22 h exposure to AuNP3). This would contribute to the penetrated amount due to decreased skin integrity [94]. Therefore, a supplementary experiment was performed which involves application of AuNP3 for only 2 h after skin treatment with chloroform/methanol mixture for 22 h, i.e. a total of only 24 h skin experiment.

(2) SC was completely removed by 30 times tape stripping followed by application of AuNP3 for 22 h. The experimental setup was carefully adjusted to insure that the stripped skin area is the same area exposed to nanoparticles. At the end of the penetration experiment, the skin surface was cleaned before further sectioning and examination by multiphoton microscopy.

As shown in Figure 3.4.3c, removal of the skin lipids using chloroform/methanol mixture resulted in AuNP3 penetrating the SC after 22 h of skin exposure. Even on skin exposure to AuNP3 for 2 h (Data not shown), 2-fold increase in penetration into the DSL was observed, compared to skin penetration of AuNP3 after 2 h skin pre-exposure to toluene. This again confirms that as for drug molecules, the intercellular lipids are the main barrier for skin penetration of nanoparticles. Intercellular localization of nanoparticles was previously reported for QD [79, 89].

On the other hand, for tape-stripping, previous reports did not show satisfactory results concerning particle penetration on the tape stripping part of the SC for QD of diameter ~ 4 nm [52], 6 nm [90] and ~ 37 nm [47] through human (20 tape-strips), rat (10 tape-strips) and mouse (5-20 tape-strips) skin, respectively. In this study,

complete removal of the SC by tape-stripping resulted, however, in about 16-fold further increase in penetration into DSL. This would rather indicate that the barrier function of the SC to particle penetration does not only rely on the intercellular lipids, however it is a complex mechanism that overall provides the rate-limiting step to penetration of nanoparticles.

For both conducted experiments, the number of AuNP3 penetrating into DSL was 2- and 53-fold, respectively, higher than that after 2 h exposure to toluene (Figure 3.4.3c). This again supports our previously drawn conclusion that toluene does have an effect on skin penetration of AuNP, however it is only a contributing factor and not the main factor.

Effect of concentration of applied AuNP dispersion and skin exposure time. All studies investigating skin penetration of nanoparticles so far based their conclusion, whether the particles are penetrating or not on a single point concentration. This does not imply that their conclusion applies for dispersions with higher or lower concentrations leaving the reader sometimes with a degree of uncertainty about the results. This also partly explains the current controversy among researchers on the status of skin penetration of nanoparticles. Moreover, the time of skin exposure to nanoparticles is very critical on studying possible skin penetration of nanoparticles since they diffuse slower. Yet, variable exposure times, e.g. 0.5 [182], 5 [115], 6 [169], 18 [183] and 24 [60] h, were reported in literature for *in vitro* particle penetration studies. Only few studies checked skin penetration on different time intervals. For instance, Baroli *et al.* [53] studied the penetration of magnetic nanoparticles through human skin after 3, 6, 12 and 24 h in which penetration was indicated by TEM images starting from 6 h skin exposure to the applied nanodispersion.

In this study, AuNP1 were applied on skin with two different concentrations, 90 and 437 $\mu\text{g/ml}$ of gold, for exposure times of 0.5, 2, 6 and 24 h (Table 3.4.2). AuNP1 in both concentrations could penetrate the SC at 24 h. Applying AuNP1 dispersion with a concentration of 437 $\mu\text{g/ml}$ resulted in higher number of AuNP in z-sections of longitudinal skin sections of 10 μm thickness in the SC as well as in DSL (Figure 3.4.6). For the two tested concentrations, incubation time showed a strong effect on the amount of AuNP penetrating into the SC and DSL. An exposure time of 6 h was

required for AuNP1 with a concentration of 90 µg/ml to permeate the SC whereas 2 h were enough for the high concentration AuNP dispersion (437 µg/ml) to penetrate into the DSL though this was a negligible amount. The longer the skin exposure time, the larger the amount of AuNP1 penetrating into the SC and DSL (Figure 3.4.6). This is also attributed to the amount of particles necessary to be detected favoring high concentrations to be visualized.

Maximum penetration depths of AuNP1 inside the skin were further determined for these skin penetration experiments (Table 3.4.4). The same trend was also observed on changing the concentration and the skin exposure time. The higher the concentration and/or the longer the skin exposure time, the longer the distance that could be travelled by AuNP1 inside the skin. The longest penetration depth by AuNP1 in DSL after crossing the whole thickness of the SC was 51.38 µm (Table 3.4.4). Knowing that the average thickness of the viable epidermis is 50-100 µm [184], particles could only reach the viable epidermis of human skin after 24 h of skin exposure. Longer exposure times could be needed for the particles to penetrate more into the dermis however skin penetration experiments were terminated at 24 h to avoid loss of skin integrity [94].

On further analysis of Figure 3.4.6, one could observe a gradually increasing difference between the densities of particle localization in the DSL for the two applied concentrations with time, reaching maximum at 24 h. This could be attributed to:

- (a) The higher the concentration of the nanodispersion the more the particles are available for penetration leading to much more particle accumulation in the deeper skin layers.
- (b) The higher concentration dispersion requires also a shorter exposure time (2 h) than that at low concentration (6 h) to cross the stratum corneum (Table 3.4.4) leading to a higher cumulative concentration of particles in the deeper skin layer.

It should be noted here that the whole area of the deeper skin layer in the image field is included in analysis. This means that the concentration measured is a more or less “cumulative” concentration.

Based on this, care should be taken on meta-analysis of the available literature on skin nanoparticle penetration. This means that extrapolation of the studies based on a single concentration or a short exposure time to indicate safety of nanoparticles or the opposite case should be avoided

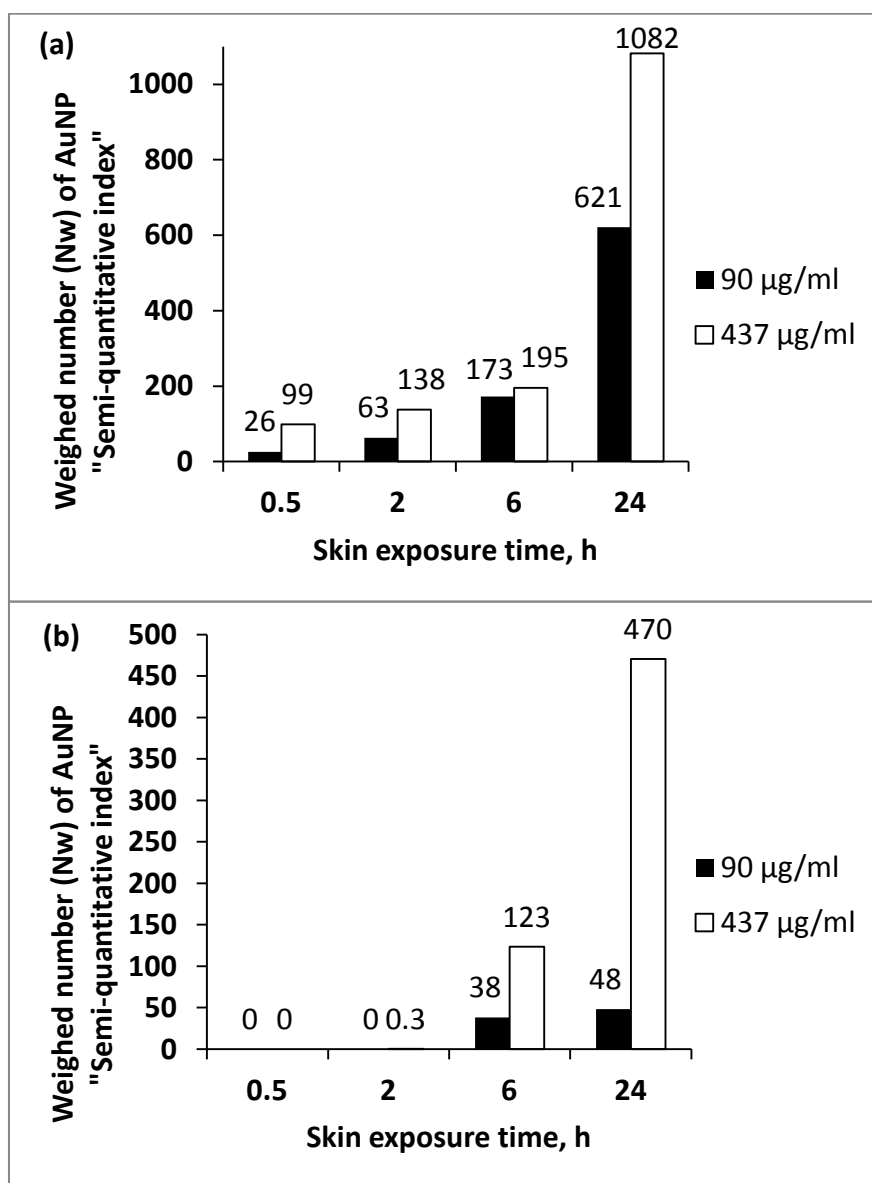


Figure 3.4.6: Effect of concentration of applied AuNP1 (6 nm thiol-coated AuNP, dispersed in toluene) and skin exposure time on their penetration into the SC (a) and to DSL (b) after 24 h of skin exposure.

Table 3.4.4: Maximum skin penetration depths of AuNP1 (6 nm thiol-coated AuNP, dispersed in toluene) in 90 and 437 $\mu\text{g/ml}$ concentration after 0.5, 2, 6 and 24 h of skin exposure, normalized to the thickness of the SC (i) and penetration depth inside DSL after crossing the whole thickness of SC (ii).

(i)

Incubation time [h]	^a Percentage depth of SC penetrated by AuNP1, %	
	90 $\mu\text{g/ml}$	437 $\mu\text{g/ml}$
0.5	48.55	77.99
2	92.65	100
6	100	100
24	100	100

^a Percentage SC penetrated = penetration depth in SC / thickness of SC x 100

(ii)

Incubation time, h	^b Penetration depth of AuNP1 in DSL, μm	
	90 $\mu\text{g/ml}$	437 $\mu\text{g/ml}$
0.5	0	0
2	0	23.86
6	7.21	29.82
24	35.72	51.38

^b Penetration depth in DSL = Total penetration depth - thickness of SC

3.4.4. Conclusions

As for drug molecules, the main barrier for particle penetration is the SC lipids, however it is not only the intercellular lipids that limit penetration of particles but the whole microstructure of the SC with its tortuous intercellular aqueous and lipidic channels. Furthermore, the varying polarities of the skin layers further reduce permeation into deeper skin layers. AuNP are expected to penetrate mainly through intercellular pathways. This penetration behavior is primarily dependent on their physicochemical attributes, of which the size is the most significant determinant of

penetration where 6 nm AuNP showed a greater extent of penetration than 15 nm AuNP. Similar to drug penetration, the surface hydrophobicity was also found as an important factor favoring skin penetration. This again implies that nanoparticles at this size range (6-15 nm) behave similar to drug molecules in permeation through the skin barrier but to a lower extent. On the other hand, the vehicle was found to have a minimal effect on skin penetration of AuNP.

Skin exposure time was also found to be of crucial impact. Incubation times of at least 6 h were required to have a significant penetration extent for studying the effect of the different physicochemical, formulation and environmental factors. Shorter exposure time is thus not recommended by the authors for conducting experiments focusing on determination of skin penetration of nanoparticles. For a certain skin exposure time, the concentration of the applied nanodispersion could greatly influence or even determine the status of skin penetration of nanoparticles, whether they could be detected or not in the DSL. This should be regarded in future studies. The results obtained in this study are of great importance especially for the basic understanding of the interaction of nanoparticles with the skin barrier.

3.5. Could chemical enhancement of gold nanoparticle penetration be extrapolated from established approaches for drug permeation?

Hagar I. Labouta, Labiba K. El-Khordagui and Marc Schneider

In due publication.(submitted)

Abstract

Investigations on chemical enhancement of skin penetration of gold nanoparticles are considered crucial not only for the high clinical significance, but also for designing an ideal nanocarrier for transdermal drug delivery and to have a deeper insight into the main barrier of particle penetration. In this study, penetration of gold nanoparticles in presence of several chemical enhancers -urea, sodium lauryl sulphate, polysorbate 80 and dimethyl sulphoxide (DMSO)- through human skin was studied. Among the tested chemical enhancers, DMSO could induce the penetration of hydrophilic (citrate-stabilized) gold colloid of no intrinsic penetration ability, in a concentration-dependent manner. Pretreatment of the skin with DMSO however reduced penetration of hydrophobic (thiol-coated) gold nanoparticles as a result of aggregation in the top layers of the stratum corneum limiting penetration into the deeper skin layers. In addition, nanoparticles-vehicle interaction and the stability of the nanoparticles in the applied vehicle were found important determinants of skin penetration. Our results demonstrate that the already established approaches for chemical permeation enhancement of drug molecules and their postulated mechanisms could be used as preliminary guidelines for enhancing the penetration of nanoparticles. At this size range, 15 nm, intercellular lipids provide the main barrier to particle permeation through the stratum corneum.

3.5.1. Introduction

The main barrier of the skin resides in the stratum corneum (SC) due to its complex micro- and macrostructure. Several pathways are postulated for drug transport across the skin including intercellular, intracellular and transappendageal pathways, of which the intercellular route is regarded as the most likely route for transdermal drug permeation. In this context, the barrier function of the SC against penetration of drugs or molecules in general depends mainly on the intercellular lipids [175]. Currently, the most widely used approach to drug permeation enhancement is the use of chemical penetration enhancers with already several theories and postulated mechanisms of action of the different classes of chemical enhancers in favoring transdermal drug permeation. They work mainly by temporarily reducing the barrier function of the SC allowing for more drug transport [104].

Skin penetration of nanoparticles in presence of these chemical enhancers would be of interest to evaluate if data from skin penetration enhancement of drug molecules can be extrapolated to particles. Among formulation factors influencing skin penetration, stand both the vehicle nature and vehicle-nanoparticles interaction as important parameters that should be carefully studied. In this context, changing the vehicle composition together with investigating the effect of chemical permeation enhancers on skin penetration of nanoparticles would ultimately lead to more insight into the possible barrier of skin penetration of nanoparticles. Kuo *et al.* [85] studied the effect of oleic acid and ethanol on the penetration of zinc oxide nanoparticles ($\varnothing = 10$ nm) through mouse skin. They showed enhanced transport values for nanoparticles in presence of oleic acid, ethanol and oleic acid-ethanol mixture. However, no penetration of quantum dots ($\varnothing = 37$ nm) was observed on pretreatment of mouse skin with acetone [47]. Yet, in these two studies, mouse skin, known to have different penetration and structural characteristics than human skin, was used as the skin model.

The aim of this work was therefore to study the penetration of gold nanoparticles (AuNP) through human skin in presence of selected chemical enhancers from different classes: Urea (amide), sodium lauryl sulphate (SLS) (anionic surfactant), polysorbate 80 (non-ionic surfactant) and dimethyl sulphoxide (DMSO) (sulphoxide/solvent) proved effective in promoting transdermal drug permeation.

AuNP were used as a model due to their multiphoton-induced luminescence [134]. Hydrophilic citrate-stabilized AuNP, 15 nm in diameter at a gold concentration of 90 µg/ml (2.7×10^{12} particles/ml) were selected for this study, since they were shown to lack an intrinsic ability to penetrate human skin after 24 h skin contact [55]. Furthermore, the enhancement of penetration of hydrophobic AuNP was studied.

3.5.2. Materials and methods

Preparation of AuNP. Ionically-stabilized, polar gold nanoparticles (AuNP1) were prepared according to Turkevich method [25, 132]. Briefly, 70 ml solution of hydrogen tetrachloroaurate ($\text{HAuCl}_4 \cdot 3\text{H}_2\text{O}$, Sigma-Aldrich Chemie GmbH, Steinheim, Germany) containing about 100 µg/ml gold was reduced by trisodium citrate dihydrate ($\text{Na}_3\text{C}_6\text{H}_5\text{O}_7 \cdot 2\text{H}_2\text{O}$, Sigma-Aldrich) containing 5-fold the molar concentration of the gold salt at 100°C.

Phase transfer of AuNP into toluene. Thioglycolic acid (TGA) (Sigma-Aldrich Chemie GmbH, Steinheim, Germany) equivalent to 1.29×10^{-3} moles was added to 2 ml of AuNP dispersion, with a concentration of 198.1 µg/ml gold and stirred until the solution gets purple. Cetrimide (Merck KGaA, Darmstadt, Germany) was then introduced to the AuNP dispersion. The molar ratio between TGA and cetrimide was 2:1. Stirring was continued for 30 min to allow for the adsorption of surfactant molecules through electrostatic interaction between TGA and cetrimide. The dispersion was then mixed with 2 ml toluene for 10 min, resulting in O/W emulsion. Finally, 2 ml ethanol, containing 0.21 M cetrimide, was added to break the emulsion, in addition to 3 ml toluene for better extraction of AuNP2 with hydrophobized surface. The whole two-phase system was vigorously shaken for 20 min. Extracted AuNP in toluene were further treated with cetrimide (6.86×10^{-6} moles for each 1 ml of AuNP dispersion) to enhance stability.

Characterization of the optical and colloidal properties for the prepared AuNP.

The optical properties of prepared AuNP were checked using a UV/Vis Spectrophotometer (lambda 35, Perkin Elmer, Rodgau-Jürgesheim, Germany) in the range of 400-800 nm. The mean particle size and the morphology of the gold core were determined by transmission electron microscopy (TEM) using a JOEL Model

JEM 2010 instrument (JOEL GmbH, Eching, Germany) operated at an accelerating voltage of 120 kV. Finally, the surface charge was estimated by measuring the zeta potential based on the electrophoretic mobility (Zetasizer Nano, Malvern Instruments, Malvern, UK).

Study of the penetration of AuNP through human skin.

Skin preparation. Healthy human skin was obtained from female patients, who had undergone abdominal plastic surgery after approval of the ethic committee of Saarland, Germany (Ärzttekammer des Saarlandes, Dec. 2008). Immediately after excision, the subcutaneous fatty tissue was removed from the skin specimen using a scalpel. Afterwards the surface of each specimen was cleaned with water, dried, wrapped in aluminum foil and stored in polyethylene bags at -26°C until use. Previous investigations have shown that no change in the penetration characteristics occurs during the storage time of 6 months [159].

Skin discs, 25 mm in diameter, were punched out from frozen skin, thawed, cleaned with water and transferred into a Franz diffusion cell.

Skin penetration study. *In vitro* penetration experiments were run in static Franz diffusion cells having a diffusion area of 1.76 cm^2 and a receptor compartment of 12 ml, containing phosphate buffer saline, pH 7.4 magnetically stirred at 500 rpm. A volume of 500 μl of AuNP dispersion was placed on the skin then the donor compartment was occluded. The diffusion cells were maintained at 32°C throughout the experiment. Following exposure, the skin was removed and the skin surface was gently cleaned with cotton. Collected skin was examined after longitudinal cryo-sectioning.

Longitudinal skin cryo-sectioning. Cross-sections of 10 μm thickness were performed at -26°C using a cryomicrotome (Slee, Mainz, Germany). The skin punch was placed in a perpendicular direction to the cutting blade piece to avoid dislocation of the particles from outside into DSL or vice versa, thus limiting sectioning artifacts [134]. Skin sections were placed on microscopical slides and mounted by an aqueous mounting medium (FluorSaveTM reagent, Calbiochem, San Diego, USA) and covered with glass cover slips.

Multiphoton Laser Microscopy. Imaging was performed using an inverted confocal/two photon excitation fluorescence microscope (ZEISS LSM 510 META system, Carl Zeiss, Jena, Germany). The objective used was water immersion lens 63X (NA=1.2). A wavelength of 800 nm was used for both excitation of AuNP and scanning the skin using an energy of 0.485 and 0.647 mW, respectively. The optical settings, discussed in detail earlier [55], allowed for separation of both signals with no signal interference among tracks. Z-stacks of the skin samples were taken with steps every 1 μm . Each optical scan is composed of 512 x 512 pixel² and a size of 0.14 x 0.14 μm^2 . The gain settings were adjusted for each measurement individually.

Data analysis. Detailed description of the method of analysis is published earlier [134]. In short, semiquantitative data for the distribution of AuNP in the SC and DSL were extracted based on calculation of \sum pixel frequency due to AuNP in the optical layers, 1 μm thickness, of the respective z-stacks of the examined longitudinal skin sections. These values were then used to calculate the total number of AuNP in the SC and DSL according to Equation 3.5.1:

$$N_w = \frac{\sum \text{Pixel} \times A_{\text{pixel}}}{A_{\text{particle}}} \quad \text{Equation 3.5.1 [134],}$$

,where $A_{\text{pixel}} = 0.139 \times 0.139 \mu\text{m}^2$ and A_{particle} (area of diffraction-limited AuNP) = 0.365 μm^2 for the optical settings used in this study as detailed elsewhere [134].

3.5.3. Results and discussion

AuNP1 (hydrophilic, negatively charged (zeta-potential -35.1 ± 1.87 mV), citrate-stabilized, $\text{Ø} = 14.90 \pm 1.76$ nm) were shown earlier not to penetrate the SC into DSL (deeper skin layers) [55]. Skin penetration of AuNP1 was studied in presence of different chemical enhancers at concentrations reported in literature to enhance transdermal drug permeation, as shown in Table 3.5.1. AuNP1 were stable for at least 2 days in all the tested systems (data not shown).

Figure 3.5.1a shows the behavior of AuNP1, at a concentration of 90 $\mu\text{g/ml}$, when topically applied on human skin dispersed in 5% urea solution. The particles can be found exclusively within the SC. Hence, Urea was found ineffective to drive AuNP to penetrate into DSL. Urea is known to promote transdermal drug permeation by

facilitating hydration of the SC and formation of hydrophilic diffusion channels, and by acting on the SC corneocytes (protein deformation). Yet, urea itself is a hydrophilic compound of no lipid disruption mechanism [104]. This suggests that the intercellular lipids represent the barrier to skin penetration of hydrophilic AuNP1. Moreover, as suggested for drugs [185], the physicochemical parameters of the nanoparticles and the chemical enhancer should be considered on selecting an appropriate enhancer, for example, the penetration of hydrophilic nanoparticles maybe increased by using a lipophilic enhancer. On the other hand, the aggregation state of the applied nanodispersion, is considered critical and should be analyzed carefully in parallel with skin penetration study. Aggregation of AuNP is indicated by a big redshift of the spectral peak and/or peak broadening [161]. Aggregation of AuNP result in big redshift of λ_{max} . Depending on the number of particles in the aggregate, the shift can easily exceed 150 nm [161]. This is in addition to significant peak broadening. Weisbecker *et al.* [186] calculated the AUC from 600 to 800 nm as a marker for broadening of gold colloids. As shown in Figure 3.5.2, AuNP1 in water aggregate on skin contact (an index higher than 6 is assumed to indicate strong aggregation). Similarly, topical application of AuNP1 in 5% urea solution for 24 h resulted in strong aggregation and precipitation of AuNP (Figure 3.5.2). This reduces the ability of the nanodispersion to penetrate through the SC into DSL.

Table 1: Conditions of skin penetration experiments for the prepared AuNP dispersions, at a concentration of 90 µg/ml.

Nanoparticles code	Chemical enhancer*	Concentration of chemical enhancer [%]	Skin exposure time to AuNP dispersion, [h]
AuNP1**	-	-	24
	Urea	5	24
	Sodium lauryl sulphate (SLS)	5	24
	Polysorbate 80	5	24
		20	24
	Dimethyl sulphoxide (DMSO)	50	24
		80	24
		-	22 (after 2 h exposure to 100% DMSO)
AuNP2***	-	-	24
	-	-	22 (after 2 h exposure to 100% DMSO)

*added to the nanodispersion.

**hydrophilic, citrate-stabilized AuNP, ~15 nm in diameter

***hydrophobic, coated with thioglycolic acid and cetrimide, ~15 nm in diameter.

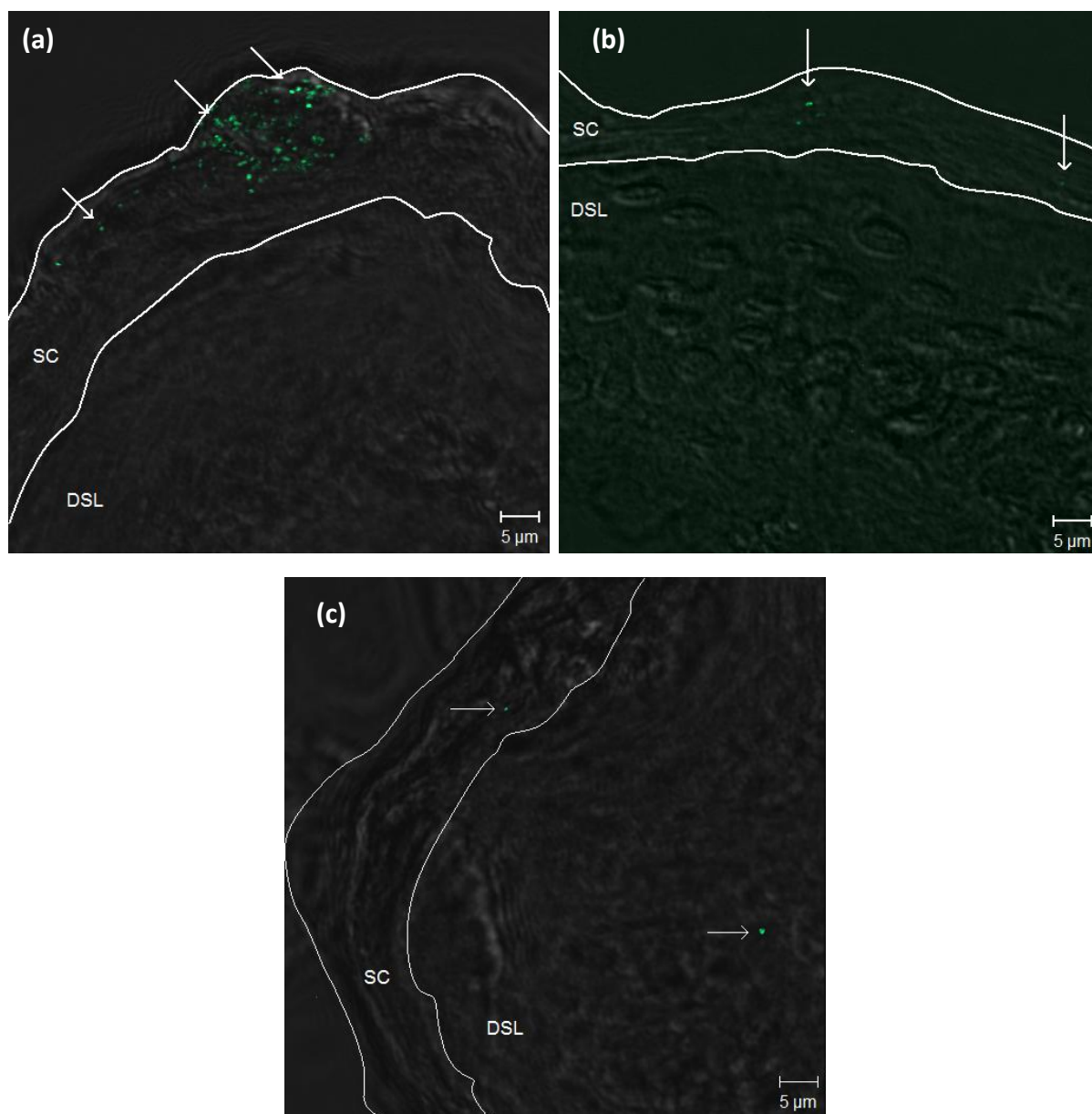


Figure 3.5.1 (a-c): Overlaid multiphoton/transmission images of AuNP1 (indicated as green spots) at a concentration of 90 μg/ml in longitudinal skin sections, showing exclusive localization of AuNP in the SC (stratum corneum) when applied in 5% concentration of urea (a) or SLS (sodium lauryl sulphate) (b) after 24 h of skin exposure or penetration of minute amounts into DSL (deeper skin layers) in case of polysorbate 80, 5% in concentration (c).

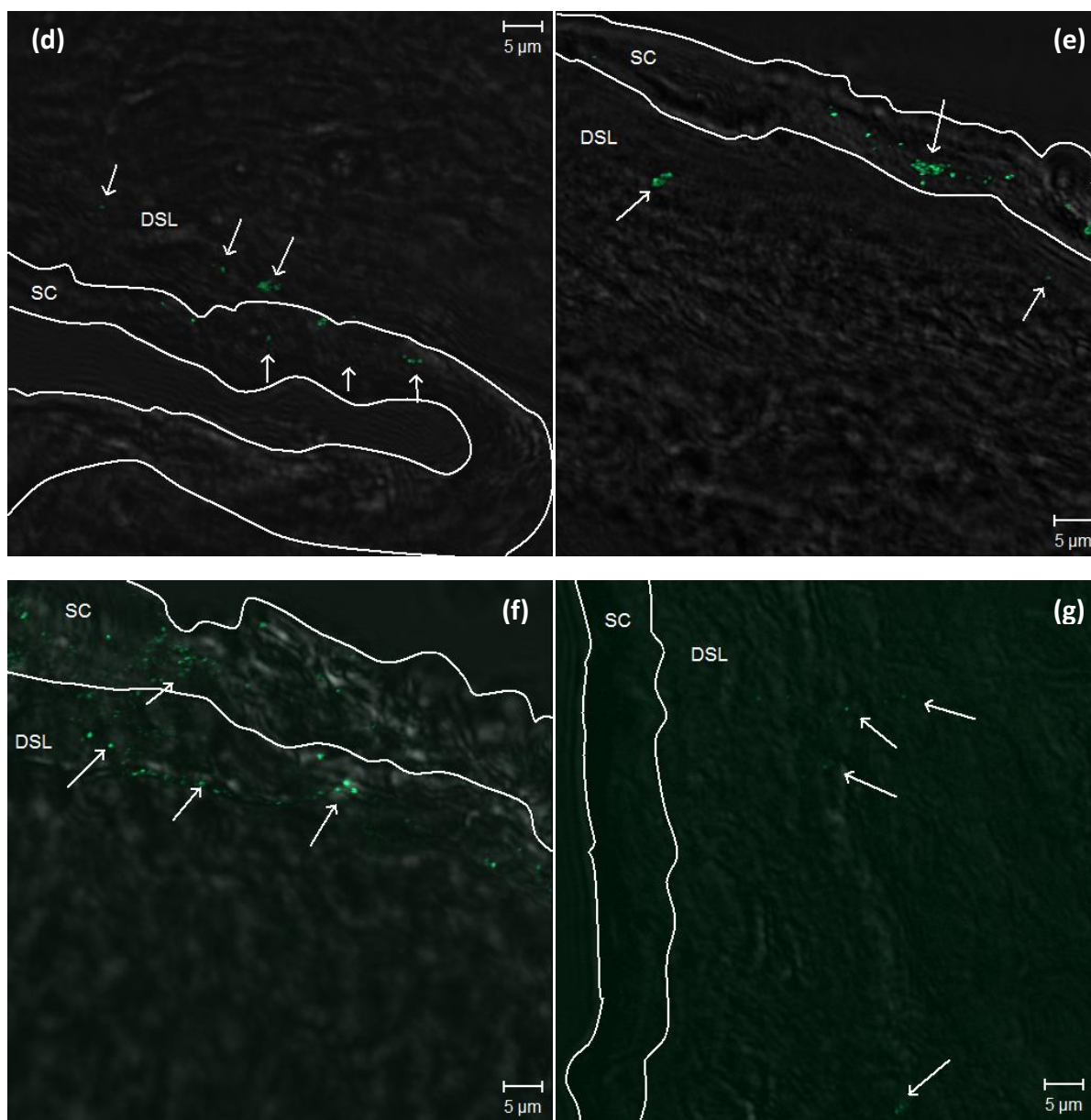


Figure 3.5.1 (d-g): Overlaid multiphoton/transmission images of AuNP1 (indicated as green spots) at a concentration of 90 $\mu\text{g/ml}$ in longitudinal skin sections. AuNP1 applied in 20% (d), 50% (e) and 80% DMSO (dimethyl sulphoxide) (f) for 24 h, as well as pre-exposure of the skin to 100% DMSO for 2 h, followed by 22 h exposure to AuNP1 (g) resulted in permeation of AuNP1 of the SC (stratum corneum) into DSL (deeper skin layers).

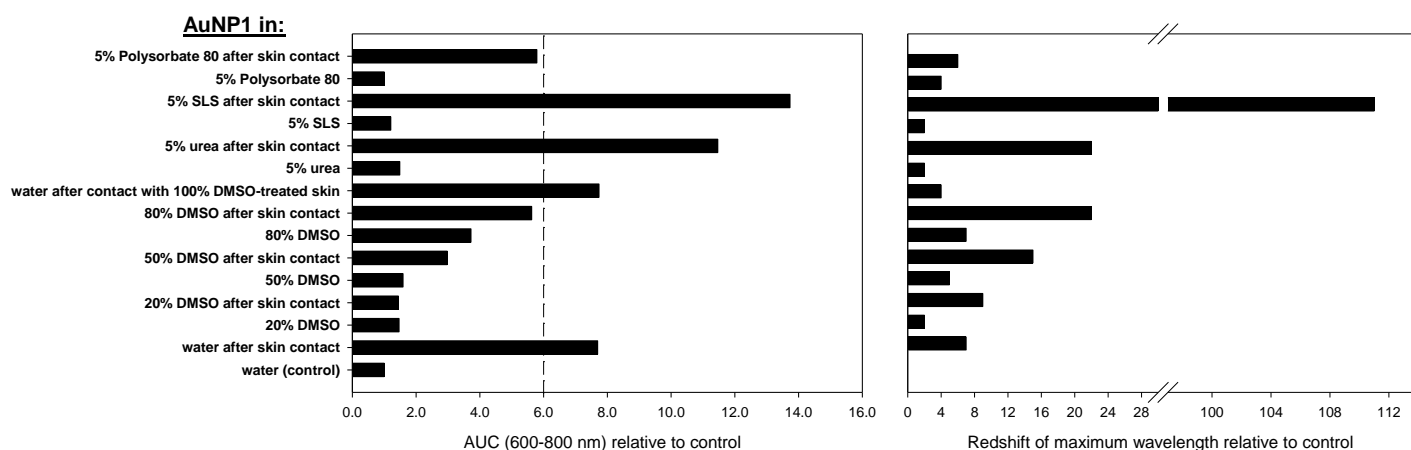


Figure 3.5.2: Plasmon peak broadening over wavelengths from 600 to 800 nm of AuNP1 in the prepared polysorbate 80, SLS (sodium lauryl sulphate), urea and DMSO (dimethyl sulphoxide) at a concentration of 90 $\mu\text{g/ml}$ and redshift of the respective maximum wavelength compared to that of AuNP1 dispersion in water, designated as “control”, as markers for particle stability before and after 24 h skin contact.

As an alternative strategy, anionic (SLS) and non-ionic (polysorbate 80) surfactants were investigated as potential chemical penetration enhancers for nanoparticles through human skin. The use of cationic surfactants was excluded due to possible electrostatic interaction with the negatively charged AuNP1. SLS and polysorbate 80 are water-soluble with fatty acid moieties, lauric and oleic acid, respectively, providing a lipophilic character for better penetration of the nanoparticles. However, both applied surfactants, applied at a concentration of 5% (above critical micelle concentration “CMC”) were found ineffective for driving AuNP1 to penetrate the SC in considerable amounts (Figure 3.5.1b, c).

In general, the mechanisms of action of the different classes of surfactants for promoting drug permeation are still not clear. Yet, the action of anionic surfactants, including SLS, on skin was previously postulated to be mainly due to their ability to interact with and bind to epidermal proteins, thus causing a reversible denaturation and an uncoiling of the filaments, exposing more water binding sites, possibly increasing the hydration level of the tissue. This is in addition to possible effect on the lipid organization above CMC concentration, though penetration into the skin lipid channels is likely hindered by micelle formation [187]. On the other hand, nonionic surfactants, e.g. polysorbate 80 were generally reported to have little effect in

promoting percutaneous drug absorption. Unexpectedly, however, minute amounts of AuNP were found in DSL in case of polysorbate 80 but not on applying AuNP1 in SLS solution. This observation could be related to the aggregation behavior of the AuNP1 in surfactant solutions on topical application. The different chemical enhancers after being in contact with the skin affected the plasmon resonance peak of the particles. Peak broadening of AuNP1 in presence of SLS after 24 h of skin contact, as well as the big redshift of λ_{\max} (111 nm) is a clear indication of aggregation (Figure 3.5.2). This would rather limit the probability of skin penetration due to the bigger sized objects. On the other hand, aggregation was also observed in case of polysorbate 80, but to a lesser extent (Figure 3.5.2). Nevertheless, application of AuNP1 in surfactant solutions was not an effective strategy in promoting skin penetration of nanoparticles in this study.

Therefore, it was important at this stage to choose a penetration enhancer with an evident effect on the intercellular lipids. DMSO is a solvent that is absorbed into the corneocytes changing the keratin conformation. However, at a concentration $\geq 60\%$, DMSO has an additional evident effect on the intercellular lipid domains. It causes reversible disorder or fluidization of the lipid structure of the SC. It forms microcavities within the lipid bilayers and increases the drug partitioning across the skin [188]. DMSO has a long clinical history of topical use to treat allergy, inflammation, especially in combination with NSAIDs; the applied concentrations varies largely reaching to 90 or 100% concentration [189-194].

AuNP1 were applied in DMSO solutions of 20 and 50% concentrations on human skin for 24 h, in which the main mechanism of penetration enhancement should be through the effect of DMSO on skin proteins resulting in higher intracellular transport. AuNP1 was also applied in a higher DMSO concentration, 80% to study the effect of lipid fluidization on penetration of AuNP1. For these three experiments, there was a possible change in the surface properties of AuNP that could also have an influence on penetration. Therefore, another skin experiment was conducted involving skin exposure to DMSO (100%) for 2 h followed by application of AuNP1 in water for another 22 h to study the intrinsic effect of DMSO.

All skin penetration experiments involving the use of DMSO as a chemical penetration enhancer resulted in penetration of AuNP1 into DSL (Figure 3.5.1d-g).

The sum of the pixels due to gold luminescence was then determined in the SC and DSL in representative optical z-stacks, 1 μm thickness for each layer, of the examined longitudinal skin sections and finally the weighed number of AuNP in the SC and DSL was calculated using a method we developed earlier [134]. Results of semiquantitative analysis are shown in Figure 3.5.3. In all skin experiments, more AuNP were found in the SC rather than DSL. Depending on the concentration of DMSO, variable amounts of AuNP penetrated into the SC and DSL. Application of AuNP1 in 20% resulted in 261 and 38 fold increase in the SC and DSL, respectively, compared to control AuNP1 (no penetration). Increasing the concentration of DMSO from 20 to 50% resulted in 1.4 and 1.6 fold further increase in the amount of AuNP penetrating into the SC and DSL, respectively. This is possibly due to looser and more permeable SC. An equivalent increase in DMSO concentration from 50 to 80% resulted however in more pronounced skin penetration of AuNP into the SC and DSL (3.1 and 5.7 fold, respectively). This underlines the expectation that as for drug molecules, intercellular lipids provide the main barrier to penetration of nanoparticles.

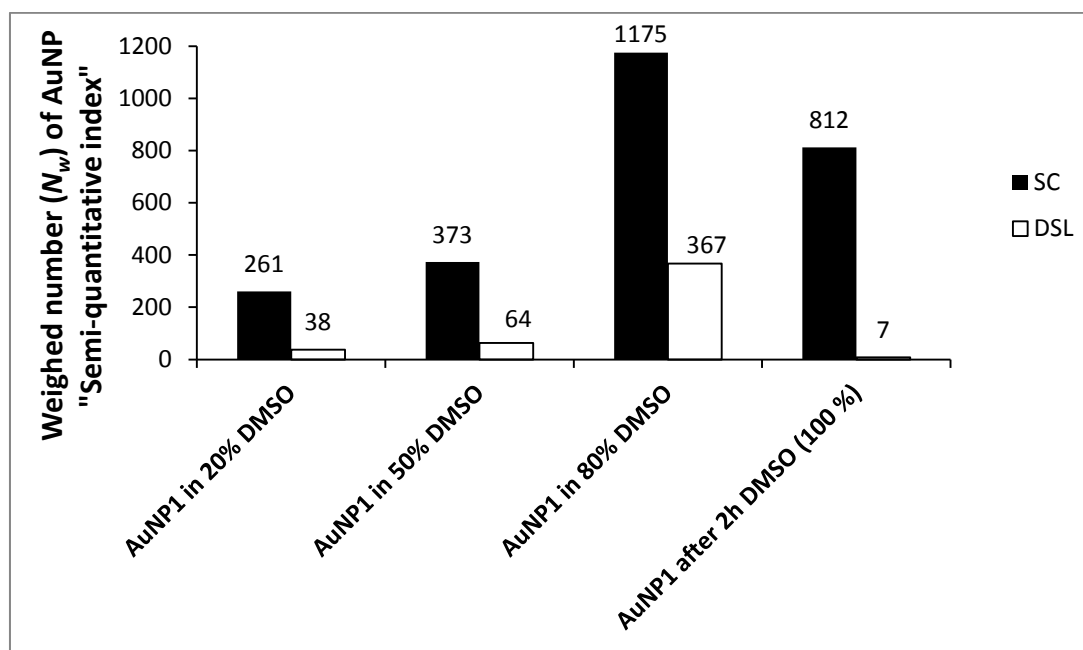


Figure 3.5.3: Effect of DMSO (dimethyl sulphoxide) in a concentration of 20%, 50% and 80% on skin penetration of AuNP1, at a concentration of 90 $\mu\text{g}/\text{ml}$ into the SC (stratum corneum) and DSL (deeper skin layers) on 24 h skin exposure, in comparison to pre-exposure of the skin to 100% DMSO for 2 h, followed by 22 h exposure to AuNP1, expressed as the total number of AuNP in optical layers, 1 μm thickness, of 10 μm longitudinal skin sections imaged by multiphoton microscopy.

Spectrophotometric analysis of the applied AuNP1 in DMSO dispersions was also performed in parallel with skin penetration study in order to determine the physical state of nanoparticles under the variable experimental conditions. Results of spectrophotometric analysis, shown in Figure 3.5.2, indicate the stability of AuNP1 in DMSO solutions on skin contact compared to control AuNP1 dispersion without DMSO. This is evident from the only small plasmon redshifts of 8, 11 and 17 nm for the applied AuNP1 in 20, 50 and 80% DMSO, respectively after 24 h contact with human skin in addition to unobvious peak broadening (Figure 3.5.2). However, application of hydrophilic citrate-stabilized AuNP without DMSO on human skin resulted in clear aggregation, as shown in Figure 3.5.2. This indicates that DMSO increased the stability of AuNP1 and prevented their aggregation when coming in contact with the skin surface. This represents an additional mechanism by which DMSO favors skin penetration of AuNP1 into DSL from these applied dispersions keeping the number of single dispersed nanoparticles high. On the other hand, application of AuNP1 dispersion on human skin following 2 h skin exposure to DMSO does not prevent aggregation of nanoparticles as shown by peak broadening in Figure 3.5.2. This explains the decrease in the population of AuNP that could penetrate into the SC by 1.4 fold compared to those on application of AuNP1 in 80% DMSO solution. This also explains an even higher decrease in AuNP penetration into the DSL, relative to all other experiments involving application of AuNP1 in DMSO solutions (Figure 3.5.3). This is despite the fact that DMSO at this high concentration, 100%, acts on both the corneocytes' keratin and the intercellular lipids compromising the barrier function of the SC to a great extent. This implies that nanoparticles-vehicle interaction is a critical determinant of skin penetration of nanoparticles and should be carefully considered when choosing a suitable chemical penetration enhancer. This is of even more importance as the particle aggregation is not instantaneous and hence might be overlooked.

The results so far show that DMSO is effective as a skin penetration enhancer for the hydrophilic nanoparticles, AuNP1. Therefore, it was employed in further experiments were conducted to investigate the effect of the physicochemical properties of nanoparticles on skin penetration enhancement mechanism using hydrophobic AuNP2, prepared by phase transfer of AuNP1 into toluene using thioglycolic acid and cetrimide. AuNP2 are uncharged and of the same core-diameter as for AuNP1. However, due to instability of AuNP2 in DMSO even at very

low concentration, 2.4% (data not shown), AuNP2 was applied on human skin for 22 h after 2 h pre-exposure to DMSO. The weighed number of AuNP in the SC and in DSL in a representative optical z-stack of the examined longitudinal skin sections were then determined. The results were compared to those of a control experiment involving skin exposure to AuNP2 for 24 h in absence of DMSO as shown in Figure 3.5.4a. Skin exposure to DMSO for 2 h before AuNP2 application resulted in 1.6 and 1.5 fold decrease in the number of AuNP penetrating into the SC and DSL, respectively, relative to the control experiment. This is despite the fact that AuNP2 in the donor compartment was stable on skin contact for 24 h (Figure 3.5.4b). It is assumed that DMSO could not enhance the penetration of the hydrophobic AuNP2 as much as for hydrophilic particles since the intercellular lipids, fluidized by DMSO, are less barrier to their transport than for the hydrophilic nanoparticles, AuNP1. Yet, the decrease in skin penetration of AuNP2 following skin exposure to DMSO can be explained by the assumption that particle aggregation could have taken place in the upper layers of the SC due to absorption of a trace amount of DMSO during the pre-incubation stage with the solvent. This would decrease the probability of their penetration into the deeper layers of the SC and furthermore into the DSL. To prove this assumption, circular discs of a dialysis membrane MW-cut-off 12-14 kDa (Medicell International Ltd, London, UK), 15 mm in diameter (the same skin exposure area in Franz diffusion experiment) were placed in small vials and exposed to aqueous solutions with increasing concentration of DMSO (0, 20, 50, 80 and 100%) for 2 h. DMSO was then removed and the dialysis membranes in the vials were left to dry in the hood, then AuNP2 were added for another 22 h. At the end of the experiment, AuNP2 dispersions were analyzed using UV/Vis spectrophotometry and the results are shown in (Figure 3.5.5). The higher the initial concentration of the applied DMSO solution, the more aggregation of the nanodispersion was observed. This represents a proof of concept that the trace amount of DMSO absorbed into the upper layers of the SC which could not be removed by cleaning the skin surface resulted in aggregation of AuNP2. Hence penetration deeper inside the skin was hindered.

In conclusion, chemical enhancement of skin penetration of gold nanoparticles could be extrapolated from already established approaches for transdermal permeation of drug molecules. In the size range of 15 nm, the intercellular lipids provide the main

barrier for penetration. As for drugs, the physicochemical attributes of nanoparticles and the chemical enhancer determine the success of the approach. However, the nanoparticles-vehicle interaction and the stability of the nanoparticles in the applied vehicle represent critical parameters in transdermal delivery of nanoparticles.

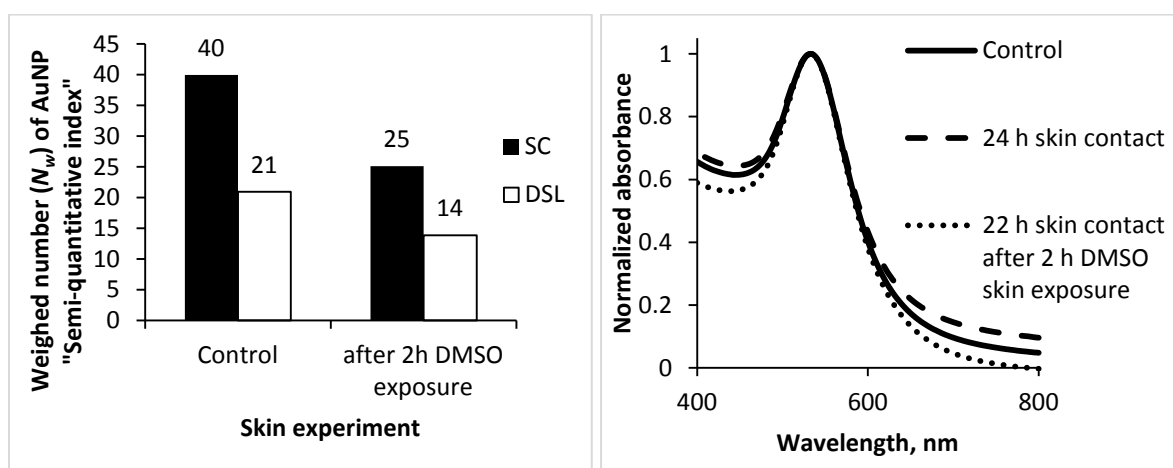


Figure 3.5.4: (a) Effect of skin pre-exposure to 100% DMSO (dimethyl sulphoxide) for 2 h on skin penetration of AuNP2, at a concentration of 90 $\mu\text{g/ml}$ into the SC (stratum corneum) and DSL (deeper skin layers) on 22 h skin exposure, expressed as the total number of AuNP in optical layers, 1 μm thickness, of a representative Z-stack in a 10 μm thickness longitudinal skin section imaged by multiphoton microscopy, in comparison to control skin penetration experiment of AuNP2 for 24 h. (b) UV/Vis spectra of AuNP2 at a concentration of 90 $\mu\text{g/ml}$ showing particle stability before, designated as "control", and after 24 h skin contact in comparison to their stability following 22 h contact with a skin pre-exposed to 100% DMSO for 2 h.

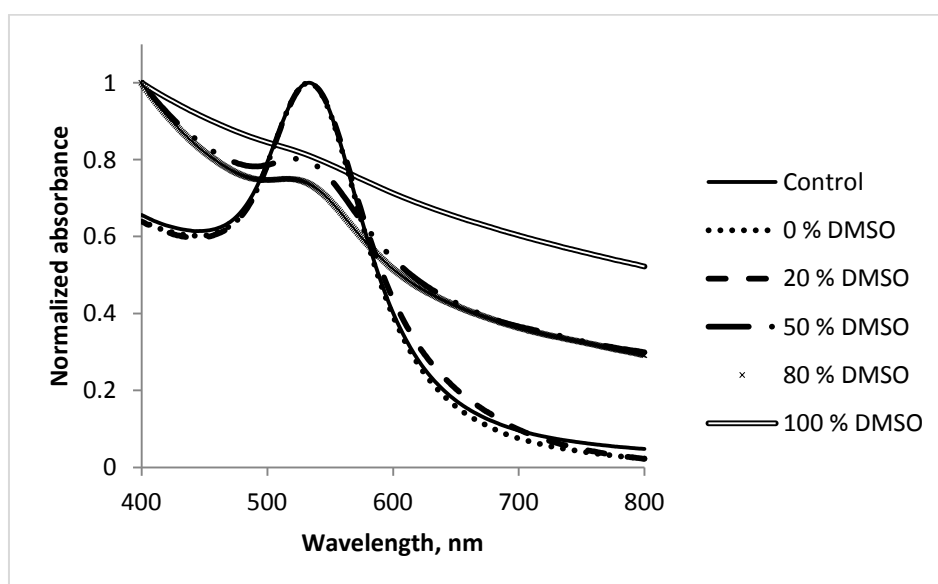


Figure 3.5.5: Stability of AuNP2 dispersions of a concentration of 90 $\mu\text{g/ml}$ after 22 h contact with dialysis membranes presoaked in increasing concentrations of DMSO (0-100%) in comparison to control AuNP2 dispersion.

3.6. Statements of effort

ad publication 3.1

The author of the thesis performed all the skin experiments, multiphoton microscopy, data analysis and interpretation, as well as writing the manuscript and planning for the experiments under the guidance of the supervisor and the other authors. Tobias Kraus was responsible for gold nanoparticles preparation and characterization.

ad publication 3.2

The author of the thesis prepared the gold nanoparticles, treatment of human skin with the prepared particle dispersion, preparation of all skin specimens for microscopy, multiphoton microscopy, data analysis, as well as writing the manuscript and planning for the experiments under the guidance of the supervisor and the other authors. Dr. Martina Hampel, Sibylle Thude and Katharina Reutlinger prepared the reconstructed human skin models.

ad publication 3.3

The author of this thesis prepared and characterized AuNP-Aq and performed thawed skin experiments (skin preparation, penetration experiments and multiphoton microscopy). Dr. Tobias Kraus was responsible for preparation and characterization of AuNP-TOL. Our partners from Australia performed the other experiments done on viable human skin (skin preparation, penetration experiments, cryosectioning, dermoscopy and reflectance confocal microscopy, TEM of skin samples). Both laboratories contributed equally in terms of practical work and writing the manuscript.

ad publication 3.4

The author of this thesis prepared and characterized AuNP3 and AuNP4. The author performed all the skin experiments, multiphoton microscopy, semiquantitative analysis, gravimetry and high performance thin layer chromatography, as well as writing the manuscript and planning for the experiments under the guidance of the supervisor and the other authors. Dr. Tobias Kraus was responsible for preparation and characterization of the two gold nanoparticles of diameter 6 nm.

ad publication 3.5

The author of this thesis prepared the nanoparticles and characterized them, performed skin experiments, microscopy, data analysis, as well as writing the manuscript and planning for the experiments under the guidance of the supervisor and the other author.

All the work done was directly supervised by Junior Prof. Dr. Marc Schneider, my principal supervisor. In addition, since the work done throughout the thesis was initially funded by the Egyptian government and the DAAD as a joint channel project, part of this work was also co-supervised by Prof. Dr Labiba K. El-khordagui, Dept. of Pharmaceutics, Faculty of Pharmacy, Alexandria University, Egypt.

4. Summary

4.1. Results and discussion

The potential ability of nanoparticles to overcome the skin barrier, attributed mainly to the stratum corneum (SC), has been the subject of recent research. Studying skin penetration of nanoparticles is considered crucial in the field of nanotoxicology, as well as on the basic research level for future pharmaceutical and clinical applications.

We have established a method by multiphoton microscopy for investigating skin penetration of gold nanoparticles (AuNP) based on gold luminescence. The optimized optical settings allowed for the separation of both skin and gold signals with no signal interference among tracks. This was also confirmed by examination of control skin (Figure 4.1).

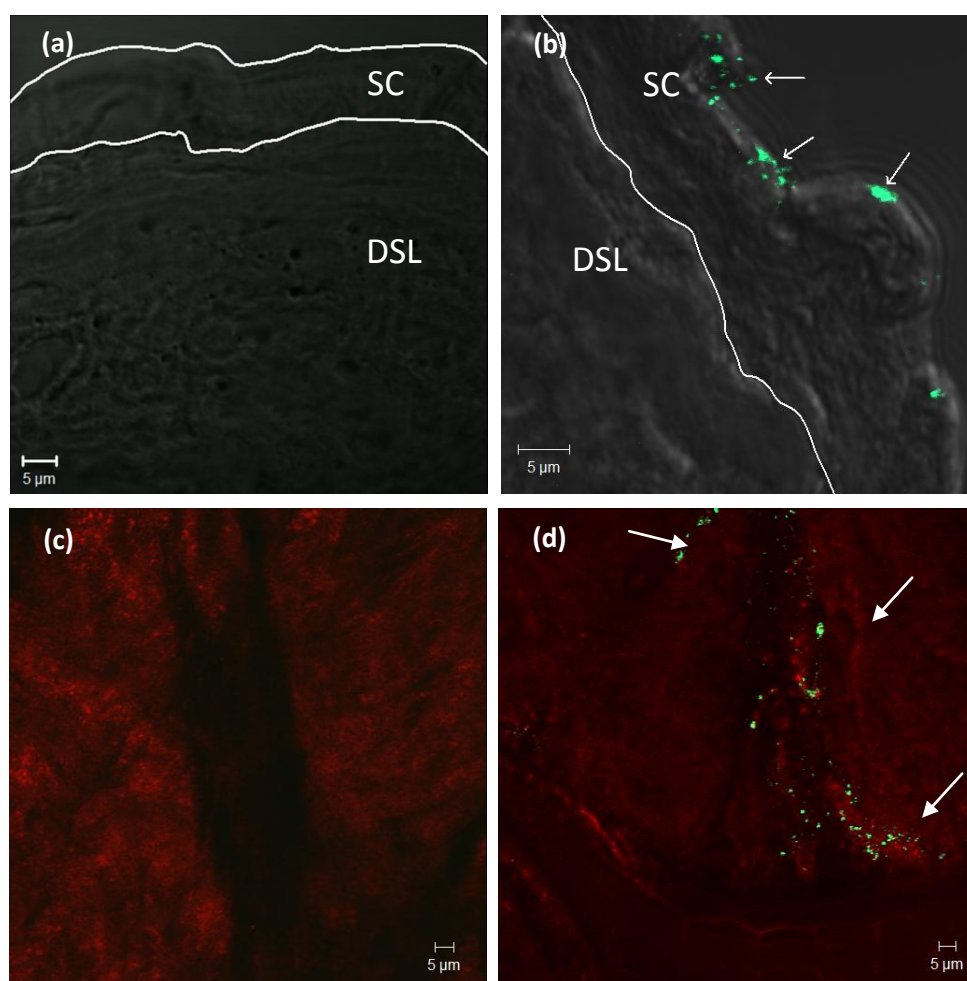


Figure 4.1: Overlaid multiphoton/transmission images of AuNP (indicated as green spots) in longitudinal skin sections (b), in comparison to control longitudinal skin section (a). Multiphoton images of skin-treated with AuNP from the top view (d), in comparison to control skin (c).

A combined multiphoton imaging-pixel analysis approach was then developed for semiquantitation of AuNP population in the SC and deeper skin layers (DSL) in terms of pixels, from which the weighed number of particles could be calculated (Figure 4.2). This method offers a relatively higher degree of accuracy and more freedom on selecting the optical settings and thus overrides previous approaches involving intensity measurement of fluorescence [89] and confocal [52] images. The latter approach necessitates fixed optical settings for all the experiments. This would rather limit the imaging capability of nanoparticles deep inside the skin using optical sectioning.

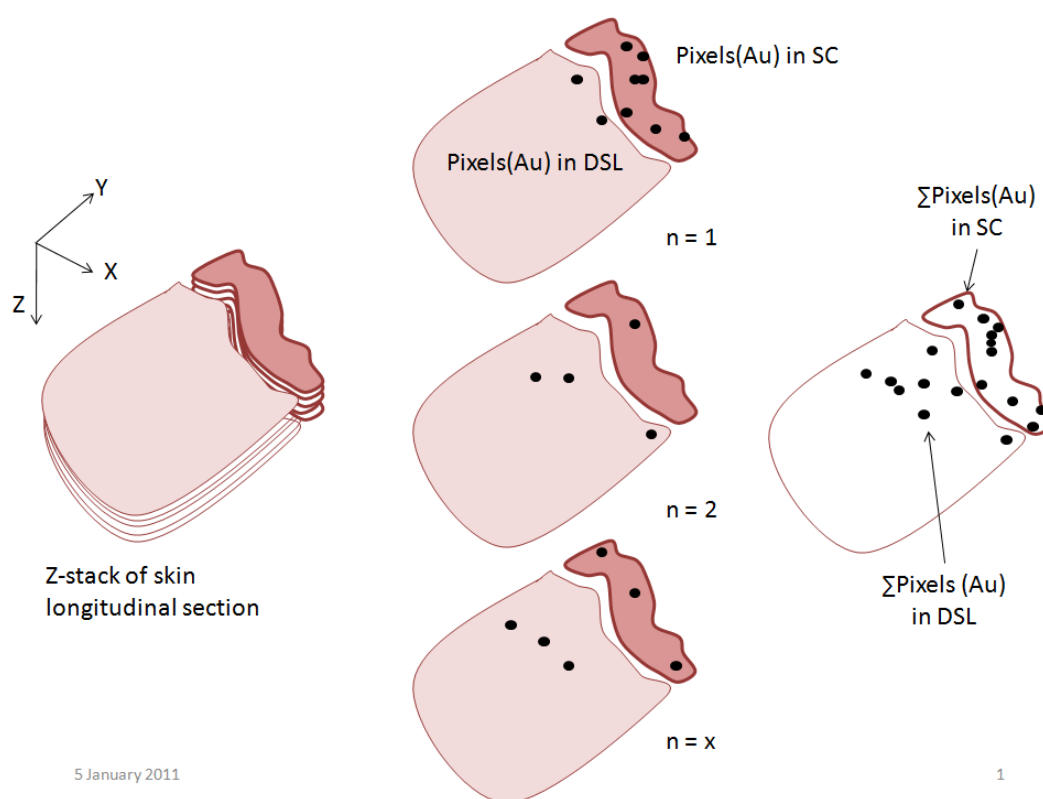


Figure 4.2: A schematic presentation of the combined multiphoton imaging-pixel analysis developed throughout the thesis [134].

Further work has been directed to the determination of the imaging parameters of multiphoton microscopy in skin in terms of achievable detection depths and the resolution limit. Multiphoton microscopy was shown to be a promising non-invasive technique with some limitations. Factors such as skin compactness and presence of wrinkles were found to deteriorate the accuracy of depth profiling. Lateral ($0.5 \pm 0.1 \mu\text{m}$) and axial ($1.0 \pm 0.3 \mu\text{m}$) point spread functions (PSF) in reconstructed and human skin specimens were determined practically. Both determined values

were higher than experimental values determined in water [128], glycerol [129] and turbid media (gel and lipid emulsion) [130]. This was explained by the higher optical density of the skin as an imaging medium. Surprisingly, lateral and axial PSF did not deteriorate with depth. This was attributed to the low tissue compactness, in case of reconstructed human skin or due to dominance of optical distortions caused by the optical system along the relatively short detection depth ($\sim 14 \mu\text{m}$) in human skin. More importantly, our results in human skin showed that AuNP could be tracked up to a shallow depth, $\sim 14 \mu\text{m}$, less than or equal to the average thickness of the SC due to scattering phenomenon in the heterogeneous skin tissue with depth, representing a major problem when tracking the penetration of nanoparticles into the DSL. According to our findings, examination of longitudinal skin sections was found more accurate and informative, rather than examination of non-sectioned skin from the top view. Therefore, longitudinal skin sections were used for further examinations.

AuNP of diameter 6 and 15 nm differing in surface polarity and vehicle nature (water and toluene) were successfully prepared and characterized. Their penetration through the skin was studied using multiphoton microscopy after validating the method as discussed earlier. Before studying the penetration of nanoparticles through the skin barrier, the effect of two selected nanoparticle dispersions (citrate-stabilized 15 nm AuNP in water and thiol-coated 6 nm AuNP in toluene) on the metabolic machinery of the skin was investigated using MP-FLIM (Multiphoton-fluorescence life-time imaging microscopy). Our results showed that the viability of the epidermis was deteriorated with distinct morphological changes after skin exposure to toluene regardless of AuNP presence. This was also shown by TEM and dermoscopy. The toluene-extracts after skin application were then analyzed gravimetrically and by means of HPTLC (high performance thin layer chromatography). Toluene was shown to have an effect on the barrier function of the SC by means of lipid extraction. Yet, only about 17% of the epidermal lipids were extracted after 24 h of skin application. Moreover, there were no drastic changes in the intercellular lipid structure on toluene application. Ceramides, known as the most important component of the SC multilamellar lipid structure with definite physicochemical properties necessary for the barrier function of the skin [178], were not extracted by toluene. This was supported by further results of the skin

penetration experiments conducted in this thesis indicating that the vehicle did not have a major effect on the penetration of the prepared nanoparticles.

Penetration studies involved skin application of four types of AuNP differing in size (6 and 15 nm), surface chemistry and vehicle (water and toluene). Results indicated penetration of all applied AuNP after 24 h of skin exposure except for citrate-stabilized AuNP, 15 nm in diameter. The physicochemical parameters were found key factors governing their skin penetration and permeation. Surface hydrophobicity of the nanoparticles was shown to favor skin penetration of AuNP through human skin. Citrate-stabilized ~ 15 nm AuNP could not penetrate human skin after 24 h of skin exposure. However, surface modification having cetrimide on the outer surface, i.e., hydrophobic surface, resulted in skin penetration into the deeper layers. A similar pattern was observed for smaller ~ 6 nm AuNP, in which surface modification of hydrophobic thiol-coated AuNP using lecithin yielded relatively hydrophilic AuNP with lower skin penetration ability under the same experimental conditions.

Away from the particle physicochemical and formulation factors, concentration of the applied nanodispersion and skin exposure time could greatly influence the skin penetration of nanoparticles. We applied thiol-coated AuNP on human skin with two different concentrations, 90 and 437 $\mu\text{g/ml}$ of gold, for exposure times of 0.5, 2, 6 and 24 h. Both the amount of AuNP penetrating into the DSL and the penetration depth increased with higher concentration and longer skin exposure time. Some other studies investigated skin particle penetration on different time intervals. For instance, Baroli *et al.* [53] studied the penetration of magnetic nanoparticles through human skin after 3, 6, 12 and 24 hr, where particle penetration was reported starting from 6 h skin exposure time. Based on these studies, generalized conclusions indicating safety of nanoparticles on topical application or the opposite case, based on studying a single concentration, is inappropriate.

The effect of deteriorating the barrier function of human skin by removal of the all epidermal lipids (using chloroform/methanol mixture) or by even total removal of the SC via tape-stripping on the skin penetration of citrate-stabilized 15 nm AuNP (no intrinsic penetration ability) was investigated. Removal of the epidermal lipids resulted in penetration of the tested AuNP indicating that the intercellular lipids are the main barrier for skin penetration of nanoparticles. Complete removal of the SC resulted, however, in about 28 fold further increase in penetration into DSL. This

would rather indicate that the barrier function of the SC to particle penetration does not rely only on the intercellular lipids but on the whole microstructure of the SC with its tortuous intercellular aqueous and lipidic channels.

Finally, attempts to induce the penetration of citrate-stabilized 15 nm AuNP were conducted. Penetration in presence of selected chemical enhancers from different classes, urea (amides), sodium lauryl sulphate (SLS) (anionic surfactant), polysorbate 80 (non-ionic surfactant) and dimethyl sulphoxide (DMSO) (sulphoxides) was investigated. The nanoparticles-vehicle interaction and the stability of the nanoparticles in the applied vehicle were shown to be a critical parameter in transdermal delivery of nanoparticles. DMSO could significantly induce the penetration of the applied gold colloid, in a concentration-dependent manner. On the other hand, pretreatment of the skin with DMSO reduced the penetration of cetrimide-coated 15 nm gold nanoparticles. This was experimentally shown to be attributed to aggregation in the top layers of the stratum corneum limiting penetration into the deeper skin layers, since the latter particles were found unstable in DMSO solutions. In addition, nanoparticles-vehicle interaction and the stability of the nanoparticles in the applied vehicle were found important determinants of skin penetration.

4.2. Conclusion

Multiphoton microscopy was found a promising technique in tracking skin penetration of nanoparticles with several limitations. Hence, the results based on this technique should be interpreted with care. Our results showed that examination of longitudinal skin sections, though suffering possible sectioning artifacts, still provides more accurate information on the status of AuNP penetration rather than optical sectioning of skin specimens examined from the top.

A combined multiphoton imaging-pixel analysis was successfully developed to semiquantify gold nanoparticles in the stratum corneum (SC) and DSL. Detection of gold nanoparticles in skin by multiphoton microscopy was based on gold luminescence. This experimental approach should be used as a tool in future studies to advance our basic understanding of nanoparticle interaction with the skin barrier.

As for molecules, the main barrier to particle penetration through the skin barrier was found to be the intercellular lipids. However, the whole microstructure of the SC with its intercellular aqueous and lipidic channels significantly limited particle penetration. This was shown from experiments performed using different grades of skin integrity.

The penetration behavior was primarily dependent on their physicochemical attributes, of which the size is the most significant determinant of penetration where 6 nm AuNP showed much higher extent of penetration rather than 15 nm AuNP. Our results however indicate a minimal effect of the vehicle on particle penetration. Furthermore, experimental considerations in setting-up a penetration experiment for nanoparticles were also studied. For instance, exposure times of at least 6 h are recommended for future studies on skin penetration of nanoparticles.

Findings obtained in the thesis are very important for the basic understanding of the interaction of nanoparticles with the skin barrier. This would find future pharmaceutical and clinical applications, e.g. designing optimal topical and transdermal delivery systems. This has also a direct impact on the field of nanotoxicology, especially in the area of work-place exposure.

5. References

1. Balogh, L.P., (2010) Why do we have so many definitions for nanoscience and nanotechnology?, *Nanomedicine: Nanotechnology, Biology and Medicine*, 6(3), 397-398.
2. Ramsden, J.J., (2009) What is Nanotechnology?, in *Applied Nanotechnology*, William Andrew Publishing, Boston, pp. 3-12.
3. Everts, M., (2007) Thermal scalpel to target cancer, *Expert Rev Med Devices*, 4(2), 131-136.
4. The United States National Nanotechnology Initiative. [accessed 2010 November 23]; Available from: <http://www.nano.gov/>.
5. Labouta, H.I. and Schneider, M., (2010) Tailor-made biofunctionalized nanoparticles using layer-by-layer technology, *Int J Pharm*, 395(1-2), 236-242.
6. Mazumder, S., Dey, R., Mitra, M.K., Mukherjee, S., and Das, G.C., (2009) Review: Biofunctionalized quantum dots in biology and medicine, *J Nanomater*, Article ID 815734, 17 pages.
7. Peng, C.-W. and Li, Y., (2010) Application of quantum dots-based biotechnology in cancer diagnosis: Current status and future perspectives, *J Nanomater*, Article ID 676839, 11 pages.
8. Gao, X., Cui, Y., Levenson, R.M., Chung, L.W., and Nie, S., (2004) In vivo cancer targeting and imaging with semiconductor quantum dots, *Nat Biotechnol*, 22(8), 969-976.
9. Michalet, X., Pinaud, F.F., Bentolila, L.A., Tsay, J.M., Doose, S., Li, J.J., Sundaresan, G., Wu, A.M., Gambhir, S.S., and Weiss, S., (2005) Quantum dots for live cells, in vivo imaging, and diagnostics, *Science*, 307(5709), 538-544.
10. Knopp, D., Tang, D., and Niessner, R., (2009) Review: bioanalytical applications of biomolecule-functionalized nanometer-sized doped silica particles, *Anal Chim Acta*, 647(1), 14-30.
11. Wang, L., Zhao, W., and Tan, W., (2008) Bioconjugated silica nanoparticles: Development and applications, *Nano Research*, 1(2), 99-115.
12. Atiyeh, B.S., Costagliola, M., Hayek, S.N., and Dibo, S.A., (2007) Effect of silver on burn wound infection control and healing: review of the literature, *Burns*, 33(2), 139-148.
13. Yen, H.J., Hsu, S.H., and Tsai, C.L., (2009) Cytotoxicity and immunological response of gold and silver nanoparticles of different sizes, *Small*, 5(13), 1553-1561.
14. Jose Ruben, M. and et al., (2005) The bactericidal effect of silver nanoparticles, *Nanotechnology*, 16(10), 2346.
15. Wong, K.K.Y. and Liu, X., (2010) Silver nanoparticles-the real "silver bullet" in clinical medicine?, *Med Chem Comm*, 1(2), 125-131.
16. Rai, M., Yadav, A., and Gade, A., (2009) Silver nanoparticles as a new generation of antimicrobials, *Biotechnol Adv*, 27(1), 76-83.
17. Pal, S., Tak, Y.K., and Song, J.M., (2007) Does the antibacterial activity of silver nanoparticles depend on the shape of the nanoparticle? A study of the gram-negative bacterium *Escherichia coli*, *Appl. Environ. Microbiol.*, 73(6), 1712-1720.
18. Sperling, R.A., Rivera Gil, P., Zhang, F., Zanella, M., and Parak, W.J., (2008) Biological applications of gold nanoparticles, *Chem Soc Rev*, 37(9), 1896-1908.
19. El-Brolossy, T.A., Abdallah, T., Mohamed, M.B., Abdallah, S., Easawi, K., Negm, S., and Talaat, H., (2008) Shape and size dependence of the surface plasmon resonance of gold nanoparticles studied by Photoacoustic technique, *Eur Phys J - Special Topics*, 153(1), 361-364.
20. Bhattacharya, R. and Mukherjee, P., (2008) Biological properties of "naked" metal nanoparticles, *Adv Drug Deliv Rev*, 60(11), 1289-1306.
21. Jain, P.K., El-Sayed, I.H., and El-Sayed, M.A., (2007) Au nanoparticles target cancer, *Nano Today*, 2(1), 18-29.
22. Huang, X., Qian, W., El-Sayed, I.H., and El-Sayed, M.A., (2007) The potential use of the enhanced nonlinear properties of gold nanospheres in photothermal cancer therapy, *Lasers Surg Med*, 39(9), 747-753.

23. Ghosh, P., Han, G., De, M., Kim, C.K., and Rotello, V.M., (2008) Gold nanoparticles in delivery applications, *Adv Drug Deliv Rev*, 60(11), 1307-1315.
24. Pissuwan, D., Niidome, T., and Cortie, M.B., (2011) The forthcoming applications of gold nanoparticles in drug and gene delivery systems, *J Control Release*, 149(1), 65-71.
25. Reum, N., Fink-Straube, C., Klein, T., Hartmann, R.W., Lehr, C.M., and Schneider, M., (2010) Multilayer coating of gold nanoparticles with drug-polymer coadsorbates, *Langmuir*, 26(22), 16901–16908.
26. Brown, S.D., Nativo, P., Smith, J.-A., Stirling, D., Edwards, P.R., Venugopal, B., Flint, D.J., Plumb, J.A., Graham, D., and Wheate, N.J., (2010) Gold nanoparticles for the improved anticancer drug delivery of the active component of oxaliplatin, *J Am Chem Soc*, 132(13), 4678-4684.
27. Chen, Y.-H., Tsai, C.-Y., Huang, P.-Y., Chang, M.-Y., Cheng, P.-C., Chou, C.-H., Chen, D.-H., Wang, C.-R., Shiau, A.-L., and Wu, C.-L., (2007) Methotrexate conjugated to gold nanoparticles inhibits tumor growth in a syngeneic lung tumor model, *Mol Pharmaceutics*, 4(5), 713-722.
28. Bhumkar, D., Joshi, H., Sastry, M., and Pokharkar, V., (2007) Chitosan reduced gold nanoparticles as novel carriers for transmucosal delivery of insulin, *Pharm Res*, 24(8), 1415-1426.
29. Wang, H., Huang, H., and Huang, X., (2007) Differential effects of abscisic acid and ethylene on the fruit maturation of Litchi chinensis Sonn., *Plant Growth Regul*, 52(3), 189-198.
30. Thomas, M. and Klibanov, A.M., (2003) Conjugation to gold nanoparticles enhances polyethylenimine's transfer of plasmid DNA into mammalian cells, *Proceedings of the National Academy of Sciences of the United States of America*, 100(16), 9138-9143.
31. Oishi, M., Nakaogami, J., Ishii, T., and Nagasaki, Y., (2006) Smart PEGylated gold nanoparticles for the cytoplasmic delivery of siRNA to induce enhanced gene silencing, *Chem. Lett.*, 35(9), 1046-1047.
32. Häfeli, U.O., (2004) Magnetically modulated therapeutic systems, *Int J Pharm*, 277(1-2), 19-24.
33. Vatta, L.L., Sanderson, R.D., and Koch, K.R., (2006) Magnetic nanoparticles: Properties and potential applications, *Pure Appl. Chem.*, 78(9), 1793-1801.
34. Pankhurst, Q.A. and et al., (2003) Applications of magnetic nanoparticles in biomedicine, *J Phys D: App Phys*, 36(13), R167-R181.
35. Berry, C.C. and Curtis, A.S.G., (2003) Functionalisation of magnetic nanoparticles for applications in biomedicine, *J. Phys. D: Appl. Phys.*, 36, R198–R206.
36. Gao, J., Gu, H., and Xu, B., (2009) Multifunctional magnetic nanoparticles: Design, synthesis, and biomedical applications, *Acc Chem Res*, 42(8), 1097-1107.
37. Newman, M.D., Stotland, M., and Ellis, J.I., (2009) The safety of nanosized particles in titanium dioxide- and zinc oxide-based sunscreens, *J Am Acad Dermatol*, 61(4), 685-692.
38. Jones, N., Ray, B., Ranjit, K.T., and Manna, A.C., (2008) Antibacterial activity of ZnO nanoparticle suspensions on a broad spectrum of microorganisms, *FEMS Microbiol Lett*, 279(1), 71-76.
39. Menon, G.K., (2002) New insights into skin structure: scratching the surface, *Adv Drug Deliv Rev*, 54(Supplement 1), S3-S17.
40. Lee, S.H., Jeong, S.K., and Ahn, S.K., (2006) An update of the defensive barrier function of skin, *Yonsei Med J*, 47(3), 293-306.
41. Cevc, G. and Vierl, U., (2010) Nanotechnology and the transdermal route: A state of the art review and critical appraisal, *J Control Release*, 141(3), 277-299.
42. Schneider, M., Stracke, F., Hansen, S., and Schaefer, U.F., (2009) Nanoparticles and their interactions with the dermal barrier, *Dermatoendocrinol*, 1(4), 197-206.
43. Hahn, T., Schaefer, U.F., and Lehr, C.M., (2010) Measuring skin absorption in vitro, *SOFW Journal*, 136, 28-38.

44. Chu, M., Wu, Q., Wang, J., Hou, S., Miao, Y., Peng, J., and Sun, Y., (2007) In vitro and in vivo transdermal delivery capacity of quantum dots through mouse skin, *Nanotechnology*, 18(45).
45. Sonavane, G., Tomoda, K., Sano, A., Ohshima, H., Terada, H., and Makino, K., (2008) In vitro permeation of gold nanoparticles through rat skin and rat intestine: Effect of particle size, *Colloids Surf B Biointerfaces*, 65(1), 1-10.
46. Wu, J., Liu, W., Xue, C., Zhou, S., Lan, F., Bi, L., Xu, H., Yang, X., and Zeng, F.D., (2009) Toxicity and penetration of TiO₂ nanoparticles in hairless mice and porcine skin after subchronic dermal exposure, *Toxicol Lett*, 191(1), 1-8.
47. Gopee, N.V., Roberts, D.W., Webb, P., Cozart, C.R., Siitonen, P.H., Latendresse, J.R., Warbitton, A.R., Yu, W.W., Colvin, V.L., Walker, N.J., and Howard, P.C., (2009) Quantitative determination of skin penetration of PEG-coated CdSe quantum dots in dermabraded but not intact SKH-1 hairless mouse skin, *Toxicol Sci*, 111(1), 37-48.
48. Godin, B. and Touitou, E., (2007) Transdermal skin delivery: Predictions for humans from in vivo, ex vivo and animal models, *Adv Drug Deliv Rev*, 59(11), 1152-1161.
49. Netzlaff, F., Schaefer, U.F., Lehr, C.M., Meiers, P., Stahl, J., Kietzmann, M., and Niedorf, F., (2006) Comparison of bovine udder skin with human and porcine skin in percutaneous permeation experiments, *Altern Lab Anim*, 34(5), 499-513.
50. Jeong, S.H., Kim, J.H., Yi, S.M., Lee, J.P., Kim, J.H., Sohn, K.H., Park, K.L., Kim, M.-K., and Son, S.W., (2010) Assessment of penetration of quantum dots through in vitro and in vivo human skin using the human skin equivalent model and the tape stripping method, *Biochem Bioph Res Co* 394(3), 612-615.
51. Netzlaff, F., Lehr, C.M., Wertz, P.W., and Schaefer, U.F., (2005) The human epidermis models EpiSkin®, SkinEthic® and EpiDerm®: An evaluation of morphology and their suitability for testing phototoxicity, irritancy, corrosivity, and substance transport, *Eur J Pharm Biopharm*, 60(2), 167-178.
52. Gratieri, T., Schaefer, U.F., Jing, L., Gao, M., Lopez, R.F.V., and Schneider, M., (2010) Penetration of quantum dot particles through human skin, *J. Biomed. Nanotechnol.*, 6(5), 586-595.
53. Baroli, B., Ennas, M.G., Loffredo, F., Isola, M., Pinna, R., and Lopez-Quintela, M.A., (2007) Penetration of metallic nanoparticles in human full-thickness skin, *J Invest Dermatol*, 127(7), 1701-1712.
54. Krishnan, G., Edwards, J., Chen, Y., and Benson, H.A., (2010) Enhanced skin permeation of naltrexone by pulsed electromagnetic fields in human skin in vitro, *J Pharm Sci*, 99(6), 2724-2731.
55. Labouta, H.I., Liu, D.C., Lin, L.L., Butler, M.K., Jeffrey, G.E., Raphael, A., Kraus, T., El-Khordagui, L.K., Soyer, H.P., Roberts, M.S., Schneider, M., and Prow, T.W., (2011) Gold nanoparticle penetration and reduced metabolism in human skin by toluene, *Pharm Res*, in press. DOI: 10.1007/s11095-011-0561-z.
56. Labouta, H.I., Kraus, T., El-Khordagui, L.K., and Schneider, M., (2011) Mechanism and determinants of nanoparticle penetration through human skin, *Nanoscale*, in press. DOI:10.1039/C1NR11109D.
57. Tan, M.H., Commens, C.A., Burnett, L., and Snitch, P.J., (1996) A pilot study on the percutaneous absorption of microfine titanium dioxide from sunscreens, *Australas J Dermatol*, 37(4), 185-187.
58. Larese Filon, F., Crosera, M., Adami, G., Bovenzi, M., Rossi, F., and Maina, G., (2011) Human skin penetration of gold nanoparticles through intact and damaged skin, *Nanotoxicology*.
59. Labouta, H.I., El-Khordagui, L.K., and Schneider, M., (in due publication) Could chemical enhancement of gold nanoparticle penetration be extrapolated from established approaches for drug permeation?

60. Cross, S.E., Innes, B., Roberts, M.S., Tsuzuki, T., Robertson, T.A., and McCormick, P., (2007) Human skin penetration of sunscreen nanoparticles: in-vitro assessment of a novel micronized zinc oxide formulation, *Skin Pharmacol Physiol*, 20(3), 148-154.
61. Mavon, A., Miquel, C., Lejeune, O., Payre, B., and Moretto, P., (2007) In vitro percutaneous absorption and in vivo stratum corneum distribution of an organic and a mineral sunscreen, *Skin Pharmacol Physiol*, 20(1), 10-20.
62. Filipe, P., Silva, J.N., Silva, R., Cirne de Castro, J.L., Marques Gomes, M., Alves, L.C., Santus, R., and Pinheiro, T., (2009) Stratum corneum is an effective barrier to TiO₂ and ZnO nanoparticle percutaneous absorption, *Skin Pharmacol Physiol*, 22(5), 266-275.
63. Zvyagin, A.V., Zhao, X., Gierden, A., Sanchez, W., Ross, J.A., and Roberts, M.S., (2008) Imaging of zinc oxide nanoparticle penetration in human skin in vitro and in vivo, *J Biomed Opt*, 13(6), 064031.
64. Durand, L., Habran, N., Henschel, V., and Amighi, K., (2009) In vitro evaluation of the cutaneous penetration of sprayable sunscreen emulsions with high concentrations of UV filters, *Int J Cosmet Sci*, 31(4), 279-292.
65. Filon, F.L., D'Agostin, F., Crosera, M., Adami, G., Rosani, R., Romano, C., Bovenzi, M., and Maina, G., (2007) In vitro percutaneous absorption of silver nanoparticles, *G Ital Med Lav Ergon*, 29(Suppl 3), 451-452.
66. Larese, F.F., D'Agostin, F., Crosera, M., Adami, G., Renzi, N., Bovenzi, M., and Maina, G., (2009) Human skin penetration of silver nanoparticles through intact and damaged skin, *Toxicology*, 255(1-2), 33-37.
67. Roberts, M.S., Roberts, M.J., Robertson, T.A., Sanchez, W., Thorling, C., Zou, Y., Zhao, X., Becker, W., and Zvyagin, A.V., (2008) In vitro and in vivo imaging of xenobiotic transport in human skin and in the rat liver, *J Biophotonics*, 1(6), 478-493.
68. Pflucker, F., Wendel, V., Hohenberg, H., Gartner, E., Will, T., Pfeiffer, S., Wepf, R., and Gers-Barlag, H., (2001) The human stratum corneum layer: an effective barrier against dermal uptake of different forms of topically applied micronised titanium dioxide, *Skin Pharmacol Appl Skin Physiol*, 14(Suppl 1), 92-97.
69. Schulz, J., Hohenberg, H., Pflucker, F., Gartner, E., Will, T., Pfeiffer, S., Wepf, R., Wendel, V., Gers-Barlag, H., and Wittern, K.P., (2002) Distribution of sunscreens on skin, *Adv Drug Deliv Rev*, 54 Suppl 1, S157-163.
70. Dussert, A.S., Gooris, E., and Hemmerle, J., (1997) Characterization of the mineral content of a physical sunscreen emulsion and its distribution onto human stratum corneum, *Int J Cosmet Sci*, 19(3), 119-129.
71. Chen, H.-Y., Zhao, Q., Su, K.-L., and Lin, Y.-C., (2008) Development of transdermal delivery chip system: Deliver gold nanoparticles into human stratum corneum, in: *3rd annual IEEE international conference on nano-micro engineered and molecular system*, Hainan island, China.
72. Pinheiro, T., Pallon, J., Alves, L.C., Veríssimo, A., Filipe, P., Silva, J.N., and Silva, R., (2007) The influence of corneocyte structure on the interpretation of permeation profiles of nanoparticles across skin, *Nuclear Instruments and Methods in Physics Research Section B: Beam Interactions with Materials and Atoms*, 260(1), 119-123.
73. Prow, T.W., Monteiro-Riviere, N.A., Inman, A.O., Grice, J.E., Chen, X., Zhao, X., Sanchez, W.H., Gierden, A., Kendall, M.A., Zvyagin, A.V., Erdmann, D., Riviere, J.E., and Roberts, M.S., (2011) Quantum dot penetration into viable human skin, *Nanotoxicology*, DOI:10.3109/17435390.2011.569092.
74. Seto, J.E., Polat, B.E., Lopez, R.F.V., Blankschtein, D., and Langer, R., (2010) Effects of ultrasound and sodium lauryl sulfate on the transdermal delivery of hydrophilic permeants: Comparative in vitro studies with full-thickness and split-thickness pig and human skin, *J Control Release*, 145(1), 26-32.

75. Ryman-Rasmussen, J.P., Riviere, J.E., and Monteiro-Riviere, N.A., (2006) Penetration of intact skin by quantum dots with diverse physicochemical properties, *Toxicol Sci*, 91(1), 159-165.
76. Paliwal, S., Menon, G.K., and Mitragotri, S., (2006) Low-frequency sonophoresis: ultrastructural basis for stratum corneum permeability assessed using quantum dots, *J Invest Dermatol*, 126(5), 1095-1101.
77. Samberg, M.E., Oldenburg, S.J., and Monteiro-Riviere, N.A., (2010) Evaluation of silver nanoparticle toxicity in skin in vivo and keratinocytes in vitro, *Environ Health Perspect*, 118(3), 407-413.
78. Senzui, M., Tamura, T., Miura, K., Ikarashi, Y., Watanabe, Y., and Fujii, M., (2010) Study on penetration of titanium dioxide (TiO₂) nanoparticles into intact and damaged skin in vitro, *J Toxicol Sci*, 35(1), 107-113.
79. Zhang, L.W., Yu, W.W., Colvin, V.L., and Monteiro-Riviere, N.A., (2008) Biological interactions of quantum dot nanoparticles in skin and in human epidermal keratinocytes, *Toxicol Appl Pharmacol*, 228(2), 200-211.
80. Menzel, F., Reinert, T., Vogt, J., and Butz, T., (2004) Investigations of percutaneous uptake of ultrafine TiO₂ particles at the high energy ion nanoprobe LIPSION, *Nuclear Instruments and Methods in Physics Research Section B: Beam Interactions with Materials and Atoms*, 219-220, 82-86.
81. Gamer, A.O., Leibold, E., and van Ravenzwaay, B., (2006) The in vitro absorption of microfine zinc oxide and titanium dioxide through porcine skin, *Toxicol In Vitro*, 20(3), 301-307.
82. Kendall, M., Rishworth, S., Carter, F., and Mitchell, T., (2004) Effects of relative humidity and ambient temperature on the ballistic delivery of micro-particles to excised porcine skin, *J Invest Dermatol*, 122(3), 739-746.
83. Sadrieh, N., Wokovich, A.M., Gopee, N.V., Zheng, J., Haines, D., Parmiter, D., Siitonen, P.H., Cozart, C.R., Patri, A.K., McNeil, S.E., Howard, P.C., Doub, W.H., and Buhse, L.F., (2010) Lack of significant dermal penetration of titanium dioxide from sunscreen formulations containing nano- and submicron-size TiO₂ particles, *Toxicol Sci*, 115(1), 156-166.
84. Lee, S.E., Choi, K.J., Menon, G.K., Kim, H.J., Choi, E.H., Ahn, S.K., and Lee, S.H., (2010) Penetration pathways induced by low-frequency sonophoresis with physical and chemical enhancers: iron oxide nanoparticles versus lanthanum nitrates, *J Invest Dermatol*, 130(4), 1063-1072.
85. Kuo, T.R., Wu, C.L., Hsu, C.T., Lo, W., Chiang, S.J., Lin, S.J., Dong, C.Y., and Chen, C.C., (2009) Chemical enhancer induced changes in the mechanisms of transdermal delivery of zinc oxide nanoparticles, *Biomaterials*, 30(16), 3002-3008.
86. Huang, Y., Yu, F., Park, Y.S., Wang, J., Shin, M.C., Chung, H.S., and Yang, V.C., (2010) Co-administration of protein drugs with gold nanoparticles to enable percutaneous delivery, *Biomaterials*, 31(34), 9086-9091.
87. Mortensen, L.J., Oberdorster, G., Pentland, A.P., and Delouise, L.A., (2008) In vivo skin penetration of quantum dot nanoparticles in the murine model: the effect of UVR, *Nano Lett*, 8(9), 2779-2787.
88. Mortensen, L., Zheng, H., Faulknor, R., De Benedetto, A., Beck, L., and DeLouise, L.A., (02 December 2009) Increased in vivo skin penetration of quantum dots with UVR and in vitro quantum dot cytotoxicity, in: *Colloidal Quantum Dots for Biomedical Applications IV*, San Jose, CA, USA: SPIE, pp. 718919-718912.
89. Upadhyay, P., (2006) Enhanced transdermal-immunization with diphtheria-toxoid using local hyperthermia, *Vaccine*, 24(27-28), 5593-5598.
90. Zhang, L.W. and Monteiro-Riviere, N.A., (2008) Assessment of quantum dot penetration into intact, tape-stripped, abraded and flexed rat skin, *Skin Pharmacol Physiol*, 21(3), 166-180.
91. Lekki, J., Stachura, Z., Dabros, W., Stachura, J., Menzel, F., Reinert, T., Butz, T., Pallon, J., Gontier, E., Ynsa, M.D., Moretto, P., Kertesz, Z., Szikszai, Z., and Kiss, A.Z., (2007) On the follicular pathway of percutaneous uptake of nanoparticles: Ion microscopy and

- autoradiography studies, Nuclear Instruments and Methods in Physics Research Section B: Beam Interactions with Materials and Atoms. Nuclear Microprobe Technology and Applications (ICNMTA2006) and Proton Beam Writing (PBW II), 10th International Conference on Nuclear Microprobe Technology and Applications and 2nd International Workshop on Proton Beam Writing, 260(1), 174-177.
92. Gontier, E., Ynsa, M.-D., Biro, T., Hunyadi, J., Kiss, B., Gaspar, K., Pinheiro, T., Silva, J.-N., Filipe, P., Stachura, J., Dabros, W., Reinert, T., Butz, T., Moretto, P., and Surleve-Bazeille, J.-E., (2008) Is there penetration of titania nanoparticles in sunscreens through skin? A comparative electron and ion microscopy study, *Nanotoxicology*, 2(4), 218-231.
 93. Kertész, Z., Szikszai, Z., Gontier, E., Moretto, P., Surlève-Bazeille, J.E., Kiss, B., Juhász, I., Hunyadi, J., and Kiss, Á.Z., (2005) Nuclear microprobe study of TiO₂-penetration in the epidermis of human skin xenografts, *Nuclear Instruments and Methods in Physics Research Section B: Beam Interactions with Materials and Atoms*, 231(1-4), 280-285.
 94. OECD (23 November 2004) Draft Guideline 428: Skin absorption: in vitro method. OECD Guideline for the Testing of Chemicals.
 95. Marro, D., Guy, R.H., and Begoña Delgado-Charro, M., (2001) Characterization of the iontophoretic permselectivity properties of human and pig skin, *J Control Release*, 70(1-2), 213-217.
 96. Jiang, S.J., Chen, J.Y., Lu, Z.F., Yao, J., Che, D.F., and Zhou, X.J., (2006) Biophysical and morphological changes in the stratum corneum lipids induced by UVB irradiation, *J Dermatol Sci*, 44(1), 29-36.
 97. Dixit, N., Bali, V., Baboota, S., Ahuja, A., and Ali, J., (2007) Iontophoresis - an approach for controlled drug delivery: a review, *Curr Drug Deliv*, 4(1), 1-10.
 98. Ogura, M., Paliwal, S., and Mitragotri, S., (2008) Low-frequency sonophoresis: Current status and future prospects, *Adv Drug Deliv Rev*, 60(10), 1218-1223.
 99. FDA (1998) Guidance for Industry: Topical dermatological drug product NDAs and ANDAs — In vivo bioavailability, bioequivalence, in vitro release, and associated studies.
 100. Choi, M.J., Zhai, H., Löffler, H., Dreher, F., and Maibach, H.I., (2003) Effect of tape stripping on percutaneous penetration and topical vaccination, *Exog Dermatol*, 2(5), 262-269.
 101. Brown, M.B., Martin, G.P., Jones, S.A., and Akomeah, F.K., (2006) Dermal and Transdermal Drug Delivery Systems: Current and Future Prospects, *Drug Delivery*, 13(3), 175-187.
 102. Gill, H.S., Andrews, S.N., Sakthivel, S.K., Fedanov, A., Williams, I.R., Garber, D.A., Priddy, F.H., Yellin, S., Feinberg, M.B., Staprans, S.I., and Prausnitz, M.R., (2009) Selective removal of stratum corneum by microdermabrasion to increase skin permeability, *Eur J Pharm Sci*, 38(2), 95-103.
 103. Lee, W.-R., Shen, S.-C., Wang, K.-H., Hu, C.-H., and Fang, J.-Y., (2003) Lasers and microdermabrasion enhance and control topical delivery of vitamin C, *J Invest Dermatol*, 121(5), 1118-1125.
 104. Thong, H.Y., Zhai, H., and Maibach, H.I., (2007) Percutaneous penetration enhancers: an overview, *Skin Pharmacol Physiol*, 20(6), 272-282.
 105. Baroli, B., (2010) Penetration of nanoparticles and nanomaterials in the skin: fiction or reality?, *J Pharm Sci*, 99(1), 21-50.
 106. Potts, R.O. and Francoeur, M.L., (1991) The influence of stratum corneum morphology on water permeability, *J Invest Dermatol*, 96(4), 495-499.
 107. Schaefer, H. and Redelmeier, T.E., *Skin barrier: Principles of percutaneous absorption*, 1996, Basel, Switzerland: Karger, 310 pages.
 108. Lademann, J., Patzelt, A., Richter, H., Antoniou, C., Sterry, W., and Knorr, F., (2009) Determination of the cuticula thickness of human and porcine hairs and their potential influence on the penetration of nanoparticles into the hair follicles, *J Biomed Opt*, 14(2), 021014.

109. Patzelt, A., Richter, H., Knorr, F., Schafer, U., Lehr, C.M., Dahne, L., Sterry, W., and Lademann, J., (2011) Selective follicular targeting by modification of the particle sizes, *J Control Release*, 150(1), 45-48.
110. Guldbbrand, S., Simonsson, C., Smedh, M., and Ericson, M.B., (1 July 2009) Point spread function measured in human skin using two-photon fluorescence microscopy, in: *Proc. of SPIE*.
111. Guldbbrand, S., Simonsson, C., Goksor, M., Smedh, M., and Ericson, M.B., (2010) Two-photon fluorescence correlation microscopy combined with measurements of point spread function; investigations made in human skin, *Opt Express*, 18(15), 15289-15302.
112. Mahe, B., Vogt, A., Liard, C., Duffy, D., Abadie, V., Bonduelle, O., Boissonnas, A., Sterry, W., Verrier, B., Blume-Peytavi, U., and Combadiere, B., (2009) Nanoparticle-based targeting of vaccine compounds to skin antigen-presenting cells by hair follicles and their transport in mice, *J Invest Dermatol*, 129(5), 1156-1164.
113. Kiss, B., Biro, T., Czifra, G., Toth, B.I., Kertesz, Z., Szikszai, Z., Kiss, A.Z., Juhasz, I., Zouboulis, C.C., and Hunyadi, J., (2008) Investigation of micronized titanium dioxide penetration in human skin xenografts and its effect on cellular functions of human skin-derived cells, *Exp Dermatol*, 17(8), 659-667.
114. Schmid, G., (1992) Large clusters and colloids. Metals in the embryonic state, *Chemical Reviews*, 92(8), 1709-1727.
115. Stracke, F., Weiss, B., Lehr, C.M., Konig, K., Schaefer, U.F., and Schneider, M., (2006) Multiphoton microscopy for the investigation of dermal penetration of nanoparticle-borne drugs, *J Invest Dermatol*, 126(10), 2224-2233.
116. Patlolla, R.R., Desai, P.R., Belay, K., and Singh, M.S., (2010) Translocation of cell penetrating peptide engrafted nanoparticles across skin layers, *Biomaterials*, 31(21), 5598-5607.
117. Sugata, K., Osanai, O., Sano, T., and Takema, Y., (2011) Evaluation of photoaging in facial skin by multiphoton laser scanning microscopy, *Skin Res Technol*, 17(1), 1-3.
118. Farrer, R.A., Butterfield, F.L., Chen, V.W., and Fourkas, J.T., (2005) Highly efficient multiphoton-absorption-induced luminescence from gold nanoparticles, *Nano Lett*, 5(6), 1139-1142.
119. Jonkman, J.E.N. and Stelzer, E.H.K., (2002) Resolution and contrast in confocal and two-photon microscopy, in *Confocal and two-photon microscopy - Foundations, applications, and advances*, (Diaspro, A., Editor), Wiley-Liss, Inc., New York, pp. 101-125.
120. Diaspro, A., Schneider, M., Bianchini, P., Caorsi, V., Mazza, D., Pesce, M., Testa, I., Vicidomini, G., Usai, C., and Bos, A., (2007) Two-Photon Excitation Fluorescence Microscopy, in *Science of Microscopy*, (Hawkes, P.W. and Spence, J.C.H., Editors), Springer New York, pp. 751-789.
121. Tsai, T.H., Jee, S.H., Dong, C.Y., and Lin, S.J., (2009) Multiphoton microscopy in dermatological imaging, *J Dermatol Sci*, 56(1), 1-8.
122. Theer, P. and Denk, W., (2006) On the fundamental imaging-depth limit in two-photon microscopy, *J Opt Soc Am A Opt Image Sci Vis*, 23(12), 3139-3149.
123. Theer, P., Hasan, M.T., and Denk, W., (2003) Two-photon imaging to a depth of 1000 microm in living brains by use of a Ti:Al₂O₃ regenerative amplifier, *Opt Lett*, 28(12), 1022-1024.
124. de Grauw, C.J., Frederix, P.L.T.M., and Gerritsen, H.C., (2002) Aberrations and penetration in in-depth confocal and two-photon-excitation microscopy, in *Confocal and two-photon microscopy - Foundations, applications, and advances*, (Diaspro, A., Editor), Wiley-Liss, Inc., New York, pp. 153-169.
125. Niesner, R., Andresen, V., Neumann, J., Spiecker, H., and Gunzer, M., (2007) The power of single and multibeam two-photon microscopy for high-resolution and high-speed deep tissue and intravital imaging, *Biophys J*, 93(7), 2519-2529.
126. Muriello, P.A. and Dunn, K.W., (2008) Improving Signal Levels in Intravital Multiphoton Microscopy using an Objective Correction Collar, *Opt Commun*, 281(7), 1806-1812.

127. Poland, S.P., Wright, A.J., Cobb, S., Vijverberg, J.C., and Girkin, J.M., (2011) A demonstration of the effectiveness of a single aberration correction per optical slice in beam scanned optically sectioning microscopes, *Micron*, 42(4), 318-323.
128. Gerritsen, H.C. and De Grauw, C.J., (1999) Imaging of optically thick specimen using two-photon excitation microscopy, *Microsc Res Tech*, 47(3), 206-209.
129. Periasamy, A., Skoglund, P., Noakes, C., and Keller, R., (1999) An evaluation of two-photon excitation versus confocal and digital deconvolution fluorescence microscopy imaging in *Xenopus* morphogenesis, *Microsc Res Tech*, 47(3), 172-181.
130. Dong, C.Y., Koenig, K., and So, P., (2003) Characterizing point spread functions of two-photon fluorescence microscopy in turbid medium, *J Biomed Opt*, 8(3), 450-459.
131. Fischer, F., Konig, K., Puschmann, S., Wepf, R., Riemann, I., Ulrich, V., and Fischer, P., (8 September 2004) Characterization of multiphoton laser scanning device optical parameters for image restoration, in: *Proc. of SPIE*, pp. 140-145.
132. Turkevich, J., Stevenson, P.C., and Hillier, J., (1951) A study of the nucleation and growth processes in the synthesis of colloidal gold, *Discuss, Faraday Soc.*, 55-57.
133. Choi, H.R., Kim, S.K., Kwon, S.B., and Park, K.C., (2006) The fixation of living skin equivalents, *Appl Immunohistochem Mol Morphol*, 14(1), 122-125.
134. Labouta, H.I., Kraus, T., El-Khordagui, L.K., and Schneider, M., (2011) Combined multiphoton imaging-pixel analysis for semiquantitation of skin penetration of gold nanoparticles, *Int J Pharm*, 413, 279-282.
135. Ding, H., Lu, J.Q., Wooden, W.A., Kragel, P.J., and Hu, X.H., (2006) Refractive indices of human skin tissues at eight wavelengths and estimated dispersion relations between 300 and 1600 nm, *Phys Med Biol*, 51(6), 1479-1489.
136. Benham, G.S., (2002) Practical aspects of objective lens selection for confocal and multiphoton digital imaging techniques, in *Cell biological applications of confocal microscopy*, (Matsumoto, B., Editor), Elsevier science, San Diego, California, pp. 245-299.
137. Mooradian, A., (1969) Photoluminescence of Metals, *Physical Review Letters*, 22(5), 185-187.
138. Prow, T.W., Chen, X., Prow, N.A., Fernando, G.J., Tan, C.S., Raphael, A.P., Chang, D., Ruutu, M.P., Jenkins, D.W., Pyke, A., Crichton, M.L., Raphaelli, K., Goh, L.Y., Frazer, I.H., Roberts, M.S., Gardner, J., Khromykh, A.A., Suhrbier, A., Hall, R.A., and Kendall, M.A., (2010) Nanopatch-targeted skin vaccination against West Nile Virus and Chikungunya virus in mice, *Small*, 6(16), 1776-1784.
139. On regulatory aspects of nanomaterials. [accessed 2010 15th September]; Available from: http://ec.europa.eu/health/ph_risk/commithttp://www.schneiderchildrenshospital.org/peds_html_fixed/peds/derm/burns.htmtees/04_sccp/docs/sccp_o_123.pdf.
140. Robertson, T.A., Sanchez, W.Y., and Roberts, M.S., (2010) Are commercially available nanoparticles safe when applied to the skin?, *J Biomed Nanotechnol*, 6(5), 452-468.
141. Monteiro-Riviere, N.A. and Tran, C.L., *Nanotoxicology: Characterization, dosing and health effects*, 2007, New York: Informa Healthcare pages.
142. Prow, T.W., Grice, J.E., Lin, L.L., Faye, R., Butler, M., Becker, W., Wurm, E.M., Yoong, C., Robertson, T.A., Soyer, H.P., and Roberts, M.S., (2011) Nanoparticles and microparticles for skin drug delivery, *Adv Drug Deliv Rev*, 63(6), 470-491.
143. Kuchler, S., Abdel-Mottaleb, M., Lamprecht, A., Radowski, M.R., Haag, R., and Schäfer-Korting, M., (2009) Influence of nanocarrier type and size on skin delivery of hydrophilic agents, *Int J Pharm*, 377(1-2), 169-172.
144. Rouse, J.G., Yang, J., Ryman-Rasmussen, J.P., Barron, A.R., and Monteiro-Riviere, N.A., (2007) Effects of mechanical flexion on the penetration of fullerene amino acid-derivatized peptide nanoparticles through skin, *Nano Lett*, 7(1), 155-160.

145. Coulman, S.A., Anstey, A., Gateley, C., Morrissey, A., McLoughlin, P., Allender, C., and Birchall, J.C., (2009) Microneedle mediated delivery of nanoparticles into human skin, *Int J Pharm*, 366(1-2), 190-200.
146. Crosera, M., Bovenzi, M., Maina, G., Adami, G., Zanette, C., Florio, C., and Filon Larese, F., (2009) Nanoparticle dermal absorption and toxicity: a review of the literature, *Int Arch Occup Environ Health*, 82(9), 1043-1055.
147. Roberts, M.S., Dancik, Y., Prow, T.W., Thorling, C.A., Lin, L.L., Grice, J.E., Robertson, T.A., König, K., and Becker, W., (2011) Non-invasive imaging of skin physiology and percutaneous penetration using fluorescence spectral and lifetime imaging with multiphoton and confocal microscopy, *Eur J Pharm Biopharm*, 77(3), 469-488.
148. Xia, X.R., Monteiro-Riviere, N.A., and Riviere, J.E., (2010) Skin penetration and kinetics of pristine fullerenes (C60) topically exposed in industrial organic solvents, *Toxicol Appl Pharmacol*, 242(1), 29-37.
149. Harper, M., (2004) Assessing workplace chemical exposures: the role of exposure monitoring, *J Environ Monit*, 6(5), 404-412.
150. Hoover, M.D., Stefaniak, A.B., Day, G.A., and Geraci, C.L., (2007) Exposure assessment considerations for nanoparticles in the workplace, in *Nanotoxicology: characterization, dosing, and health effects*, Informa Healthcare, pp. 71-84.
151. Riviere, J.E. and Brooks, J.D., (2011) Predicting skin permeability from complex chemical mixtures: Dependency of quantitative structure permeation relationships on biology of skin model used, *Toxicological Sciences*, 119(1), 224-232.
152. Riviere, J.E. and Brooks, J.D., (2005) Predicting skin permeability from complex chemical mixtures, *Toxicol Appl Pharmacol*, 208(2), 99-110.
153. Xia, X.R., Monteiro-Riviere, N.A., and Riviere, J.E., (2010) Intrinsic biological property of colloidal fullerene nanoparticles (nC60): lack of lethality after high dose exposure to human epidermal and bacterial cells, *Toxicol Lett*, 197(2), 128-134.
154. Boyd, G.T., Yu, Z.H., and Shen, Y.R., (1986) Photoinduced luminescence from the noble metals and its enhancement on roughened surfaces, *Phys Rev B Condens Matter*, 33(12), 7923-7936.
155. Yang, Y., Qu, Y., and Lu, X., (2010) Global gene expression analysis of the effects of gold nanoparticles on human dermal fibroblasts, *J Biomed Nanotechnol*, 6(3), 234-246.
156. Schaeublin, N.M., Braydich-Stolle, L.K., Schrand, A.M., Miller, J.M., Hutchison, J., Schlager, J.J., and Hussain, S.M., (2011) Surface charge of gold nanoparticles mediates mechanism of toxicity, *Nanoscale*, 3(2), 410-420.
157. Lu, S., Xia, D., Huang, G., Jing, H., Wang, Y., and Gu, H., (2010) Concentration effect of gold nanoparticles on proliferation of keratinocytes, *Colloids and Surfaces B: Biointerfaces*, 81(2), 406-411.
158. Zheng, N., Fan, J., and Stucky, G.D., (2006) One-Step one-phase synthesis of monodisperse noble-metallic nanoparticles and their colloidal crystals, *J Am Chem Soc*, 128(20), 6550-6551.
159. Wagner, H., Kostka, K.H., Adelhardt, W., and Schaefer, U.F., (2004) Effects of various vehicles on the penetration of flufenamic acid into human skin, *Eur J Pharm Biopharm*, 58(1), 121-129.
160. Lin, L., Grice, J., Butler, M., Zvyagin, A., Becker, W., Robertson, T., Soyer, H., Roberts, M., and Prow, T., (2011) Time-correlated single photon counting for simultaneous monitoring of zinc oxide nanoparticles and NAD(P)H in intact and barrier-disrupted volunteer skin, *Pharm Res*, 28(11), 2920-2930.
161. Schneider, G. and Decher, G., (2008) Functional core/shell nanoparticles via layer-by-layer assembly. Investigation of the experimental parameters for controlling particle aggregation and for enhancing dispersion stability, *Langmuir*, 24(5), 1778-1789.

162. Bird, D.K., Yan, L., Vrotsos, K.M., Eliceiri, K.W., Vaughan, E.M., Keely, P.J., White, J.G., and Ramanujam, N., (2005) Metabolic mapping of MCF10A human breast cells via multiphoton fluorescence lifetime imaging of the coenzyme NADH, *Cancer Res*, 65(19), 8766-8773.
163. Sanchez, W.Y., Prow, T.W., Sanchez, W.H., Grice, J.E., and Roberts, M.S., (2010) Analysis of the metabolic deterioration of ex vivo skin from ischemic necrosis through the imaging of intracellular NAD(P)H by multiphoton tomography and fluorescence lifetime imaging microscopy, *J Biomed Opt*, 15(4), 046008.
164. Okyar, A., Nuriyev, M., Yildiz, A., Pala-Kara, Z., Ozturk, N., and Kaptan, E., (2010) The effect of terpenes on percutaneous absorption of tiaprofenic acid gel, *Arch Pharmacol Res*, 33(11), 1781-1788.
165. Parfenov, A.S., Salnikov, V., Lederer, W.J., and Lukyánenko, V., (2006) Aqueous diffusion pathways as a part of the ventricular cell ultrastructure, *Biophys J*, 90(3), 1107-1119.
166. Lacerda, S.H., Park, J.J., Meuse, C., Pristinski, D., Becker, M.L., Karim, A., and Douglas, J.F., (2010) Interaction of gold nanoparticles with common human blood proteins, *ACS Nano*, 4(1), 365-379.
167. Wester, R.C. and Maibach, H.I., (1993) Percutaneous absorption of topical corticosteroids, *Curr Probl Dermatol*, 21, 45-60.
168. Wester, R.C., Melendres, J., Sedik, L., Maibach, H., and Riviere, J.E., (1998) Percutaneous absorption of salicylic acid, theophylline, 2, 4-dimethylamine, diethyl hexyl phthalic acid, and p-aminobenzoic acid in the isolated perfused porcine skin flap compared to man in vivo, *Toxicol Appl Pharmacol*, 151(1), 159-165.
169. Wu, X., Landfester, K., Musyanovych, A., and Guy, R.H., (2010) Disposition of charged nanoparticles after their topical application to the skin, *Skin Pharmacol Physiol*, 23(3), 117-123.
170. Kohli, A.K. and Alpar, H.O., (2004) Potential use of nanoparticles for transcutaneous vaccine delivery: Effect of particle size and charge, *Int J Pharm*, 275(1-2), 13-17.
171. Zhu, H., Tao, C., Zheng, S., Wu, S., and Li, J., (2005) Effect of alkyl chain length on phase transfer of surfactant capped Au nanoparticles across the water/toluene interface, *Colloids and Surfaces A: Physicochemical and Engineering Aspects*, 256(1), 17-20.
172. Hahn, T., Hansen, S., Neumann, D., Kostka, K.H., Lehr, C.M., Muys, L., and Schaefer, U.F., (2010) Infrared densitometry: a fast and non-destructive method for exact stratum corneum depth calculation for in vitro tape-stripping, *Skin Pharmacol Physiol*, 23(4), 183-192.
173. Kligman, A.M. and Christophers, E., (1963) Preparation of Isolated Sheets of Human Stratum Corneum, *Arch Dermatol*, 88, 702-705.
174. Labouta, H.I., Hampel, M., Thude, S., Reutlinger, K., Kostka, K.H., and Schneider, M., (2011) Depth profiling of gold nanoparticles and characterization of point spread functions in reconstructed and human skin using multiphoton microscopy, *J Biophotonics*, in press. DOI: 10.1002/jbio.201100069.
175. Wertz, P.W., (2000) Lipids and barrier function of the skin, *Acta Derm Venereol Suppl (Stockh)*, 208, 7-11.
176. Magnusson, B.M., Anissimov, Y.G., Cross, S.E., and Roberts, M.S., (2004) Molecular size as the main determinant of solute maximum flux across the skin, *J Invest Dermatol*, 122(4), 993-999.
177. Parfenov, A.S., Salnikov, V., Lederer, W.J., and Lukyánenko, V., (2006) Aqueous diffusion pathways as a part of the ventricular cell ultrastructure, *Biophysical Journal*, 90(3), 1107-1119.
178. Glombitza, B. and Müller-Goymann, C.C., (2002) Influence of different ceramides on the structure of in vitro model lipid systems of the stratum corneum lipid matrix, *Chem Phys Lipids*, 117(1-2), 29-44.

179. Monteiro-Riviere, N.A., Inman, A.O., Mak, V., Wertz, P., and Riviere, J.E., (2001) Effect of selective lipid extraction from different body regions on epidermal barrier function, *Pharm Res*, 18(7), 992-998.
180. Vaddi, H.K., Wang, L.Z., Ho, P.C., and Chan, S.Y., (2001) Effect of some enhancers on the permeation of haloperidol through rat skin in vitro, *Int J Pharm*, 212(2), 247-255.
181. Zhou, H., Yue, Y., Liu, G., Li, Y., Zhang, J., Gong, Q., Yan, Z., and Duan, M., (2009) Preparation and characterization of a lecithin nanoemulsion as a topical delivery system, *Nanoscale Res Lett*, 5(1), 224-230.
182. Luengo, J., Weiss, B., Schneider, M., Ehlers, A., Stracke, F., Konig, K., Kostka, K.H., Lehr, C.M., and Schaefer, U.F., (2006) Influence of nanoencapsulation on human skin transport of flufenamic acid, *Skin Pharmacol Physiol*, 19(4), 190-197.
183. Shim, J., Seok Kang, H., Park, W.S., Han, S.H., Kim, J., and Chang, I.S., (2004) Transdermal delivery of mixnoxidil with block copolymer nanoparticles, *J Control Release*, 97(3), 477-484.
184. Cevc, G., (2004) Lipid vesicles and other colloids as drug carriers on the skin, *Adv Drug Deliv Rev*, 56(5), 675-711.
185. Asbill, C.S. and Michniak, B.B., (2000) Percutaneous penetration enhancers: local versus transdermal activity, *Pharm Sci Technolo Today*, 3(1), 36-41.
186. Weisbecker, C.S., Merritt, M.V., and Whitesides, G.M., (1996) Molecular Self-Assembly of Aliphatic Thiols on Gold Colloids, *Langmuir*, 12, 3763-3772.
187. Walters, K.A., Bialik, W., and Brain, K.R., (1993) The effects of surfactants on penetration across the skin, *Int J Cosmet Sci*, 15(6), 260-271.
188. Anigbogu, A.N.C., Williams, A.C., Barry, B.W., and Edwards, H.G.M., (1995) Fourier transform raman spectroscopy of interactions between the penetration enhancer dimethyl sulfoxide and human stratum corneum, *Int J Pharm*, 125(2), 265-282.
189. Lawrence, H.J., Walsh, D., Zapotowski, K.A., Denham, A., Goodnight, S.H., and Gandara, D.R., (1989) Topical dimethylsulfoxide may prevent tissue damage from anthracycline extravasation, *Cancer Chemother Pharmacol*, 23(5), 316-318.
190. Roth, S.H. and Fuller, P., (2011) Diclofenac topical solution compared with oral diclofenac: a pooled safety analysis, *J Pain Res*, 4, 159-167.
191. Wong, K.K., Wang, G.M., Dreyfuss, J., and Schreiber, E.C., (1971) Absorption, excretion, and biotransformation of dimethyl sulphoxide in man and miniature pigs after topical application as as 80% gel, *J Investig Dermatol*, 56(1), 44-48.
192. Sulzberger, M.B., Cortese, T.A., Jr., Fishman, L., Wiley, H.S., and Peyakovich, P.S., (1967) Some effects of DMSO on human skin in vivo, *Ann N Y Acad Sci*, 141(1), 437-450.
193. John, H. and Laudahn, G., (1967) Clinical experiences with the topical application of DMSO in orthopedic diseases: evaluation of 4180 cases, *Ann N Y Acad Sci*, 141(1), 506-516.
194. Brechner, V.L., Cohen, D.D., and Pretsky, I., (1967) Dermal anesthesia by the topical application of tetracaine base dissolved in dimethyl sulfoxide, *Ann N Y Acad Sci*, 141(1), 524-531.

Curriculum Vitae

NAME Hagar Ibrahim Mohamed Ibrahim Labouta
BIRTH DATE AND PLACE: 4 September 1980- Copenhagen, Denmark
NATIONALITY: Egyptian
E-MAIL: h.ibrahim@mx.uni-saarland.de
hagar80im@gmail.com

Education

- **2007:** MSc. at the Department of Pharmaceutics, Faculty of Pharmacy, University of Alexandria. The thesis was entitled: "**Modulation of Drug Release from Polymer-based Controlled Delivery Systems**".
- **1998-2000:** BSc. of pharmaceutical sciences, Faculty of pharmacy, University of Alexandria. Egypt. Excellent grade with honor, top 2% among class.
- **1998:** Completed high school education at the E.G.C. "English Girls College", top 2% among class.

Career Summary:

- **2009- Present:** PhD student at Department of Pharmaceutical Nanotechnology, Saarland University, Saarbrücken, Germany.
- **2007- 2009:** Assistant lecturer at Faculty of Pharmacy, University of Alexandria, Egypt.
- **2003- 2007:** Demonstrator (Teaching Assistant) at Faculty of pharmacy, University of Alexandria, Egypt.
- **2006- 2008:** Research investigator at the bioequivalence center at the Faculty of Pharmacy, University of Alexandria, Egypt.

Publications:

Research articles:

- **Hagar I. Labouta**, Labiba K. El-Khordagui, Tobias Kraus and Marc Schneider, Mechanism and determinants of nanoparticle penetration through human skin, *Nanoscale*, 3 (2011), 4989-4999.
- **Hagar I. Labouta**, Martina Hampel, Sibylle Thude, Katharina Reutlinger, Karl-Heinz Kostka and Marc Schneider, Depth profiling of gold nanoparticles and characterization of point spread functions in reconstructed and human skin using multiphoton microscopy, *Journal of Biophotonics*, 5 (2011) 85-96.
- **Hagar I. Labouta**, David C. Liu, Lynlee L. Lin, Margaret K. Butler, Jeffrey E. Grice, Anthony P. Raphael, Tobias Kraus, Labiba K. El-Khordagui, H. Peter Soyer, Michael S. Roberts, Marc Schneider and Tarl W. Prow, Gold nanoparticle penetration and reduced metabolism in human skin by toluene, *Pharmaceutical Research*, 28:11 (2011) 2931-2944, DOI: 10.1007/s11095-011-0561-z.
- **Hagar I. Labouta**, Tobias Kraus, Labiba K. El-Khordagui and Marc Schneider, "Combined multiphoton imaging-pixel analysis for semiquantitation of skin penetration of gold nanoparticles" *International Journal of Pharmaceutics*, 413 (2011) 279– 282.
- **Hagar I. Labouta** and Labiba K. El-Khordagui, "Polymethacrylate microparticles gel for topical drug delivery", *Pharmaceutical Research*, Vol. 27 (10): 2106-2118, 2010.
- **Hagar I. Labouta**, Labiba K. El-Khordagui, Abdullah M. Molokhia and Ghaly M. Ghaly, "Multivariate modeling of encapsulation and release of an ionizable drug from polymer microspheres", *Journal of Pharmaceutical Sciences*, vol. 98 (12):4603-4615, 2009.
- **Hagar I. Labouta**, Labiba K. El-Khordagui and Marc Schneider, "Could chemical enhancement of gold nanoparticle penetration be extrapolated from established approaches for drug permeation", submitted.

Review articles:

- **Hagar I. Labouta** and Marc Schneider, "Tailor-made biofunctionalized nanoparticles using layer-by-layer technology", *International Journal of Pharmaceutics*, Vol. 395 (1-2): 236-242, 2010.
- **Hagar I. Labouta** and Marc Schneider, Interaction of inorganic nanoparticles with the skin barrier: current status and critical review, in due publication.

Conference Contributions:

Poster presentations:

- **Hagar I. Labouta**, Tobias Kraus, Karl-Heinz Kostka, and Marc Schneider, "Physicochemical parameters of gold nanoparticles influencing skin penetration", Gordon Conference on Barrier Function of Mammalian Skin, Waterville Valley, 7th-12th of August 2011.
- **Hagar I. Labouta**, Labiba K. El-Khordagui and Marc Schneider, "Chemical enhancement of skin penetration of gold nanoparticles", Skin forum, Frankfurt, March 2011.
- **Hagar I. Labouta**, Tobias Kraus, Labiba K. El-Khordagui and Marc Schneider, "Influence of the physicochemical attributes of gold nanoparticles on their interaction with the skin barrier", poster presentation, Skin forum, Frankfurt, March 2011.
- **Hagar I. Labouta**, Tsambika Hahn, Leon Muijs, Marc Schneider, "Multiphoton microscopy for investigating the penetration of AuNP through human Skin", 8th international conference and workshop on Biological Barriers- in vitro tools, nanotoxicology, and nanomedicine, Saarland University, Saarbrücken, 21st March – 1st April 2010.
- **Hagar I. Labouta** and Labiba K. El-Khordagui, "Modulation of in vitro release of hydrophilic drugs from polymeric microspheres", poster presentation, 3rd PSWC "Pharmaceutical Sciences World congress", Amsterdam, 2007.

- **Hagar I. Labouta** and Labiba K. El-Khordagui, "Development of verapamil HCl microspheres using neural modeling versus statistically-based factorial analysis", 3rd PSWC "Pharmaceutical Sciences World congress", Amsterdam, 2007.

Oral presentations:

- **Hagar I. Labouta**, Tobias Kraus, Labiba K. El-Khordagui and Marc Schneider "Determinants of skin penetration of gold nanoparticles and insight into the mechanism of action", Controlled release society- German local chapter, Jena, March 2011.
- **Hagar I. Labouta**, Tobias Kraus, Labiba K. El-Khordagui and Marc Schneider, "Study of the penetration of gold nanoparticles through human skin", European IP on Advanced Delivery Strategies for Pharmaceuticals and Cosmetics, Lyon, October 2010
- **Hagar I. Labouta** and Labiba K. El-Khordagui, "Verapamil Hydrochloride microspheres for potential topical applications", 67th International Congress of FIP, Beijing, August 2007.

Teaching Experience:

- Participated in teaching the practical course of biopharmaceutics and pharmaceutical technology "*Arzneiformenlehre I*": solid, liquid and semisolid pharmaceutical dosage forms, winter semester 2010/2011 and summer semester 2011, University of Saarland, Saarbrücken, Germany.
- Supervision of a pharmacy student in a one-month research project: "Exploring functionalities on gold nanoparticles: coating gold nanoparticles with thioglycolic acid" for an internship in the institute of Pharmaceutical Nanotechnology, University of Saarland, Saarbrücken, Germany, May 2011.
- Participated in teaching the module "Visualization of skin samples by different microscopic settings: Confocal and multiphoton laser scanning microscopy" in the lab course "In vitro models of human skin and application of modern visualization tools" during the 8th international conference and workshop on

Biological Barriers- in vitro tools, nanotoxicology, and nanomedicine, 21 March – 1 April 2010, Saarland University, Saarbrücken, Germany.

- Participated in teaching the following practical courses of pharmaceutics for undergraduates from 2003-2009 in Faculty of Pharmacy, University of Alexandria, Egypt:

Liquid Dosage Forms (solutions, suspensions, emulsions), Semisolid Dosage Forms (ointments, creams, suppositories, etc.), Solid Dosage Forms, Micromeritics, Complexation, Incompatibilities, Physical Pharmacy and Reaction Kinetics, and Cosmetics and Personal Care Products.

Other Scientific Activities:

- Participation in the assessment of the Pharmaceutical Sector in Egypt (focus on Alexandria Governorate) in collaboration with the Ministry of Health and the WHO, December 2008.
- Invited talk on the “Health Hazards of Smoking” at “Women and Children Health Institute”, Alexandria, Egypt, February 2009.
- Participation in the *translation* of a pharmacy book, entitled “Quality Assurance of Pharmaceuticals” (English to Arabic) for the WHO, December 2008.

Grants:

- German Egyptian Research Long-Term Scholarship “GERLS” 2009, a jointly funded scholarship by the Egyptian Ministry of Higher Education and Scientific research (MoHESR) and the German Academic Exchange Service (DAAD) for a 2 years study at Saarland University for a PhD degree (channel project).
- Travel grants to attend the 3rd Pharmaceutical Sciences World congress "PSWC" held at Amsterdam, April 2007 and the 67th International Congress of FIP held at Beijing, August 2007.

Acknowledgments

Above all, I am really thankful to Allah for his infinite blessings. Thanks Allah the most merciful for accepting my prayers, protecting me and keeping me on track during hard times. May Allah accept this work as one of my good deeds and make it useful for the others!

No matter whom this thesis is attributed to, the contents are the fortunate product of the efforts of many people. It is a pleasure to convey my gratitude to all of them though I can only name a fraction of them in my humble acknowledgments:

*First and foremost, I would like to express my sincere gratitude and appreciation to my supervisor (Doktorvater) **Jun. Prof. Dr. Marc Schneider** for offering me the opportunity to join his working group, his support and encouragement, spending a lot of effort and time on this work, fruitful discussions especially in the time of new ideas and difficulties and for being always willing to help. I am happy to know that I am the first official PhD student under his supervision! I want to thank him for allowing for a good scientific environment with a high degree of intellectual freedom. His friendly manner creates a calm atmosphere with absolutely no pressure on his students. I also want to thank him for being understanding and easy-going in many times! He is not only a supervisor from whom I have learnt so much, but a good friend as well. I am really thankful for everything! I also want to thank my entire working group, **Nico Reum, Ke, Qiong, Mardi, Clemens, Marius and Xavier**, for always acting like a team and helping in numerous ways.*

*I am grateful to **Prof. Dr. Ulrich Schäfer** for sharing with me his long and outstanding experience in the skin field. His valuable guidance*

and suggestions has often led me to the right scientific direction or even helped me in solving in situ technical problems. Thanks are extended to **Prof. Dr. Claus-Michael Lehr** for his encouragement and his faith and trust in me and **Dr. Nicole Daum** for sharing with me her experience in reconstructed human skin models.

I consider myself lucky to be first introduced to the skin lab by **Tsambika Hahn**. She kindly spent a lot of time and effort to show me some of the valuable skin techniques that I have practiced throughout my PhD work. She did all this with patience and a friendly attitude; she shares part of my success in the PhD. I am indebted to her more than she knows!

Many thanks to our expert technicians: **leon Muijs** for helping me with many things especially cryo-sectioning of skin punches and teaching me all the tricks for that, **Peter Meiers** for his help with HPTLC and gravimetric experiments, and **Petra König** for introducing me to the cell-culture lab.

Thanks to **Dr. Karl-Heinz Kostka** (Karitaskrankenhaus, Lebach), for supplying us with human skin essential to carry out all skin penetration experiments. Thanks to **Dr. Tobias Kraus** for preparing two types of the gold nanoparticles used in this work. Many thanks to all our partners in Melbourne especially **David C. Liu**, **Prof. Dr. Michael S. Roberts** and **Tarl W. Prow** and in Stuttgart, especially **Dr. Martina Hampel** and **Sibylle Thude**, who are co-authors in the presented publications.

I am eternally grateful to dearest **Prof. Dr. Labiba Khalil El-khordagui**, Dept. of Pharmaceutics, Faculty of Pharmacy, Alexandria University, Egypt, for her supervision during the first part of my PhD in Egypt and in Germany, as well as for preparing

me to be a good researcher during my master program. She is and will always be a good model for me and for all the young generation back home in our department. This is for her high scientific standards, creativeness, enthusiasm and her respect to the profession. I am grateful to her for all what I have achieved so far and I miss so much our casual personal talks.

Thanks to all my colleagues and friends in my home university. I miss you all and I wish you were all with me on the day of my defense. Special thanks to **Dr. Noha Nafee**, for all her help since I joined the department in Alexandria and especially here in Germany. Thanks for always being a good listener.

I would like to acknowledge the **Egyptian Ministry of Higher Education and Scientific Research** as well as the **DAAD** "Deutscher Akademischer Austausch Dienst" for their financial support during my stay in Germany.

A PhD was not only a scientific achievement for me; this was also a fascinating and an extremely rewarding personal experience. In our international institute, I was privileged to get to know and work with great colleagues and have the opportunity to share cultures and traditions with them. I enjoyed working with them all as much as I enjoyed our evenings and outings especially with **Salem, Anne Paulus**, my sweet neighbor **Nadia**, the Indian couple **Ratnesh and Prajakta**, **Nico Mell, Ana Melero**, the Finish couple **Timo and Päivi**, and all my working group. I will be waiting for your visit in Egypt!

My sincere thanks to my friends in Germany especially **Rabab, Yasmeen** and in Saarbrücken my best companion **Dina, Sahar, Doaa** and **Abou Al-Abbas, Noran, Amir, Sherif, Midu, Rawya, Asmaa** and

Alaa. Thanks for all the nice moments and memories and for being my family here! Life would have been simply difficult without you.

*Words are not there to express my gratitude to the people who shaped my life, my family. The word "Thanks" is simply meaningless, but sorry I have to say "thanks" to you my parents, for bringing me up as a good Muslim, for your unconditional love and support, for your infinite patience, for your trust and faith in me and for bringing to my life the sense of balance and happiness. I love you more than anyone else in this world. You are the best parents ever! To our engineer **Hend**, although you have grown up now but you will always remain my little sister, with all what it means "my little sister"! You should understand! To my older brother **Mohamed**, dear sister **Lamia** and my sweethearts **Jana** and **Yasin**, I share with you this success. I also want to share my success with **Dr Abdelaziz Saleh** from whom I always got a lot of confidence and strength throughout my way.*

*On writing the acknowledgments, I went with my thoughts throughout this journey in life. This journey was that much amusing and productive because of **Yasmine Abdo**, my best friend. I now look back to these days and just pray that Allah protects you my soul mate!*

It is impossible to end the acknowledgments... I finally want to thank all the important people that I could not mention here. Please accept my respect and gratitude!

Thanks!